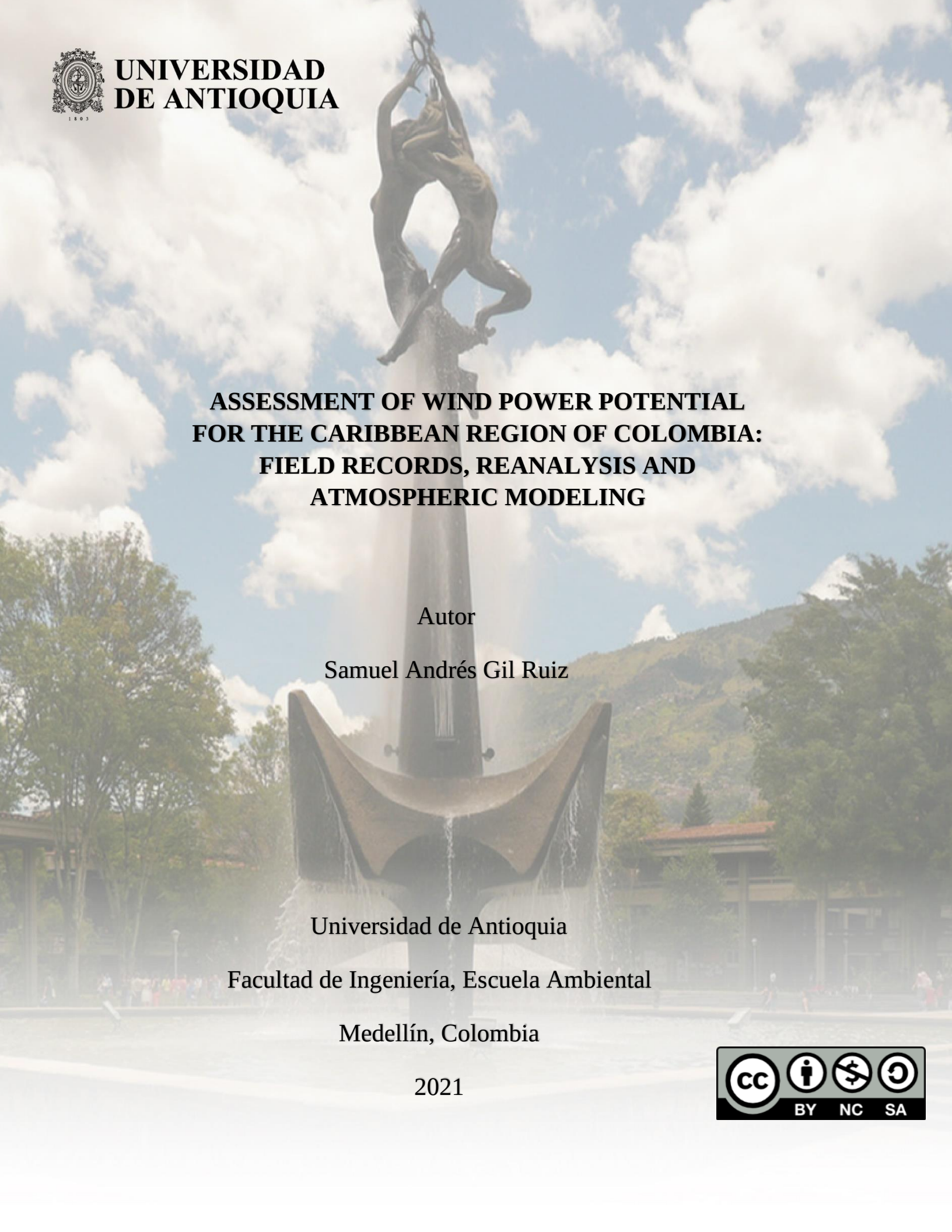

UNIVERSIDAD DE ANTIOQUIA

ASSESSMENT OF WIND POWER POTENTIAL FOR THE CARIBBEAN REGION OF COLOMBIA: FIELD RECORDS, REANALYSIS AND ATMOSPHERIC MODELING

Autor

Samuel Andrés Gil Ruiz

Universidad de Antioquia

Facultad de Ingeniería, Escuela Ambiental

Medellín, Colombia

2021

Assessment of Wind Power Potential for the Caribbean region of Colombia: Field Records, Reanalysis and Atmospheric Modelin

Samuel Andrés Gil Ruiz

Trabajo de investigación presentado como requisito parcial para optar al título de:
Magister en Ingeniería Ambiental

Asesores :
NJulio Eduardo Cañón Barriga, MSc., Ph.D.
J. Alejandro Martínez, MSc., Ph.D.

Línea de Investigación:
Energía renovable y modelación atmosférica

Universidad de Antioquia
Facultad de Ingeniería, Escuela Ambiental
Medellín, Colombia
2021.

“Somewhere, something incredible is waiting to be known.”

- *Carl Sagan*

To my family for their permanent support and understanding.

To my advisors, for their patience.

Abstract

This master's report presents an assessment of wind power potential for the Caribbean coast of Colombia. The report analyses a large set of field measurements with high temporal resolution, along with data from the reanalysis product ERA5 from the European Center for Medium-Range Predictions (ECMWF) and with high-resolution wind speed fields simulated with the Weather Research and Forecast model (WRF), validated with field measurements. The manuscript consists of two chapters. The first chapter characterizes the wind resource across a wide area that includes the Gulf of Urabá and the San Andrés Islands, with a special focus on La Guajira. The temporal aggregation in the averaging time of some variables shows how finer time intervals (10-minute to hourly) generate more accurate monthly and annual statistics than daily and monthly data, with 10-min average wind speeds in the region in the range of 2.2 m s^{-1} to 8.3 m s^{-1}. ERA5 performance at reproducing wind speed, direction, and variability compared to *in situ* measurements can be a valuable information source after identification/treatment of biases for wind characterization. Based on Weibull distributions and hourly Wind Power Density (WPD) calculations, the study finds several locations that offer commercial wind potential, with many having WPD above 800 W m^{-2}. Furthermore, estimates based on ERA5 show a wide offshore region in the Caribbean with a WPD over 800 W m^{-2} yearlong. Annual Energy Production (AEP) for the stations with promising potential reach capacity factors around 50%, which are comparable to those of the most productive wind farms worldwide. The second chapter shows the use of the WRF model to estimate the monthly wind regime, the intra diurnal wind variability, and the monthly WPD at resolutions of 9 and 3 km, which are substantially finer than the nearly 30 km equivalent grid size of ERA5. We compared the performance of three planetary boundary layer schemes in WRF (QNSE, YSU and MYJ) at reproducing the monthly average diurnal cycle of wind speeds during the months of higher (June) and lower (October) wind speeds, in four stations with high wind potential, based on metrics from Taylor diagrams. In addition, we compared WRF results with ERA5 estimates. The QNSE scheme outperforms the others in most sites and cases, with averaged fractional bias (FB) of 9.88% for QNSE, 10.83% for YSU, and 9.50% for MYJ, whereas ERA5 reached values up to 14.6%. Using the QNSE scheme, we calculated the WPD for the entire year and compared it with the ERA5 and the observed WPD by means of duration curves, for two of the analyzed points (northernmost locations). The WPD with WRF shows an almost perfect fit to the observed curves, while ERA5 only outperforms WRF in one location, and both ERA5 and WRF underrepresent in one location. Although the fields of WPD estimated with WRF are more detailed than those generated by ERA5, ERA5 information could still be valuable for offshore estimations at larger scales, e.g., the synoptic scale. The estimated WPD values for the month with higher wind speeds are up to 1200 W m^{-2} in the shoreline and up to 2000 W m^{-2} offshore, varying between 800 W m^{-2} and 1600W m^{-2} inland. WPD values during the month of lower wind speeds vary between 400 W m^{-2} and 800 W m^{-2}. Due to the high spatial resolution of the WRF model, the obtained results will serve to identify new areas with commercial wind potential in the Caribbean region of Colombia and the north coast of South America.

Keywords: Colombia wind potential, renewable energy, wind energy, ERA5, WRF, Weibull wind distribution; Colombia offshore wind power, WRF wind modeling

Acknowledgements

The author is especially grateful to Universidad de Antioquia for providing the logistics to develop this work, especially to the University's Observatorio Institucional for providing computational resources to run the models; we thank Professor Mónica M. Zambrano Ortiz and DIMAR for supplying the field data. Professor J. A. Martinez also received funding from the Program "Colombia Científica" within the framework of the called Ecosistema Científico (Contract No. FP44842-218-2018).

Table of Contents

List of Figures

List of Tables

1. Introduction

1.1 Problem statement

As the adverse effects of global warming increase, societies look for renewable energy sources to supply their needs in a sustainable manner. In this context, wind energy becomes a realistic option for both industrialized and developing countries. In industrialized countries, wind energy has been implemented successfully during the past two decades, representing nearly 19% of power generation capacity in Europe and 5% of energy use worldwide by 2018 (The Global Wind Energy Council, 2019). In developing countries, the implementation of this energy source begins to be viable both due to new regulations on the local energy markets and to continuous improvements in technology that reduce the production costs of wind energy.

In this context, countries like Colombia require reliable data about the availability, quality, and variability of winds in temporal and spatial scales that provide suitable information for the design and operation stages of new wind farms.

We focused on the study of winds over the Caribbean region of Colombia, especially in La Guajira, a region with promising wind resources (Vergara, 2010; IDEAM et al., 2017, Hoyos Guerrero et al., 2018; Rueda Bayona et al., 2019; Carvajal-Romo et al., 2019), with wind velocities in the range of 8 m s^{-1} at 10 meters height. The Colombian National Meteorological and Hydrological Service (IDEAM), based on 67 meteorological stations, generated a wind atlas for the entire country. Carvajal-Romo et al. (2019), in the assessment of wind potential for La Guajira, concluded that the entire national energy demand by 2050 could be covered by any of the wind power sources (onshore or offshore). In addition, Hoyos Guerrero et al. (2018), evaluated wind potential for La Guajira region, calculating the annual amount of energy produced in that region, and defining available areas for wind farms based on environmental, technical, and economical criteria. Rueda Bayona et al. (2019) studied the offshore wind potential of four sites in the north of Colombia, whereas Henao et al. (2020) indicated that wind power in the Caribbean coast could complement the country's hydropower sector during dry seasons and El Niño Southern Oscillation (ENSO) events. The cited sources have in common the use of information from reanalysis products such MERRA2, NAAR or derived products from these reanalyses. The cited authors made use of sparse meteorological stations with daily average data. However, both sources (reanalyses and network of meteorological stations with daily averages) lack the necessary resolution in time and space to represent the influence of local factors such as topography, the shoreline or land cover in the regional wind patterns and the intra diurnal behavior of winds.

Despite the progress made in characterizing the wind resource in this region, there is still a need for more precise assessments of wind potential for preliminary evaluation, micro-localization, and operation stages of wind farms. These assessments must use, for instance, available records of ten-

minute wind speed and air density from meteorological stations and secondary data from ERA5 (European Centre for Medium-Range Weather Forecasts reanalysis product of fifth generation), with hourly data and higher spatial resolution (Olauson, 2018; Floors & Nielsen, 2019; Ulazia et al., 2019; Betts et al., 2019; Kalverla et al., 2019; Hersbach et al., 2020). Even more, to solve issues related to the influence of local factors such as topography and land cover in the wind patterns, the assessments must take into account the atmospheric modeling of wind patterns with models such as WRF (Al-Yahyai et al., 2010; Carvalho, et al., 2014; Mattar & Borvarán, 2016; Salvação & Guedes Soares, 2018; Skamarock, et al., 2019; González-Alonso de Linaje et al., 2019), adequately validated to simulate atmospheric velocity fields in the region at high resolutions.

1.2 Research questions

Based on the previous considerations, this study tackles the following research questions:

1) What are the places of the Caribbean region of Colombia with feasible wind potential for commercial electric generation?

2) What are the performances of ERA5 and the WRF model in representing wind fields for power assessment in the Caribbean region of Colombia?

The hypotheses to address these questions are:

1) That several on-shore and off-shore locations along the Caribbean coast of Colombia, besides La Guajira, have the potential to produce wind power of commercial interest, and
2) That both ERA5 and the WRF model would provide useful information for wind potential assessment, but at different scales, being WRF more accurate than ERA5 at finer scales, since WRF considers the influence of local factors such as topography, coastline, land-sea breezes, and ground cover.

1.3 Objectives

1.3.1 Aim

This research aims at assessing high-resolution wind power potential of the Caribbean region of Colombia, suitable for preliminary evaluation, micro-localization, and operation stages of wind farms, based on field data, reanalysis, and numerical weather modeling.

1.3.2 Specific Objectives

To achieve the aim, the study states the following specific objectives:

- Characterize the surface wind regime (hourly, daily distributions, daily cycle, annual cycle), based on on-site data from three DIMAR (Dirección General Marítima de Colombia)-owned stations in the area and ERA5 reanalyses for a typical year in the region of interest.
- Determine the best high-resolution simulations that represent the observed surface winds in the region of interest, using different parameterizations of the boundary layer and surface layer in the WRF atmospheric model at the meso and convective scales.
- Estimate the hourly scale energy production of typical commercial turbines (i.e., power curves) at specific sites, defined in the high-resolution simulations, using the Wind Power Density (WPD).

To accomplish the aim and specific objectives, this research uses observations from meteorological stations, data from the reanalysis product ERA5, and the version 4.0.2 of the Weather Research and Forecasting model (WRF) (Skamarock et al., 2019). With the data from meteorological stations, the study extends previous characterizations of Wind Power Density (WPD) in the region. By using wind speed data with 10-minute frequency, we seek to contribute with more detailed wind speed distributions as with more precise estimates of the Annual Energy Production (AEP) and the expected capacity factors. With ERA5, the research seeks to understand the advantages and limitations of this kind of products when compared with observations and the possibility of extending estimates of wind potential based on this source to other regions without observations. Finally, the study looks for validating the use of WRF to represent observed winds in the studied region and to simulate not only the average, but also the intra diurnal spatial and temporal variability of the wind, and to estimate the WPD in a specific region that includes the north coast of Colombia and wide areas of the Caribbean Sea. The expectation is that, due to the physical basis of the generated information and its high resolution, it will help to identify new sites with wind power potential (inland, onshore, and offshore).

1.4 Structure of the report

This report consists of two chapters, structured as research papers. The first chapter (accepted for publication in the Journal Renewable Energy), characterizes the wind regimes in the Caribbean Region of Colombia and estimates the WPD and AEP of promising sites, based on two sources: ten-minute averaged winds of thirteen meteorological stations property of DIMAR (Dirección General Marítima de Colombia) and ERA5 estimates. The second chapter (under preparation for submission to the Journal Renewable Energy), evaluates the performance of three widely used PBL schemes of the WRF model to represent wind speeds and directions in comparison to observations and ERA5. Using the best performing scheme, we estimate the WPD for La Guajira region via the numerical modeling of the atmosphere during an entire year. A final section summarizes the general conclusions from the two chapters, followed by the references.

2. Wind Power Assessment in The Caribbean region of Colombia Using Ten-Minute Wind Observations and ERA5 Data

2.1 Abstract

The Caribbean region of Colombia is a strategic source of wind energy for Colombia's economic development. However, current estimates of wind energy potential for this region are based on low-resolution observations from a sparse set of weather stations that falls short of the temporal and spatial scales required by the wind energy sector. We present a novel characterization of the wind resource over the Caribbean region of Colombia, using 10-minute average wind records from 13 meteorological stations and compare the results with newer ERA5 reanalysis data to generate reliable information for the feasibility and operational stages of wind farms. According to the 10-min observations, average wind speeds in the region are in the range of 2.2 m s^{-1} to 8.3 m s^{-1}. Based on Weibull distributions and hourly Wind Power Density (WPD) calculations, we found several locations that offer commercial wind potential, with many having WPD above 800 W m^{-2}. Furthermore, our estimates based on ERA5 show a wide offshore region in the Caribbean with a WPD over 800 W m^{-2} yearlong. Finally, we calculate the Annual Energy Production (AEP) for the stations with promising potential, obtaining capacity factors around 50%, comparable to those of the most productive wind farms worldwide.

Keywords: Renewable energy; wind power; ERA5 wind power; Weibull wind distribution; wind power Colombia; Colombia offshore wind power

2.2 Introduction

The installed capacity of wind energy farms worldwide is expected to exceed hydroelectric and nuclear power in the current decade (Smets et al., 2016). The Global Wind Energy Council, for instance, reported that the wind power industry installed around 60.4 GW in 2019, which represents a 17% growth in only one year (Lee & Zhao, 2020). However, wind power use in countries like Colombia is still incipient. According to Vergara (2010), wind regimes in Colombia are among the

best in South America, with wind speeds up to 9 ms^{-1} at heights of 50 m on its north coast. Despite this, only in recent years, wind power is starting to be seriously considered as an important alternative in Colombia. Currently, there are only 19.5 MW of installed capacity at Jepírachi wind farm, La Guajira, over the Caribbean region of Colombia. Nonetheless, the expectations are to increase such capacity, with several wind farm projects already underway (UPME, 2019). According to XM, operator of the national interconnected electricity system, 1452 MW of wind generation could become operational by 2023 (XM, 2019).

Colombian winds have been characterized in an Atlas by the Colombian National Meteorological and Hydrological Service (IDEAM) (IDEAM, UPME, Ruiz M., Serna C., & Zapata L., 2017). This Atlas was generated with data from 67 wind stations for the entire Country. Carvajal-Romo et al (2019), for instance, used the Colombia Wind Atlas along with data from NASA Prediction of Worldwide Energy Resources (PWER) based on MERRA-2 reanalysis product (NASA, 2020), to study the wind power potential among other renewable energy sources in La Guajira, within a framework of regulations, energy demand in the Colombian market and social aspects, finding that onshore/offshore wind power may have the potential to cover the entire national energy demand by 2050. However, wind atlases have limitations to represent the effects of local factors (i.e., the surrounding topography, the differential heating of land surfaces and local circulations systems), due to their coarse resolutions in both time and space (Shi & Erdem, 2017). These factors cannot be adequately represented in resolutions of the order of tens of kilometers. Furthermore, the use of daily (in some cases monthly) wind speed averages in the atlases can also lead to miscalculations of wind potential, because they hinder the intra-diurnal variability of the wind, which is required for the feasibility and operation stages of wind power projects (the industry-standard time interval for wind power assessment is the 10-minute interval)

Based on Geographic Information Systems, in situ observations and the NASA-PWER dataset, Hoyos Guerrero et al. (2018), evaluated wind potential for the La Guajira region, determining the annual amount of energy and the capacity factor produced in that region, as well as mapping available areas for wind farms, based on environmental, technical, and economical criteria. Rueda Bayona et al. (2019) studied the offshore wind potential of four sites in the north of Colombia, based on 40 years of wind speed data from NAAR (NOAA, 2016) reanalysis database (approximately 33 km of grid size and 3-hourly data).

For the Caribbean region of Colombia, Devis-Morales et al. (2017) evaluated extreme values of winds and ocean waves, focusing on the design of offshore structures. These authors based their study on the information of the Cross-Calibrated Multi-Platform (CCMP) product (Ricciardulli et al., 2017), which uses ERA-Interim as a source of information. CCMP has a grid of 0.25° with a time resolution of 6 h, and the authors validated its data with information from five buoys.

The European Centre for Medium-Range Weather Forecasts reanalysis product of fifth generation (Hersbach et al., 2020) has been recently used, together with MERRA-2, to assess wind power potential in five Nordic countries (Olauson, 2018). Concerning the use of ERA5 in wind assessment, Floors & Nielsen (2019) present a method to estimate the air density for wind energy purposes, considering the elevation and making use of reanalysis data. The authors compared the estimates derived from ERA5, CFSR, and nearby in situ observations, finding that ERA5 exhibits lower mean absolute error than CFSR. Other recent examples of the use of ERA5 reanalysis product for wind characterization are presented by Ulazia et al. (2019) who performed a global

estimation of wind potential considering seasonal changes in the air density, demonstrating the importance of taking into account the air density variation, both in altitude and time, instead of taking a standard air density as is usually done in the case of wind turbine power curves and by Kalverla et al. (2019) who evaluated the skill of ERA5 reanalysis for representing low-level jets in northern latitudes, finding that, although the product is biased regarding observations, it represents reasonably well the stationary cycles and spatial patterns.

In this study we first characterize the mean diurnal and annual cycles of near surface wind speed and direction over the Caribbean region of Colombia, using data from 13 meteorological stations and ERA5 reanalysis. We compare the performance of ERA5 reanalysis with historical records. Afterward, we show the inter-annual variability of the diurnal cycle of in-situ measurements of wind speed and its behavior during different phases of the El Niño-Southern Oscillation (ENSO). Next, we characterize the wind speed variability with Weibull probability density functions (PDF), using daily, hourly, and 10-min aggregations (the last one being the standard for wind power characterization). We then estimate the Wind Power Density (WPD) for the locations of the stations at 100 m height, using logarithmic wind profiles at each station and wind duration curves. We compare the results with the corresponding estimates from ERA5. We also use ERA5 data to estimate the seasonal variation of WPD (at 100 m height) over the entire region; this information is then used to identify large offshore areas with significant wind potential. Finally, we calculate the Annual Energy Production (AEP) and the corresponding Capacity Factor (CF), which is corrected with real data from the Jepírachi wind farm. To the best of our knowledge, our study is the first attempt to both validate ERA5 surface wind estimates for the Caribbean region of Colombia and use ERA5 to evaluate wind power potential incorporating variations of air density. In addition, we offer the first wind characterization in 10-minute and hourly intervals for the studied area, which better represent fluctuations of wind speed and direction over periods of minutes and hours, impossible to detect with daily and monthly averages. This fine characterization is relevant for grid operators to make decisions about the operation of the entire electrical system.

The paper aims at contributing to the development of the wind energy sector in the Caribbean region of Colombia by providing useful and relevant information for wind farm developers, investors, and operators in terms of: (i) a characterization of winds at finer temporary scales (10-minute and hourly basis) with novel information on diurnal cycles of wind speed, direction, turbulence, and intra-daily variability; (ii) a comparison and validation of the performance of the new ERA5 reanalysis data to represent hourly winds over the entire Caribbean region of Colombia coast (including parts of Central America and San Andrés Island) at a grid resolution of 30 km, following recent methodologies presented in Betts et al. (2019) ; (iii) an estimation of the annual cycle of WPD from both meteorological stations and ERA5 data, based on a novel approach to improve consistency and precision of the estimates with hourly variability of air density (Ulazia et al., 2019; Floors & Nielsen, 2019); and (iv) a quantification of the AEP from both recorded data and ERA5.

2.3 Materials and Methods

2.3.1 Study area

The Caribbean coast of Colombia extends from the San Andres and Providencia archipelago in the west to the La Guajira peninsula in the east, encompassing part of the Central American Caribbean (Figure 2.1). The Caribbean coast of Colombia consists of eight political-administrative divisions known as departments (from north to south): La Guajira, Magdalena Atlantico, Bolivar, Sucre, Cordoba, Antioquia, and Chocó.

At the intra-annual scale, the trade winds, and the displacement of the Intertropical Convergence Zone (ITCZ) are the drivers of wind climatology in the Caribbean region of Colombia. The above implies that stronger winds move along the Caribbean coast of Colombia coast from the south (i.e., inner lands and Gulf of Urabá) at the beginning of the year (January to March) towards the north (i.e., San Andrés and Guajira) in June-July, due to the displacement of the ITCZ northwards (Poveda, 2004; IDEAM et al., 2017). In addition, at the intra-daily scale, wind variability is associated with local factors (i.e., topography, land cover), and with terrain-induced mesoscale systems (i.e., sea and land breezes). Since the analyzed stations are located near the coastline, their winds are highly influenced by land-sea breeze circulations (Pérez et al., 2018), conditioned by prevailing synoptic systems and the shape/orientation of the coastline.

Winds in the region are also affected by the Caribbean Low-Level Jet (CLLJ), which has been characterized by several authors (e.g., Whyte et al., 2008; Rife et al., 2010; Ranjha et al., 2013). The CLLJ strengthens the trade winds during the summer season and its intensity is linked to ENSO (Whyte et al., 2008).

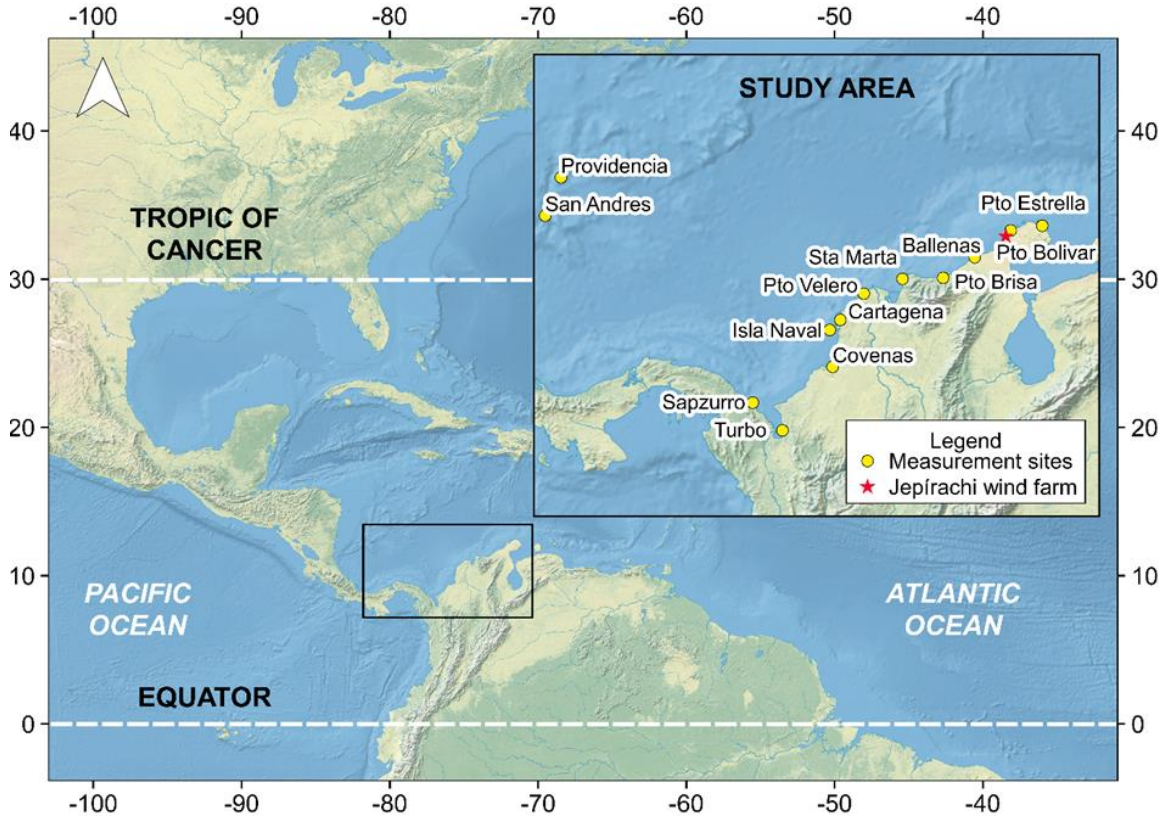

Figure 2.1: ***Location of the Caribbean region of Colombia. Analyzed region framed in black. The map shows the location of the 13 meteorological stations and the Jepírachi wind farm.***

2.3.2 Datasets

We analyzed data from 13 meteorological stations, distributed along the continental coast and in the islands of San Andrés and Providencia (see Figure 2.1). The stations provide 10-minute average records of near-surface winds (10 m above the surface), and hourly records of pressure and temperature. The stations are property of DIMAR (Dirección General Marítima de Colombia), which supplied the in-situ data for this study. The period covered by these records varies between one and six years, depending on the station (Figure 2.2).

We studied the spatial patterns of winds in the studied area with ten years of hourly wind speed and direction data (2008-2017) at 10 m over the surface from the novel ERA5 reanalysis product (ECMWF, 2017, and Hersbach et al., 2020). To estimate the WPD, we used ERA5 data of hourly temperature, pressure, dewpoint temperature, and specific humidity.

To assess the capabilities of ERA5 to represent recorded wind speeds at the stations, we used the root-mean-square error (RMSE) estimator and its percentage concerning the mean of the observations (RMSE%). In addition, we used the bias percentage to measure the overestimation or underestimation of the ERA5 product. Finally, we utilized the Pearson correlation coefficient r to know the degree of association in the fluctuations between ERA5 and the recorded data from stations.

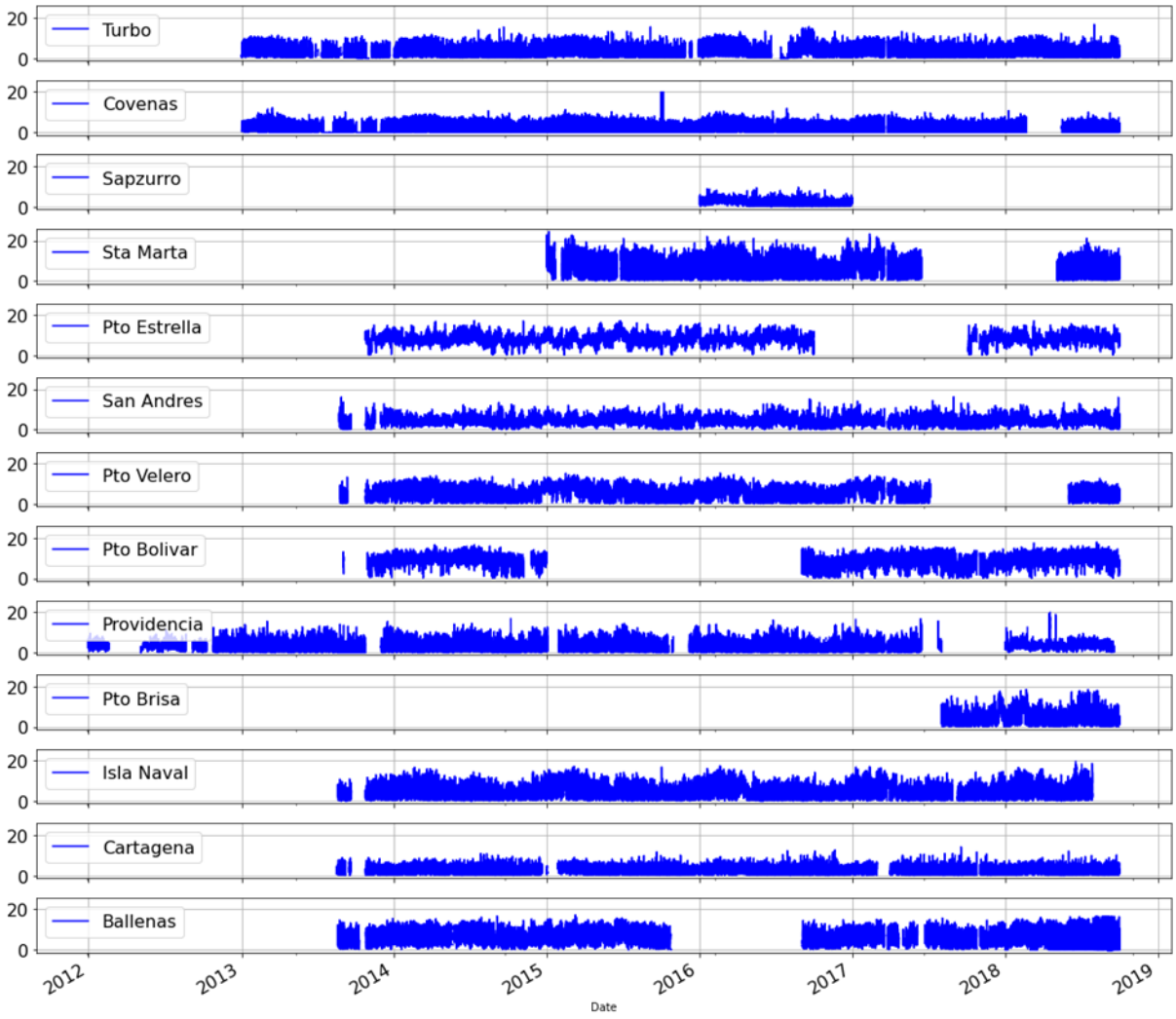

Figure 2.2: ***Length of records at each station (ten minutes averages of wind speed).***

After checking the consistency of the time series and discarding abnormal data, we characterized the wind speed at each station via statistical moments of mean, standard deviation, and the percentiles P_{25}, P_{50}, and P_{75}. We characterized wind regimes (frequency, magnitude, and direction) through wind rose plots for each station. In addition, we analyzed the diurnal wind speed cycle and the range of variation of wind speeds along the day, based on 10-minute wind speed means and the 25 and 75 quartiles. Furthermore, we estimated the diurnal wind cycle for each year of available data, to correlate the behavior with an ENSO signal.

We analyzed the variations of wind direction across the diurnal cycle with mean hourly data statistics and hodograph plots.

We used the turbulence intensity (I) to identify the turbulent nature of the wind field:

$$I = \frac{\sigma}{\bar{\mu}} \quad (1)$$

Where I = turbulence intensity; σ = standard deviation of wind speed (ms^{-1}); $\bar{\mu}$=wind speed average.

We calculated I over a moving window of an hour with 10-minute averages for all the registered periods. *The value of I* depends on local factors such as the roughness of the ground surface, height above the surface, topography, and thermal behavior of the atmosphere (Burton et al., 2001), and its magnitude weakens with height above the surface (Jacques, 2010).

2.3.3 Wind speed frequency distribution

We characterize the wind speed frequency distribution for the analyzed stations and ERA5 through two-parameter Weibull distributions, which are widely used in the wind energy field to represent wind variability. The probability density function of the Weibull distribution and its cumulative form are expressed as:

$$f(v) = \frac{\kappa}{\lambda}\left(\frac{v}{\lambda}\right)^{\kappa-1} \exp\left\{-\left(\frac{v}{\lambda}\right)^{\kappa}\right\} \qquad k>0, \lambda>0, v>0 \quad (2)$$

$$f(v) = 1 - \exp\left\{-\left(\frac{v}{\lambda}\right)^{\kappa}\right\} \quad (3)$$

Where k = Weibull shape parameter; λ = Weibull scale parameter on (ms^{-1}); v = wind speed (ms^{-1}).

The Weibull distribution consists of a scale parameter (λ) and a shape parameter (k). As explained in Jacques (2010) and Arslan et al. (2014), the scale parameter λ (ms^{-1}) represents the relative cumulative frequency of wind speed, and hence λ relates to the annual average velocity, whereas the shape parameter k represents the asymmetry of the function. High k values ($k > 2{,}5$) indicate narrow frequency distributions, meaning steadier, less variable wind, which sometimes is the case for the trade winds belts. On the other hand, low values of k ($k < 1{,}5$) indicate greater variability with respect to the mean (Burton et al., 2001).

Using the Maximum Likelihood Method (MLM) (Arslan et al., 2014; Kaplan, 2017), we estimate the shape and scale parameters for the averaged ten-minute winds, the hourly averaged winds, the daily averaged winds, and the ERA5 pixels over the area of each station (also in hourly and daily averaged time steps).

2.3.4 Wind power and wind power density

Wind power is the rate of kinetic energy flow (Kalmikov, 2017) defined as:

$$P = \frac{1}{2} * \rho * A * v^3 * C_p \qquad (W) \qquad (4)$$

Where P = wind power (W); ρ = air density (kg m^{-3}); A = sweep area (m^2); v = wind speed (m s^{-1}) and Cp = power coefficient (between 0 and 1, according to Figure 2.3).

Wind power dependency on the cube of wind speed highlights the need for an accurate wind speed characterization. With the records of each station, we estimated the hourly WPD (also known as kinetic wind energy flux) at 100 m height for each site, as:

$$WPD = \frac{1}{2} * \rho * v^3 \qquad (W\ m^{-2}) \qquad (5)$$

Where WPD = hourly wind power density (W m^{-2}); ρ = hourly air density (kg m^{-3}); v = hourly wind speed (m s^{-1}).

The 100 m height corresponds to the altitude of a current standard wind turbine. As noted in Kalmikov (2017), the WPD serves to compare wind power resources, regardless of wind turbine size.

As remarked by Gunturu & Schlosser (2012), representing the WPD only by the total mean does not describe the wind power potential appropriately, since it ignores useful information about the variability and availability of the wind resource. Therefore, we used the methodology of duration curves, which represent the frequency of occurrence of the WPD for the entire time series (season a). We also calculated the duration of WPD in the months in which average wind speed is higher than the mean wind speed of the entire time series (season c) and for the months in which mean wind speed is lower than the mean of all records (season b).

Since data in the stations were taken at 10 m above the surface, we extrapolated the wind speed to the desired height with a logarithmic wind profile (see e.g., Stull, 1988), expressed as:

$$v_z = v_m * \left(\frac{\ln(z/z_0)_*}{\ln(z_m/z_0)} \right) \qquad (m\ s^{-1}) \qquad (6)$$

Where: z0 = roughness length for momentum; u* = friction velocity (m s^{-1}); K = Von Karman constant; d = displacement height (m); vz = wind speed at the desired height (m s^{-1}); vm = wind speed at known height (m s^{-1}); zm = known height (m); z = interest height (m).

We assumed neutrally stable atmospheric (boundary layer) conditions, following the considerations of large wind shear at the speeds of wind power generation, given by Gunturu & Schlosser (2012).

For each station, the values of z0 (theoretical height at which wind speed is zero) were chosen according to the reference values presented in Bonan (2016), and the information about measurement sites available in the DIMAR's web geographic portal, that provides satellite images and photographs of each station.

With the data of mean hourly temperature and pressure, and using the Ideal Gas Law, we estimated the hourly mean wind density. Finally, assuming a well-mixed boundary layer with negligible variations of air density between heights of interest, we calculated the WPD using Equation 5, according to Gunturu & Schlosser (2012).

We use the 10-minute mean wind speed data, together with the mean hourly data of temperature and pressure available for each station, to calculate WPD, following the work of Ulazia et al. (2019). We considered the hourly variation of air density (rho in Equation 4. Similarly, we estimated WPD with hourly ERA5 data, considering the hourly variation of \rho, according to the framework and equations presented by Floors & Nielsen (2019).

2.3.5 Annual energy production (AEP)

We use a Vestas V117-3.45 wind turbine model (with a rated power of 3,45 MW), and an assumed 100 m hub's height to estimate the annual energy production (AEP). Figure 2.3 shows the turbine power curve, its main features are shown in the Table 2.1. This turbine model was chosen according to its design for high and medium wind velocity sites (although the type of turbine may vary in each site, we use only one type as a baseline for our estimates).

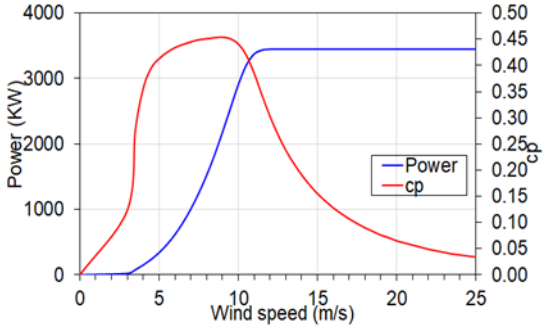

Figure 2.3 : ***Power curve of Vestas V117-3.45 wind turbine. Elaborated with information from wind-turbine-models.com (2019).***

Table 2.1 ***: Main features of Vestas V117-3.45 wind turbine. Elaborated with information from wind-turbine-models.com (2019).***

Vestas V117-3.45 wind turbine	
Rated power (MW)	3.45
Swept area (m^2)	10751
Cut-in wind speed (ms^{-1})	3
Cut out wind speed (ms^{-1})	25
Diameter (m)	117

We estimated AEP through the integration of the 10-minute mean wind speed frequency distribution for a typical year (bins of 1 ms^{-1}), with the power curve of the chosen turbine and the resultant energy given in GWh. As mentioned by Burton et al. (2001) and Jacques (2010), the above constitutes a standard practice of the wind industry. We extrapolated the wind speed data at 100 m. This calculation was performed for different time averages and ERA5 data.

We also estimated the AEP with direct measurements from several years, calculating the energy production for each time interval (10 min) directly from the records with Equation 4 and integrating the calculation into the year. We estimated the other necessary data in the same way as in the case of the WPD calculations explained in section 2.7.1.

The Cp coefficient represents the turbine efficiency (i.e., the ratio between the power extracted by the turbine and the total power of wind resources, Kalmikov, 2017). As shown in Figure 2.3, Cp varies according to wind speed, being the Betz's Limit (59%) the maximum achievable value of Cp (Burton et al., 2001). In our case, Cp reaches values of 45%.

To estimate AEP from field measurements, we considered that a turbine does not generate energy when wind speeds are above the cut-off or below the cut-in speed limits. First, we presented an AEP estimate that initially does not take into account the times of no energy generation due to technical issues (like maintenance or repair) or due to the grid restrictions for energy generation (AEP for ideal conditions). To address the lack of information about the operation, we corrected the AEP based on the capacity factor (CF) of the Jepírachi wind farm, reported by XM (2019) for 2014. The Jepírachi wind farm is located within the studied area at 12.23°N and -72.04°W, near Pto. Bolivar station located at 12.26°N and -71.97°W (Figure 2.1).

The CF quantifies the fraction of the installed generating capacity that actually generates power (Kalmikov, 2017), and it is estimated as the ratio between the actual generated energy throughout a period and the total energy that could be generated at rated power during the same period (Equation 7).

$$\mathrm{CF} = \frac{\mathrm{E_{actual}}}{\mathrm{E_{ideal}}} \tag{7}$$

Where CF = capacity factor; $\mathrm{E_{actual}}$ = actual generated energy along a period; $\mathrm{E_{ideal}}$ = energy that could be generated at rated power during the same period. Equation 8 show our proposed correction to the AEP:

$$\mathrm{Dif} = \mathrm{CF(Idealized)} - \mathrm{CF(Reported)}$$

$$\mathrm{CF_{corrected}} = \mathrm{CF(Idealized)} - \mathrm{Dif} \tag{8}$$

$$\mathrm{AEP_{Corrected}} = \mathrm{E_{ideal}} * \mathrm{CF_{corrected}}$$

where $\mathrm{CF\ (Idealized)}$ = capacity factor calculated for ideal conditions; $\mathrm{CF\ (Reported)}$ = capacity factor reported by the energy market manager.

2.4 Results and discussion

2.4.1 Wind characterization for the Caribbean region of Colombia

Table 2.2 summarizes the main statistics of 10-minute wind speed averages of the 13 stations along the Caribbean region of Colombia (Figure 2.1). From this characterization, the highest average wind speeds occur in La Guajira, with values between 5.5 m s^{-1} and 8.3 m s^{-1}. In the coastline of Magdalena (Sta. Marta and Pto. Velero stations), the average speed values oscillate between 6.0 m s^{-1} and 7.1 m s^{-1}. On the coast of the department of Bolivar (Cartagena and Isla Naval stations), mean wind speeds vary between 2.8 m s^{-1} and 5.4 m s^{-1}. In the Gulf of Urabá, the average wind speed reaches values between 2.2 m s^{-1} and 3.2 m s^{-1}, and in the archipelago of San Andrés, values oscillate between 3.4 m s^{-1} and 4.5 m s^{-1}.

According to the classification proposed by the National Renewable Energy Laboratory (NREL), sites with wind speeds higher than 5.0 m s^{-1} are suitable for energy generation on a commercial scale. As shown in Table 2.2, the Caribbean region of Colombia effectively has the potential for large-scale wind power generation, except for the Gulf of Urabá and San Andrés.

Table 2.2: ***Wind speed statistics for the studied stations. For location, see Figure 2.4.***

Wind speed statistics for analyzed stations									
Region	Station	Parameter							
		n	u (m s^{-1})	Std. Dev. (m s^{-1})	P_{25} (m s^{-1})	P_{50} (m s^{-1})	P_{75} (m s^{-1})	T (°C)	P (hPa)
Guajira	Pto. Estrella	199471	8,3	2,2	6,9	8,2	9,7	28,3	1010,75
	Pto. Bolivar	162043	8,4	2,8	6,7	8,8	10,4	27,8	1010,37
	Ballenas	203937	6,9	3,1	4,5	6,9	9,2	27,9	1009,65
	Pto. Brisa	61223	5,5	3,7	2,5	4,6	7,8	27,4	1009,44
Magdalena	Sta. Marta	144356	7,1	4,2	3,4	6,6	10,4	27,9	1004,52
	Pto. Velero	208756	6,0	2,9	3,6	6,1	8,4	28,3	1008,94
Bolívar	Cartagena	245998	2,8	1,5	1,7	2,7	3,8	28,5	1008,93
	Isla Naval	245606	5,4	3,3	2,8	4,6	7,6	28,2	1009,13
Golfo de Urabá	Covenas	277137	2,4	1,9	0,7	1,9	3,9	28,2	1010,99
	Turbo	281010	3,2	2,5	1,3	2,0	4,7	27,6	1008,42
	Sapzurro	51339	2,2	1,2	1,2	1,9	3,1	27,1	1010,07
San Andrés	San Andres	252526	4,5	1,8	3,2	4,4	5,7	28,2	1011,85
	Providencia	267112	3,4	1,9	2,1	3,2	4,5	27,9	1011,17

Regarding wind direction, wind roses in Figure 2.4 show that easterly winds, characterized by high speeds (> 5 m s^{-1}), are predominant in La Guajira region year-round. The same pattern of predominant trade winds occurs in San Andres, but with wind speeds lower than in La Guajira. Towards the Gulf of Urabá, winds from the northwest and south are common, with lower speeds. Towards the coasts of Magdalena and Bolivar, the prevalent winds are from the north, N-E and N-W, also with lower speeds than La Guajira.

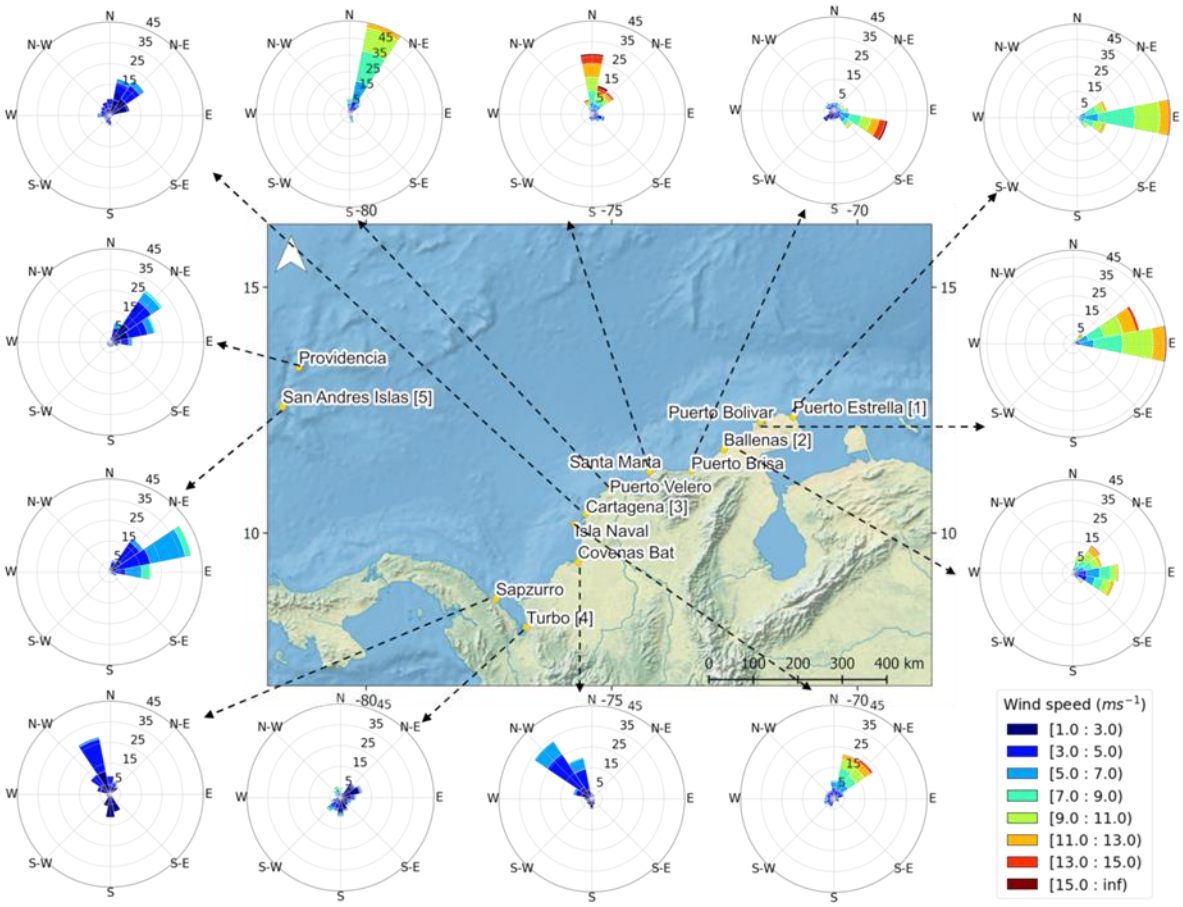

Figure 2.4 : ***Area of interest and wind roses of analyzed stations.***

Table 2.3 shows the performance of ERA5 to represent wind data for the region of interest. On the one hand, ERA5 underestimates (negative bias) the wind speed in the stations located in La Guajira and other locations of the northern shoreline of the Caribbean region of Colombia (Turbo and Isla Naval stations included). On the other hand, ERA5 reanalysis overestimates wind speed in San Andrés islands stations. Table 2.3 also shows good correlations at the hourly scale between ERA5 and the observations, except for Turbo station (r=0.23). In stations Coveñas (r=0.43), Cartagena (r=0.42) and Sta. Marta (r=0.42), correlations are low, whereas ERA5 exhibits good linear correlations with the rest of the stations.

ERA5 issues with RMSE, bias and correlation at some stations are likely associated with the limited resolution and parametrization of factors such as the influence of sub-grid gradients in topography near the stations, misrepresentation of the details of the coastline, limitations in boundary layer and

turbulence parameterizations, and inadequate specification of the land cover type used for the production of ERA5.

The results presented in Table 2.3 (for example RMSE variations between 18% and 116%) are consistent with Olauson (2018), who points out that the use of reanalysis products to directly determine the wind speed at one point is not recommended due to the inability of the reanalysis to resolve variations of local turbulent fluxes, especially over complex terrain. However, Olauson (2018) also found that, at a country level, the ERA5 product behaves better than MERRA-2 and even better than databases obtained from MERRA-2 scaling (sources cited by the same author, point out that the scaling of reanalysis data, whether statistical or dynamic, not necessarily implies better correlations with observations).

Table 2.3 : ***ERA5 performance against meteorological stations. For the location of the stations see Figure 2.4.***

ERA5 performance against meteorological stations					
Region	Station	Error measurement			
		RMSE (m s^{-1})	RMSE (%)	Bias (%)	Correlation (R)
Guajira	Pto. Estrella	1,50	18,0	-20,0	0,74
	Pto. Bolivar	1,78	21,0	-51,0	0,80
	Ballenas	2,46	36,0	-84,0	0,63
	Pto. Brisa	3,10	56,0	-202	0,70
Magdalena	Sta. Marta	4,03	57,0	-47,0	0,42
	Pto. Velero	2,04	34,0	-17,0	0,75
Bolívar	Cartagena	1,98	70,0	64,0	0,42
	Isla Naval	3,67	68,0	-245,0	0,52
Golfo de Urabá	Covenas	1,70	75,0	42,0	0,43
	Turbo	2,60	82,0	-24,0	0,23
	Sapzurro	1,77	81,0	97,0	0,68
San Andrés	San Andres	3,95	116,0	367,0	0,69
	Providencia	2,58	58,0	195,0	0,67

2.4.2 Mean annual cycle of winds

Figures 2.5 and 2.6 show the monthly wind roses of representative months for stations Pto Estrella (1), Sta. Marta (2), Turbo (3) and San Andres (4), compared with monthly wind roses from the ERA5 product for the pixel in which the stations are located.

For the stations over the north of the region of interest (e.g., Pto Estrella station), in La Guajira region, easterly winds prevail along the year (steady both in direction and speed). Higher wind

speeds occur in May, June, July, and December. As mentioned before, this behavior is due to the influence of trade winds and the displacement of the ITCZ. For this region if we compare with the station information, we can observe that ERA5 product shows a good performance in representation of winds both in frequency and prevalent direction but underestimates speeds, which is coincident with information presented in Table 2.3.

To the south, according to Santa Marta station data, we observe a notorious influence of northerly winds, which are predominant all year long, especially during the first quarter. Winds from the south occur in the second half of the year, although these are weaker than the winds from the north. In addition to the aforementioned effect of ITCZ displacement, the wind's behavior in the zone of Santa Marta station could be due to the circulation of trade winds induced by continental land. In this zone, the magnitudes of wind speed reach up to 13 m s^{-1} for all months of the year, except October and November. If we compare the wind roses presented in Figure 2.5 we can observe that for this area, for all year the prevalent wind direction according to ERA5 is E to N-E whereas for Sta Marta station prevalent wind direction is N. We can observe that also for this area ERA5 underestimates wind speed values. Regarding less frequent winds we can observe that for September month ERA5 shows a wide variety of directions which is surprise due to the coarse resolution of this reanalysis product.

In the Gulf of Urabá, according to Turbo station the monthly wind regime shows the prevalence of N-E winds for the first quarter of the year. Winds from the south prevail in the remaining months. Wind speeds in Turbo station are among the lowest recorded. We observe a predominant decreasing trend in wind speeds with latitude from La Guajira towards the Gulf of Urabá According to Figure 2.6 in this area ERA5 product shows prevalent N winds for the first quarter of the year which is not coincident with Turbo station data. For the rest of the year ERA5 shows S-W prevalent winds. In general, ERA5 does not reproduce well the wind frequency and magnitude of wind in the Urabá region, however ERA5 is capable of represent south winds which influence is less common in the studied area.

For San Andres station, East winds prevail along the year (Figure 2.6). Higher wind speeds occur in June and July, while lower speeds occur in October and November. In this case ERA5 shows a good performance regarding wind direction and frequency but tends to overestimate wind speeds.

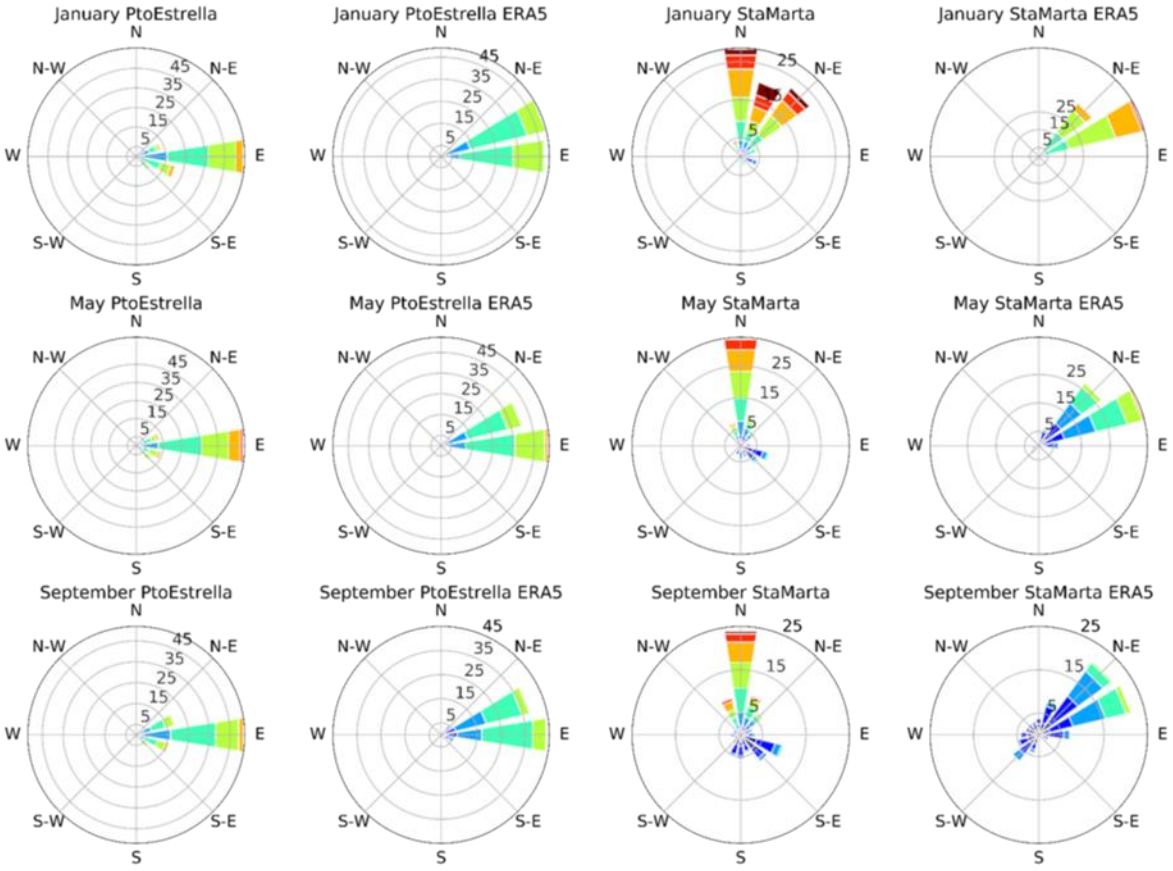

Figure 2.5: ***Wind roses for representative months, comparison with ERA5 (velocities magnitude according to Figure 2.4).***

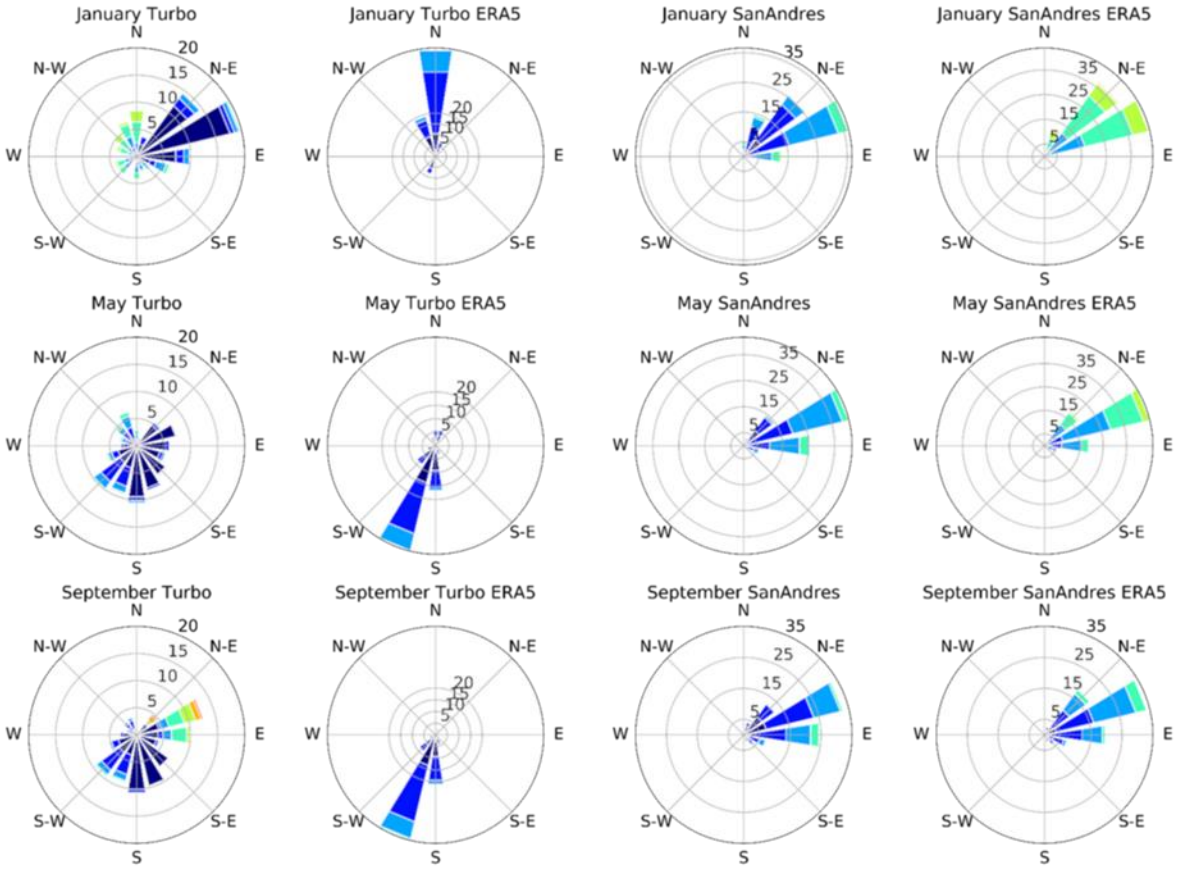

Figure 2.6: ***Wind roses for representative months, comparison with ERA5 product (velocities magnitude according to Figure 2.4).***

Regarding the spatial behavior of winds in the analyzed area, Figure 2.7 shows the annual wind regime obtained from ERA5 reanalysis product and the location of the four stations analyzed in the previous paragraph. Reanalysis data should be used only for larger space and time scales (Emeis, 2013). In this case, for example, we can appreciate the effect of ITCZ's displacement on monthly wind regimes over the north of Colombia and how in June–July the winds are stronger over La Guajira, while in January the zone of stronger winds moves southwards, influencing wind patterns in the Gulf of Urabá. Also, from figures 2.5, 2.6 and 2.7 we observe that the northern area (La Guajira) is under the influence of trade winds throughout the year which may favor wind energy generation.

If we look at the ERA5 data with respect to the measurement points (Figures 2.5, 2.6 and 2.7)), we obtain a good ERA5 performance to represent both wind speed and direction throughout the annual cycle along areas where synoptic systems like the Trade Winds have a strong influence.

The previous analysis (Figures 2.5 to 2.7) suggests that ERA5 represents adequately both wind speed and direction throughout the annual cycle over areas where regional scale patterns such as the Trade Winds have a strong influence. ERA5 does not perform as well in areas like Turbo and Sta. Marta stations, where local conditions have a strong influence on winds. This could be due to ERA5 inherent lack of representation of the influence of local factors like topography and land cover in wind speed and direction, as pointed out by Olauson (2018).

ERA5 also shows zones in front of Magdalena and Bolivar locations with mean annual wind speeds greater than 6 m s^{-1} at 10 m above the surface, which may be suitable for offshore wind energy applications. This result coincides with findings by Rueda-Bayona et al. (2019).

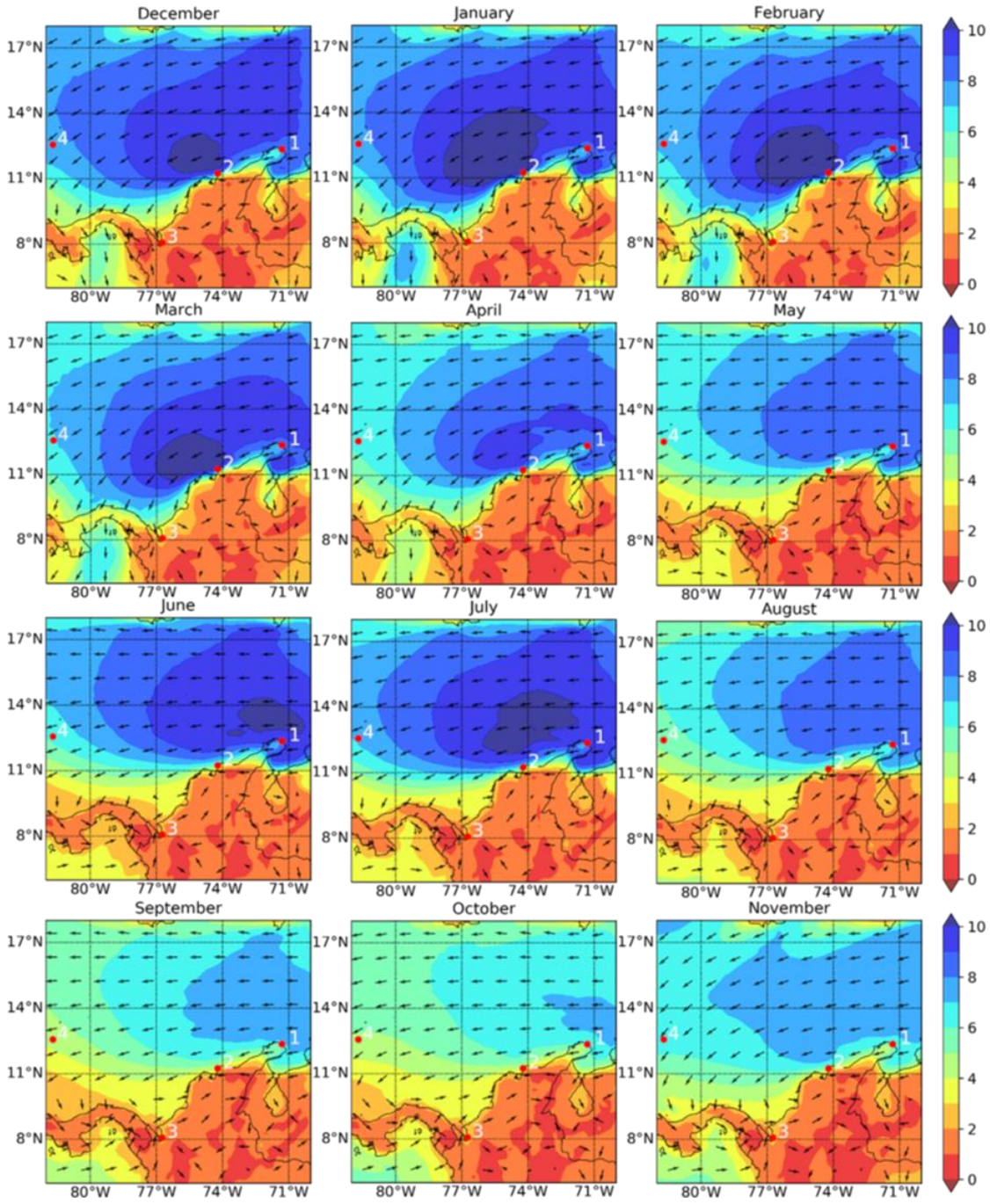

Figure 2.7 : ***Monthly mean wind magnitude (shades in m s^{-1}) and direction (normalized vectors) according to ERA5. Base period is 2008-2017. Stations: Pto Estrella (1), Sta. Marta (2), Turbo (3) and San Andres (4).***

2.4.3 Diurnal cycle of wind speed

The diurnal cycle of winds in the region, reveals a thermally driven system, in which the differential heating of the surface drives the wind speed and direction, typical of a land-sea breeze system (Pielke & Segal, 1986). In this regard, our results reinforce the results presented by Pérez et al. (2018). For instance, the hodographs in Figure 2.8 show a cyclic pattern in stations Pto. Estrella, Sta. Marta, Turbo, and San Andrés, where winds blow toward the continent at daytime (corresponding to a strong -U component of wind velocity vectors for Pto. Estrella and San Andrés, and +U component for Sta. Marta and Turbo station), and toward the sea at night (corresponding to a U+ component of velocity vectors for Pto. Estrella, and U- component for Sta. Marta, and Turbo, and a U+ component for San Andrés station). In San Andrés, other factors, such as the island size or the superposition of wind sea circulation, can modify the wind patterns. Nonetheless, we can assume that wind speeds in San Andrés are thermally driven. Given the spatial distribution of the stations analyzed in Figure 2.8, they may be considered representative of the region.

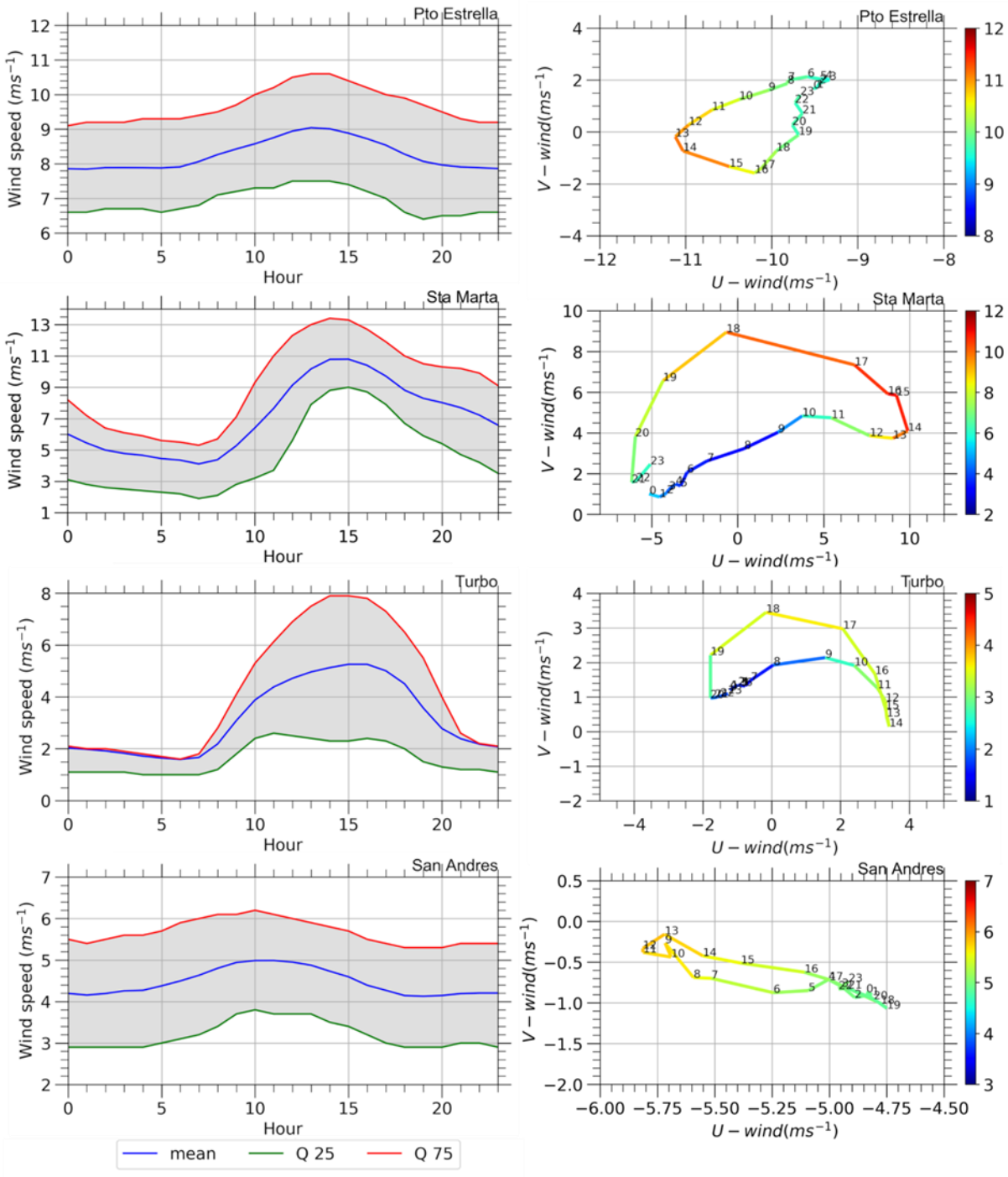

Figure 2.8 : ***Diurnal cycle of wind speed and hodographs for highest wind speed months.***

From the point of view of wind potential in the diurnal cycle, there is a coincidence between the hours of higher wind speeds (between 07:00 and 18:00 LT in the left panels of Figure 2.8) and the hours of the day in which demand is high and constant, according to Colombia's energy demand curve (XM, 2019).

Figure 2.9 shows the mean diurnal cycle of wind speeds for different years. In La Guajira, El Niño years exhibit higher wind speeds throughout the diurnal cycle, which would imply a higher availability for wind power generation. Since the hydroclimatic variability generated by El Niño has had adverse effects on hydroelectric power production in Colombia (Poveda, 2004), we can assume that wind power generation, at least in La Guajira, would add stability to the country's energy matrix during critical stages of energy availability. In this way, wind generation projects can benefit from incentives such as the Charge on Reliability, and therefore increase their economic viability.

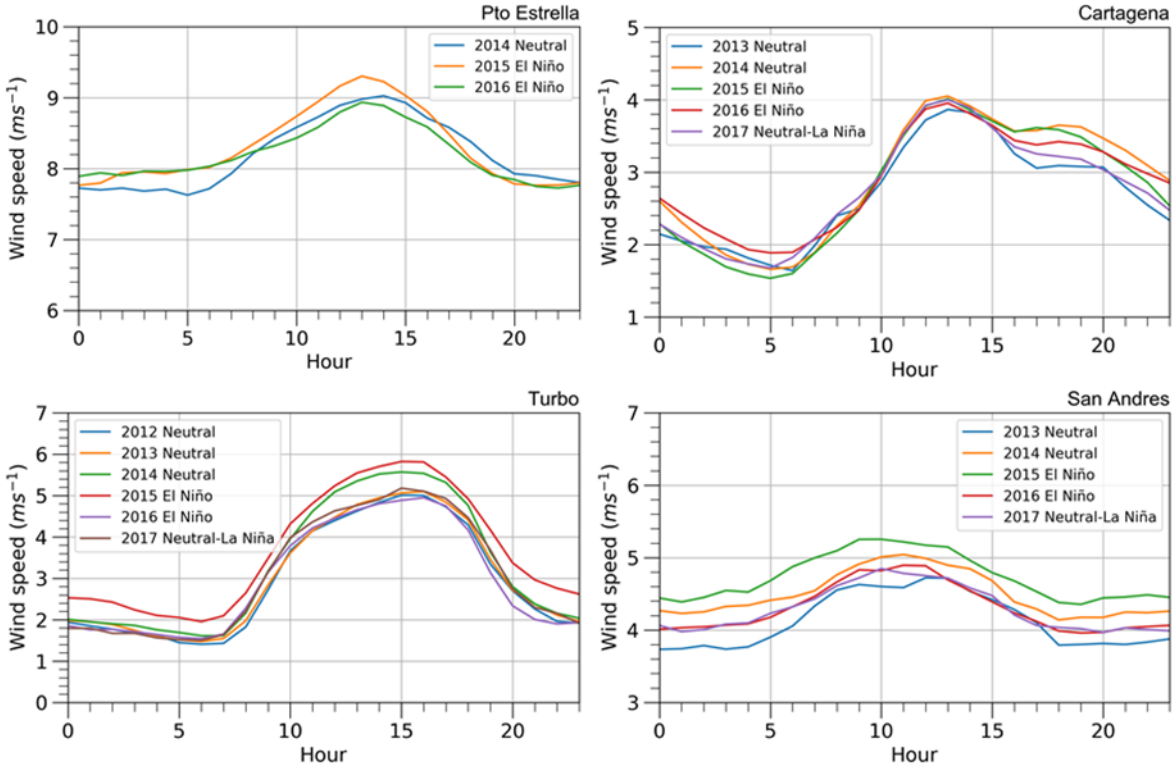

Figure 2.9 ***: Annual diurnal cycle of wind speed.***

2.4.4 Wind turbulence intensity (I)

Table 2.4 shows average values of I obtained for different stations, varying between 0.06 and 0.29. Contrasting these results with those presented in Table 2.2, winds at the stations with higher mean wind speed of La Guajira region are the less turbulent. In contrast, the highest turbulent winds occur at the Gulf of Urabá, where mean wind speeds are the lowest among the analyzed stations, and in San Andres, where the localization of station Providencia near to trees and hills plays an important role in the occurrence of its turbulence field.

Due to the time interval used to obtain the standard deviation, the calculations of I could be considered a rough estimate. However, the obtained values and behavior, according to the location of stations, are in the range of those reported by previous studies (e.g., Jacques, 2010).

Table 2.4 : ***Turbulence intensity characterization.***

Turbulence intensity *I* characterization									
Region	Station	n	mean	Std. Dev.	Min	25%	50%	75%	max
Guajira	Pto Estrella	198385	0,06	0,05	0,00	0,03	0,05	0,07	1,21
	Pto Bolivar	153641	0,08	0,07	0,00	0,04	0,06	0,08	1,14
	Ballenas	195537	0,11	0,11	0,00	0,05	0,08	0,13	1,67
	Pto Brisa	61160	0,17	0,15	0,00	0,06	0,13	0,24	1,59
Magdalena	Sta Marta	140345	0,19	0,15	0,00	0,08	0,15	0,27	1,32
	Pto Velero	207381	0,13	0,11	0,01	0,06	0,09	0,15	1,26
Bolívar	Cartagena	238058	0,18	0,13	0,00	0,10	0,14	0,23	1,47
	Isla Naval	243450	0,13	0,11	0,00	0,05	0,09	0,16	1,38
Golfo de Urabá	Covenas	453695	0,28	0,23	0,00	0,10	0,22	0,41	2,45
	Turbo	446519	0,19	0,22	0,00	0,06	0,14	0,24	2,45
	Sapzurro	86763	0,23	0,15	0,00	0,12	0,19	0,31	2,16
San Andrés	San Andres	250919	0,13	0,10	0,01	0,07	0,11	0,16	1,56
	Providencia	438336	0,29	0,19	0,00	0,14	0,25	0,41	2,45

2.4.5 Wind speed frequency distribution

Figure 2.10 show the wind frequency distribution estimated for each station. Table 2.5 summarizes the shape (k) and scale (λ) parameters for each station and data source. The shape parameter (k) criterion shows on the one hand that winds in La Guajira region are very steady. On the other hand, the more variable winds, with respect to the mean, are those measured in the Gulf of Urabá to the south, where continental orography and the presence of winds from the southwest dampens the easterly winds.

About the influence of the sampling frequency on the shape of the distributions, there is a coincidence between the distribution of the ten-minute averages and the hourly averages of wind speed. This coincidence is very important, at least for the wind power industry, given that hourly wind speed averages could be used for modeling purposes instead of ten-minute average data, which are the standard in the evaluation of wind potential.

In relation to the distributions of average daily speed, there are considerable differences compared to the ten-minute average wind speeds and hourly average wind speeds. For example, according to Figure 2.10, for Pto Bolivar station the probability of the average wind speed for higher sampling frequency (ten-minute averages) is 14%, whereas for daily average sampling it is of 20%. For Ballenas station this difference is from 13% of probability for the higher sampling frequency, to a

probability to 24% for the daily sampling frequency. This difference is important, since wind power is a cubic function of wind speed (Kalmikov, 2017):

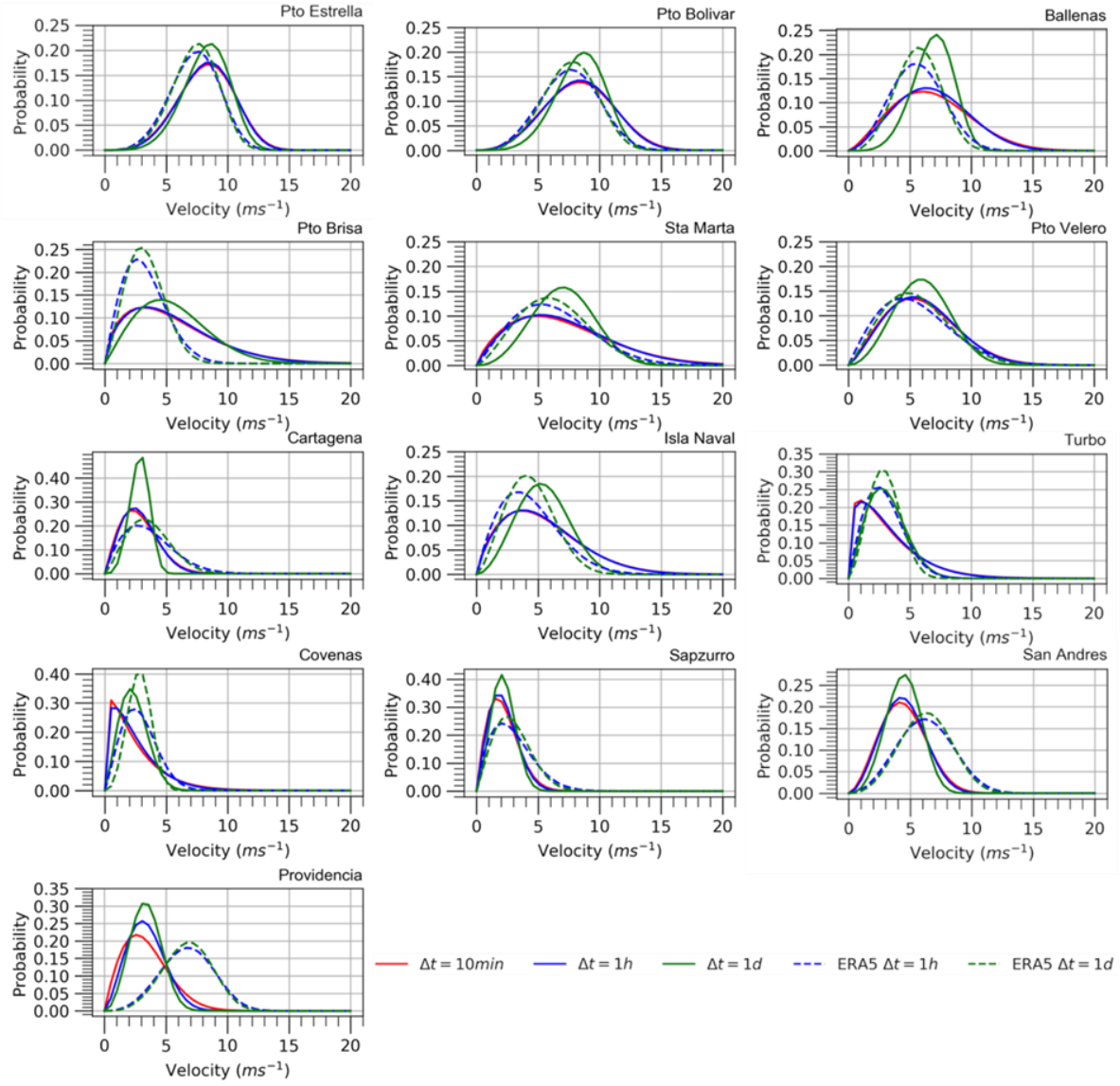

Figure 2.10 : ***Weibull distributions for analyzed sites.***

Therefore, the wind annual energy assessment with Weibull's distributions of mean daily wind speed could lead to severe errors and miscalculations of true wind potential and wind variability. These data may lead to errors in the wind power estimates of up to 20% or more according to Shi & Erdem (2017); in our case the differences are in a range of 0,1% (in station Ballenas) to 11,4% (in Sta Marta station) as is shown in Table 2.8 (see below). These results depend on the shape of wind speed distribution, and for example low differences in estimates for Ballenas station are due to high density around mean wind speed in daily sampling frequency whereas sampling frequency of 10 minutes averages have large tails in higher velocities. Likewise, that shows the importance of taking into account wind variability in the evaluation of the wind resource and how the use of

daily average winds can lead to errors. Although the purpose of the wind atlases is to offer a first approach to wind potential, we emphasize that our estimates, based on higher resolution data (10-minute), are more accurate to characterize temporal wind variability through the use Weibull PDF, the mean diurnal cycle, and the hodograph plots.

In general, the ERA5 data distribution of mean wind speed was different from the data at the stations (Figure 2.10). For stations located to the north (Pto Estrella, Pto Bolivar, Ballenas, Pto Brisa and Sta Marta) ERA5 overestimates the frequency of low wind speeds, whereas underestimating the occurrence of higher wind speeds. In case of Pto Velero station which is located in Magdalena region we can observe a good fit between Weibull distribution of ERA5 data and Weibull distribution of observed data. For the Urabá gulf stations ERA5 tends to overestimate wind speeds located in the left tail of the distribution. For stations located in San Andres islands, the distribution of wind speed of ERA5 is very skewed to the right which mean that both frequency and magnitude of ERA5 are pretty different of the recorded data distributions.

The comparison of wind distributions from observations with distributions from ERA5 suggests that this reanalysis product has difficulties in representing some of the local wind variations, as has been found in other studies for different regions (e.g., Olauson, 2018). Therefore, we do not recommend the use of the reanalysis directly to estimate mean wind speed distributions for the region of interest in this study.

Table 2.5 : ***Weibull shape (k) and scale (λ) parameters.***

Weibull shape (k) and scale (λ) parameters											
Region	Station	Time series									
		10 m		1 h		1 d		ERA5 1 h		ERA5 1 d	
		k	λ(ms^{-1})	*k*	λ (ms^{-1})	*k*	λ (ms^{-1})	*k*	λ (ms^{-1})	*k*	λ (ms^{-1})
Guajira	Pto. Estrella	4,11	9,08	4,21	9,07	5,09	8,98	4,19	8,05	4,54	8,04
	Pto. Bolivar	3,34	9,33	3,44	9,32	4,85	9,17	3,59	8,41	3,98	8,40
	Ballenas	2,31	7,73	2,51	7,77	4,80	7,50	2,91	6,33	3,51	6,31
	Pto. Brisa	1,54	6,13	1,60	6,16	2,05	6,25	1,97	3,72	2,32	3,74
Magdalena	Sta Marta	1,75	7,96	1,85	8,00	3,20	7,90	2,09	7,16	2,41	7,19
	Pto. Velero	2,20	6,79	2,27	6,80	3,00	6,76	1,97	6,28	2,22	6,32
Bolívar	Cartagena	1,97	3,20	2,09	3,21	4,06	3,11	1,86	4,07	2,26	4,09
	Isla Naval	1,73	6,08	1,76	6,09	2,84	6,07	1,90	4,95	2,47	4,96
Golfo de Urabá	Covenas	1,14	2,51	1,26	2,58	2,25	2,68	2,14	3,20	3,33	3,14
	Turbo	1,24	3,39	1,29	3,42	2,15	3,54	2,01	3,35	2,57	3,35
	Sapzurro	1,89	2,49	2,04	2,49	2,56	2,48	1,79	3,31	2,10	3,34
San Andrés	San Andres	2,64	5,02	2,81	5,01	3,54	4,95	3,08	7,01	3,37	6,99
	Providencia	1,91	3,83	2,42	3,82	2,99	3,77	3,52	7,49	3,83	7,47

2.4.6 Wind power density (WPD)

Figure 2.11 shows the WPD variability for the analyzed stations throughout the recorded period and for ERA5 in the corresponding pixel of each station (year 2014). As in the case of wind velocities, the higher wind power densities occur at La Guajira and tend to be lower as we move south. Figure 2.11 also shows an acceptable performance of the ERA5 reanalysis at representing the availability of the wind resource in time, which could be useful in the initial stages of the assessment of wind potential in the area of interest.

Table 2.6 presents the WPD discretized by the percentage of occurrence for the stations with potential for commercial wind power generation. As expected, higher WPD occurs in smaller fractions of time. Taking into account the NREL wind power classification (Kalmikov, 2017) and the WPD for 50% of the time (presented in Table 2.6), only five stations (Pto. Estrella, Pto. Bolivar, Ballenas, Sta. Marta and Pto. Velero) offer commercial wind power potential. Furthermore, only two of these stations (Pto. Estrella and Pto. Bolivar) in La Guajira, have outstanding potential.

Figure 2.12 shows the monthly WPD, obtained from ERA5 model-level data at 100 m above the surface, using hourly data of wind speed, temperature, pressure, dewpoint temperature, and specific humidity. In addition to the La Guajira region, offshore regions located north of 11°N and between 77°W and 74°W have high WPD throughout the year and could be suitable for offshore wind power generation. Since ERA5 underestimates WPD (Figure 2.11), the estimated WPD in Figure 2.12 are on the conservative side.

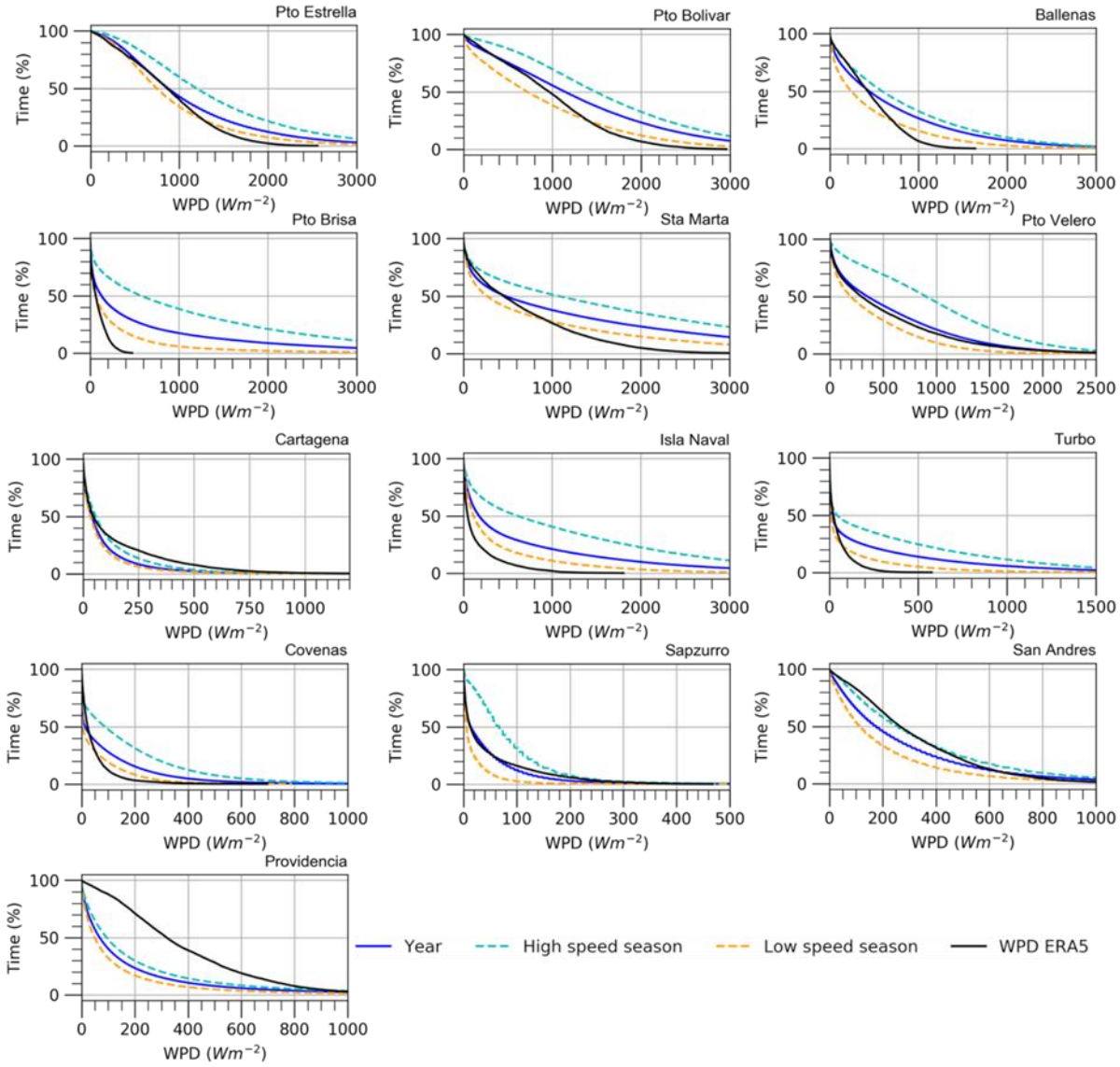

Figure 2.11: ***Wind Power Density at analyzed stations.***

Table 2.6 : ***Wind Power Density variability in stations with commercial wind potential*.**

Wind Power Density variability in stations with commercial wind potential						
Station	Season*	Fraction of the time in which WPD (W m^{-2}) is greater than indicated				
		95%	90%	50%	10%	5%
Pto Estrella	a	163	276	868	2144	2632
	b	133	236	746	1805	2234
	c	259	394	1186	2625	3143
	ERA5	115	201	862	1566	1778
Pto Bolivar	a	37	126	1146	2757	3293
	b	16	45	718	2128	2578

	c	189	409	1490	3099	3643
	ERA5	82	177	964	1831	2122
Ballenas	a	9	24	443	1759	2235
	b	6	14	238	1262	1654
	c	14	40	589	1971	2456
	ERA5	11	44	424	921	1056
Sta Marta	a	6	14	480	3625	4813
	b	5	12	265	2617	3610
	c	8	21	1073	4637	5964
	ERA5	5	16	453	1646	1985
Pto Velero	a	5	14	349	1428	1777
	b	3	9	192	986	1240
	c	21	66	906	1928	2250
	ERA5	4	11	296	1309	1685

*a= entire time series, b = low speed season, c= high speed season

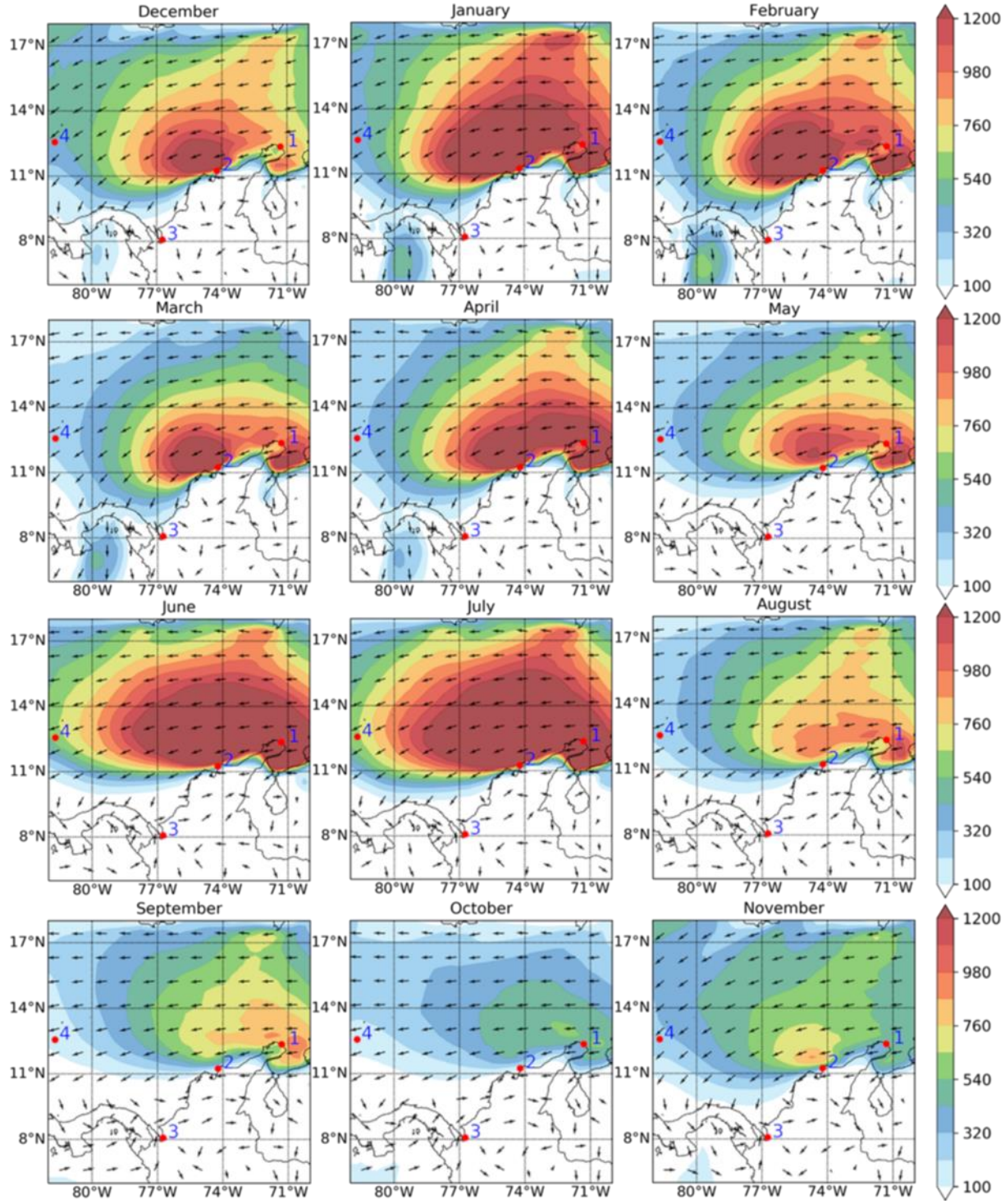

Figure 2.12: ***Monthly mean wind power density in W m^{-2} (shades) for year 2014 above 100 meters height and wind direction (normalized vectors) according to ERA5 hourly data. Stations: Pto Estrella (1), Sta. Marta (2), Turbo (3) and San Andres (4).***

2.4.7 Annual energy production estimate

AEP estimation with wind speed frequency distribution

Table 2.7 summarizes the AEP for the sites with commercial wind power potential. We obtained this estimate from the definition of a typical year with records of 10-minute averages, and the integration of the turbine power curve with wind speed distribution (100 m above the surface) (Figure 2.13).

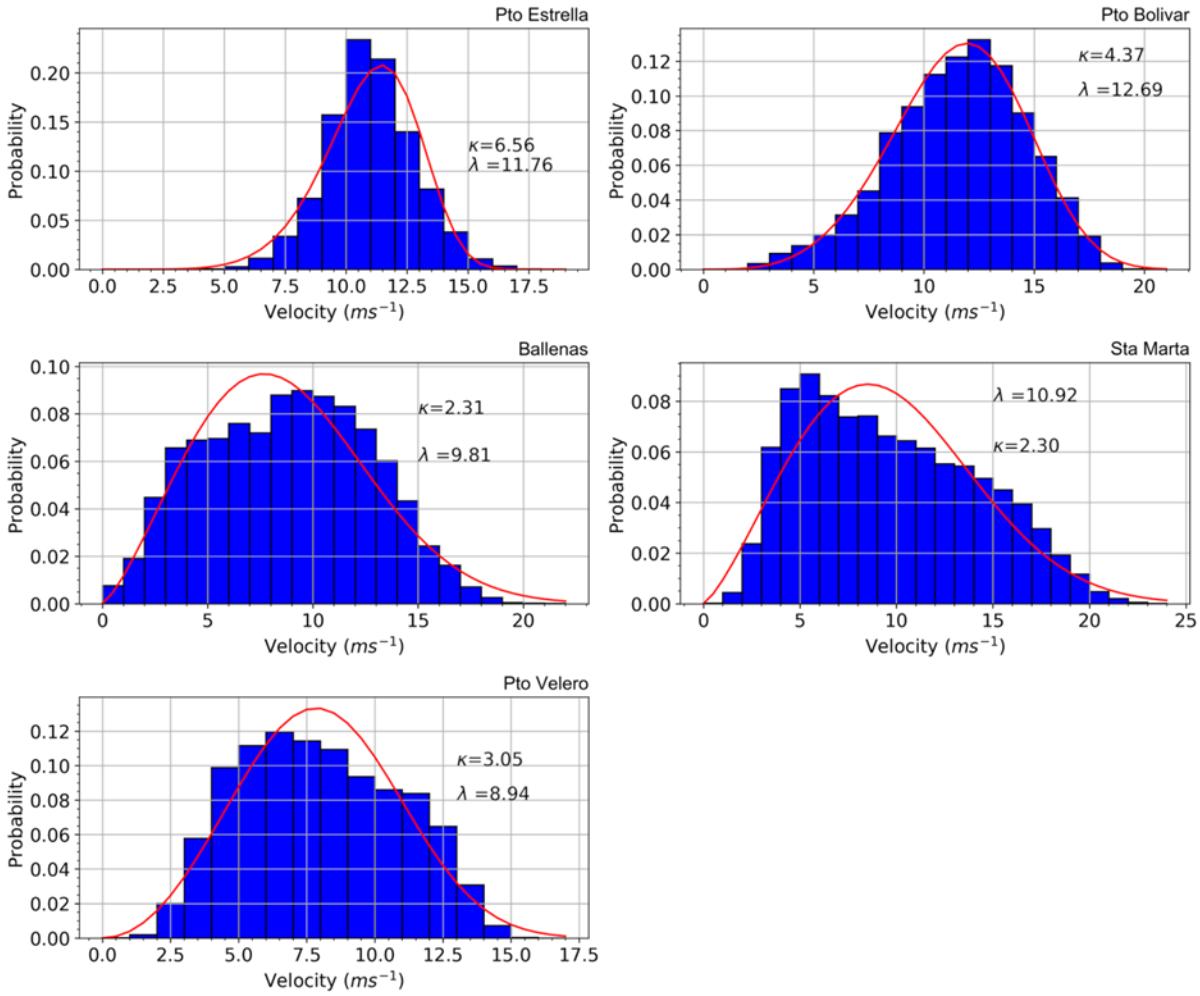

Figure 2.13: ***100 meters wind speed frequency distribution for AEP estimation.***

Table 2.7: ***AEP through wind speed frequency distribution.***

AEP from wind speed frequency distribution	
Station	AEP for typical year (GWh)
Pto Estrella	24.9
Pto Bolivar	24.2
Ballenas	15.8

Sta Marta	16.6
Pto Velero	13.2

Figure 2.14 and Table 2.8 show the sensitivity of the AEP estimates to the temporal aggregation of data. Although the standard for estimating AEP is the 10-minute averages, such as those used in this work, the comparison between different time scales, illustrates the implications of using daily, monthly, or annual averages of wind speed for the calculation. For hourly sampling frequency, the variation on AEP estimates with respect to 10-min averages is between 0.0 % and 2.2%, and for daily sampling frequency is between 0.1% and 11.4%. These differences increase according to the sampling frequency. Given that AEP depends on the shape of the distribution, the analysis of these results should be carefully addressed to avoid misinterpretations. Figure 2.14 also shows the AEP estimated with ERA5, which is very different from the AEP calculated with the 10-min averages of meteorological stations.

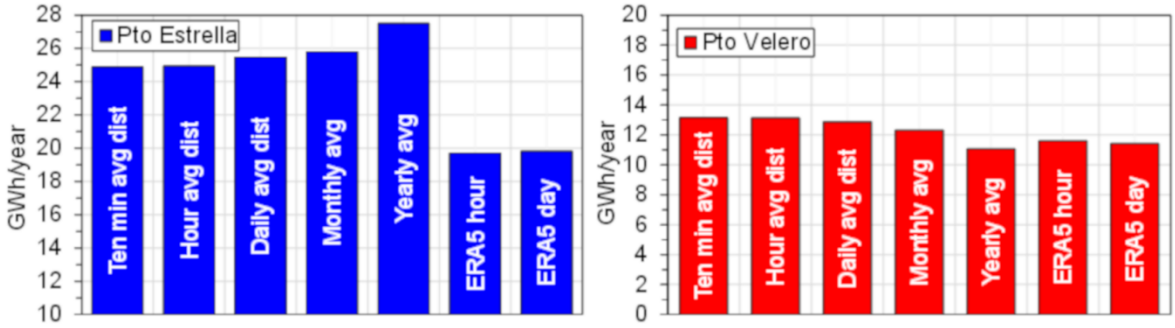

Figure 2.14: ***Sensibility of AEP estimation according to time aggregation.***

Table 2.8 : ***Variations in AEP estimates respect to sampling frequency of wind speed.***

Variation (%) of AEP estimates with respect to sampling frequency of 10 minutes averages					
Sampling frequency	Pto Estrella	Pto Velero	Pto Bolivar	Sta Marta	Ballenas
Hour avg dist	0,2	0,2	0,1	0,0	2,2
Daily avg dist	2,4	2,1	6,7	11,4	0,1
Monthly avg	3,7	6,3	7,6	18,2	2,4
Yearly avg	10,5	15,8	2,1	15,7	7,1
ERA5 hour	20,8	11,8	18,8	19,2	25,7
ERA5 day	20,4	13,2	18,4	20,8	28,6

AEP calculation from direct measurements

Table 2.9 contains the AEP estimated directly with ten-minute averages for the stations of Table 2.7. As in the case of velocities, the estimated AEP is higher in La Guajira stations, which also exhibit higher capacity factors (CF). This is due to the high and steady speeds during the year, and due to factors as the thermal driven winds like the land sea breezes (daily cyclic phenomena) and the influence of trade winds throughout the year over that region.

To contextualize our estimates, we compare them with the Jepírachi wind farm, which has an installed capacity of 19,5 MW, supplied by 15 wind turbines of 1,3 MW each (EP, 2019). This is

the only wind farm currently operating in Colombia and is located near Pto Bolivar station. In 2014, this wind farm generated 70,2 GWh (XM, 2019), which means a capacity factor (CF) of 0,41.

Table 2.9 ***: Annual energy production and capacity factors by station and year with available data under idealized conditions.***

Station	Annual energy production							
	2014		2015		2016		2017	
	GWh /year	CF	GWh /year	CF	GWh /year	CF	GWh /year	CF
Pto Estrella	24,9	0,83	25,96	0,86				
Pto Bolivar	26,1	0,86					23,5	0,78
Ballenas	17,5	0,58					14,2	0,47
Sta Marta			17,3	0,57	17,3	0,57		
Pto Velero	16,7	0,55	18,0	0,60	14,8	0,49		

With the power curve of Jepírachi's wind turbine (available on the manufacturer's web page, Nordex, 2019), we estimate the AEP of Jepírachi park by extrapolating Pto Bolivar's station wind speed to 50 m, which corresponds to the hub heights of Nordex N60/1300 turbine at Jepírachi wind farm, and then we applied the framework presented before.

With these estimations, we obtained a CF of 0,69 for 2014, which means that the estimate of the AEP, under idealized conditions, can overestimate the capacity factor in at least 0,28 (0,69idealized – 0,41actual). This difference indicates that the time in which the wind farm is not working due to factors like maintenance, repairs, and grid restrictions, at least in this case, is equivalent to 28% of the time.

Additionally, we observed that the power coefficient (Cp) of the Nordex turbine is minor than the Cp of Vestas turbine. Cut-in speed is larger in the Nordex turbine, which means that Vestas turbine can take energy at lower wind speeds at which Nordex turbine cannot work. Additionally, we have the fact that Nordex wind turbine at Jepírachi wind farm takes the wind energy at 50 meters height, meaning a minor wind speed and major wind turbulence than 100 m height, which is the altitude of our estimates.

Therefore, we can attribute the difference of Jepírachi's CF with the estimates presented in Table 2.7 both to the ideal conditions assumed in our work and to the technology gap between the park generators and the turbine utilized for our estimates.

Finally, knowing the percentage of affectation of CF (0,28) due to operative factors like maintenance, repair and grid restrictions over the AEP generated in 2014 in La Guajira, we proceed to correct the estimates presented in Table 2.9.

Table 2.10 shows the annual energy production obtained through direct measurements and corrected with Jepírachi's CF. The results give us a realistic view of the wind power potential in La Guajira, Magdalena, and Bolivar regions. The CF for La Guajira is still high but comparable to those of Burra Dale wind farm located in the Shetland Islands, which have an averaged CF of 52% (Shetland Aerogenerators, 2019).

Table 2.10 : ***Annual energy production and capacity factors by station and year with available data corrected with Jepírachi's CF.***

Station	Annual energy production corrected with Jepírachi's CF							
	2014		2015		2016		2017	
	GWh /year	CF	GWh /year	CF	GWh /year	CF	GWh /year	CF
Pto Estrella	16,5	0,55	17,5	0,58				
Pto Bolivar	17,6	0,58					15,1	0,50
Ballenas	9,1	0,30					5,7	0,19
Sta Marta			8,9	0,29	8,9	0,30		
Pto Velero	8,3	0,27	9,6	0,32	6,3	0,21		

The results of AEP are promising for the region, but the assessment of wind power projects must include also important economic aspects that are beyond the scope of our study. In this regard, wind energy is becoming more competitive. According to a report by IRENA (2019), the regional weighted average Levelized Cost of Energy (LCOE) for South America on onshore wind energy production has dropped from 0.10 USD/kWh in 2010 to 0.05 USD/kWh in 2018, while the same variable for hydraulic energy, for the same period and region, varied between 0.09 USD/kWh and 0.04 USD/kWh. The same report indicates a global weighted average LCOE of 0.127 USD/kWh for offshore wind power generation and of 0.085 USD/kWh for solar photovoltaic energy for 2018.

2.5 Conclusions

This study offers a novel characterization of the wind power potential of the Caribbean region of Colombia based on both 10-min averaged wind speed data from 13 meteorological stations and data from the recent ERA 5 reanalysis, with results that are useful and relevant for wind farm developers, investors, and operators interested in developing wind farms in Colombia.

Our 10-min and hourly analyses confirm that La Guajira has the higher wind power potential in the Caribbean coast of Colombia, with wind power densities over 850 W m^{-2}, 50% of the time. Furthermore, from the spatial analysis of ERA5 winds, which includes the average monthly wind speed and the average monthly WPD, we identify wide sea zones in the north of the country that may be suitable for offshore wind energy applications. Some of these zones are located in front of the shoreline of Magdalena, Bolivar, and La Guajira sectors, northward of 11°N and between 77°W and 74°W. The offshore WPD results obtained with ERA5 expose the viability of offshore wind energy around the studied sites.

Our WPD estimates, based on hourly variability of air density and presented as duration curves, contribute to refining information of wind variability that was not previously available from the wind atlas. The WPD estimated through the duration curves, give an accurate sense of the expected availability of wind power in the studied locations, since a unique value of this parameter based on mean wind speeds could mislead the overall calculations. In La Guajira, for instance, we observe a good potential of wind resources more than 70% of the time, similar to other stations located towards the south in the Magdalena region, which shows good wind potential 40 to 50 % of the time. Another contribution is the use of ERA5 to calculate air density on an hourly basis and at finer spatial resolution.

ERA5 offers useful information about wind availability in time and space, despite its limited capacity to represent the influence of local effects on wind patterns for localized areas. We found that ERA5 tends to underestimate near-surface wind speeds (e.g., the nominal 10 m winds) for La Guajira and other regions of the northern shoreline of the Caribbean region of Colombia (Turbo station and Isla Naval station included), while it tends to overestimate wind speeds in San Andrés and stations in the south and center shoreline of the Caribbean region of Colombia (Cartagena, Sapzurro, and Coveñas). ERA5 correlates well with the stations located under the direct influence of Trade Winds (La Guajira region and San Andrés and Providencia Islands). The RMSE for the hourly time series of ERA5 varies between 1.5 m s^{-1} and 4.0 m s^{-1}, presenting the smallest variations in La Guajira.

The turbulence intensity is high in zones with lower wind speeds (i.e., 0.28 for Coveñas in the Urabá region), whereas in places with higher wind potential, like La Guajira, the values are low (0.06 and 0.08). Lower values of turbulence intensity indicate steadier winds. Since wind turbine selection depends on turbulence intensity, our results may offer aid to choose adequate wind turbine models for wind potential evaluation and preliminary estimations of AEP, based on Weibull distribution functions.

Our results show that the estimated Weibull distributions at each station are similar at 10-min and hourly average intervals, leading to differences between 0.0% and 2.2% in the estimated AEP, with an almost perfect graphic adjustment. Therefore, any of these intervals are suitable to characterize winds in the studied stations and surrounding areas. This is of interest for wind power planners and developers during a preliminary economic evaluation of projects, through the integration of the PDF with the power curve of the wind turbines.

By contrast, the AEP estimates based on Weibull distributions of wind averages on intervals longer than one hour (similar to those of previous studies in the analyzed region) differ considerably from those of 10-min sampling frequency estimates and do not give accurate information about intra-day variability of wind speed magnitude and variability. For instance, the daily wind average sampling frequency leads to differences up to 11.4 % in AEP estimates with respect to the AEP estimated with Weibull distribution of 10-min average winds, with a poor graphic fit of distribution curves. This information is crucial for wind power assessments. AEP estimates with ERA5 data lead to differences up to 25.7% for hourly time intervals and 28.6% for daily time intervals respect to 10-min AEP estimations.

We found that Weibull distributions of ERA5 and stations' daily averages differ considerably in magnitude and frequency from the finest data on stations. This means that, even for preliminary wind potential evaluation, these data should not be used without previous treatment, since wind energy is a cubic function of wind speed and any underestimation or overestimation implies large errors on energy estimates.

Finally, our estimates of AEP with direct measurements (GWh/year) for some years in the stations with higher WPD (W m^{-2}), based on 10-min averaged wind speed and mean hourly data of temperature and pressure, are illustrative of wind potential in the analyzed sectors. AEP estimated with ERA5 differs up to 28.6% respect to estimates made with 10-min average data. Based on the corrections of the AEP with the capacity factor of the Jepírachi wind farm, the wind potential in La Guajira (CF up to 0.5) is similar to some of the higher CF reported in the literature.

In general, our analysis with 10-minute data allowed us to present valuable information on the intra-day availability and variability of wind power, not reported in previous studies. In addition, we found that ERA5 performs better in areas directly exposed to the trade wind belts like La Guajira, while its ability to recreate the winds decreases with the appearance of complex topographic patterns in areas located south of this region. Therefore, to refine the level of detail from these ERA5 coarse estimates, especially near the coastline, we suggest the use of numerical modeling schemes based on atmospheric dynamics, such as the WRF model, as a further step in research.

3. High Resolution Modeling of Wind Potential for the Caribbean Region of Colombia Using WRF

3.1 Abstract

High-resolution information about wind power potential is scarce for the Caribbean region of Colombia. In this study, we used the WRF model with two nested domains (9 km and 3 km) and 50 vertical levels with 15 minutes output to evaluate the annual wind power potential for the La Guajira region (north coast of South America). We evaluated the performance of three widely used parameterization schemes for the planetary boundary layer of the WRF model, to simulate observed winds during extreme months, finding that the QNSE scheme performs better representing the phase and amplitude of the field observations of wind speed in the studied area. With this scheme, we estimated the mean monthly wind fields, considering the monthly intra diurnal cycle. Finally, we estimated the monthly average of the Wind Power Density (WPD) at 100 meters height, finding that, for the month with higher wind speeds, the WPD reaches values up to 1200 W m^{-2} in the shoreline and up to 2000 W m^{-2} offshore, with variations between 800 W m^{-2} and 1600 W m^{-2} inland, whereas in the month of lower wind speeds, the WPD varies between 400 W m^{-2} and 800 W m^{-2}. The results constitute the first wind power assessment for this region based on high-resolution atmospheric modeling.

3.2 Introduction

The area of study covers the Caribbean coast of Colombia in the north of South America. This region has an important wind power potential, which has been reported in previous studies (Vergara, 2010; Hoyos Guerrero et al., 2018; Rueda Bayona et al., 2019). Carvajal-Romo et al. (2019), estimated that any of the wind power sources (onshore or offshore) may have the potential to cover the entire national energy demand by 2050, whereas Henao et al. (2020) indicated that wind power in the Caribbean coast can complement the country's hydropower sector during dry seasons and El Niño Southern Oscillation (ENSO) events.

Previous characterizations have been performed with both measurements from ground stations (with a very low density over the territory) or with reanalysis products. For instance, Gil et al. (2020) performed a wind potential assessment for the Caribbean region of Colombia using both reanalysis data (ERA5) and ten minutes winds data (13 meteorological stations), finding that La Guajira region has the higher wind power potential in the Caribbean coast of Colombia, with wind

power densities over 850 W m^{-2}, 50% of the time and large offshore areas with promising wind power densities, this source shows that estimates of the annual energy production (AEP) with ERA5 data lead to differences up to 25.7% for hourly time intervals and 28.6% for daily time intervals respect to 10-min AEP estimations. However, the reanalysis products cannot represent the influence of local factors such as orography, the shoreline, and land cover on wind patterns. To the authors knowledge, this is the first time in which wind power potential for the Caribbean coast of Colombia is characterized with a high-resolution numerical modeling of the atmosphere (3x3 km grid and 50 vertical levels) throughout a whole year and including validation with measurement points and reanalysis data.

According to Jacques (2010) and Shi & Erdem (2017), among others, wind resource assessment is the collection of analytical technologies and methods used to estimate the availability of winds for a wind power plant over its lifetime. Information on wind availability is the most important to determine how much energy the plant will produce, define its operation, and finally, have an estimate of its economic viability. In other words, the use of successful forecasting models is vital to provide useful predictions of wind power potential of interest for long-term development of wind farms and pricing reforms in energy markets.

In this regard, the use of atmospheric models such as the Weather Research and Forecast (WRF) is becoming popular to generate information about wind availability and variability and to describe the wind power potential of wide areas (Al-Yahyai et al., 2010), (Carvalho, et al., 2014), (Carvalho et al., 2014), (Salvação & Guedes Soares, 2018) (Mattar & Borvarán, 2016), (González-Alonso de Linaje et al., 2019) especially in areas where field measurements are scarce and expensive, and sources such as reanalysis or wind atlases are still of low spatial resolution.

Since winds in the first levels of the atmosphere are highly dependent on the exchange of turbulent fluxes of heat, momentum, and humidity between the surface and the atmospheric boundary layer (ABL or PBL), the first approach in our study is to evaluate the performance of some parametrizations for the PBL in the representation of the turbulent interactions, taking into account that this capability varies with local factors, such as land cover, topography, and latitude. The performances of the analyzed PBL schemes are valuable for implementing models such as WRF to adequately forecast the amount of energy generated on a time scale of a few days for both wind farms and electric market operators.

We applied the best performing PBL scheme to assess the wind power potential for the Caribbean coast of Colombia, characterizing monthly wind regimes, intra diurnal monthly cycles of the wind speed, and estimating wind power density (WPD) at 100 meters height with high temporal resolution data of wind speed and air density (Floors & Nielsen, 2019; Ulazia et al., 2019). The variability of winds in the region is represented by the standard deviation and duration curves of the WPD.

This study will contribute to the wind industry by identifying and quantifying wind power potential as a basis for the proper assessment and operation of wind farms, in a region that is just beginning to develop its wind power industry.

3.3 Materials and Methods

3.3.1 Study area

The area of interest in this study is the Caribbean coast of Colombia, on the north of South America (Figure 3.1), a region under a strong influence of the Intertropical Convergence Zone (ITCZ) displacement throughout the year (Poveda, 2004) as well as by the trade winds belts. Due to its coastal nature, in the region exist local wind systems like the land-sea breezes (Pérez et al. 2018.) and low-level jets (Whyte et al., 2008).

3.3.2 The WRF model

For this study, we used the 4.2 version of WRF (Skamarock et al., 2019) with two nested domains, D01 (with cells of 9 x 9 km and 240 x 160 grid points) and D02 (with cells of 3 x 3 km and 292 x 181 grid points) (Figure 3.1). D01. Both domains consider 50 vertical levels. The above configuration is similar to that of the High-Resolution Rapid Refresh (HRRR) model (Benjamin et al., 2016), which is widely used for assessment and research in the field of renewable energy (i.e., Pichugina et al., 2019, James et al., 2018, and Wilczak et al., 2015).

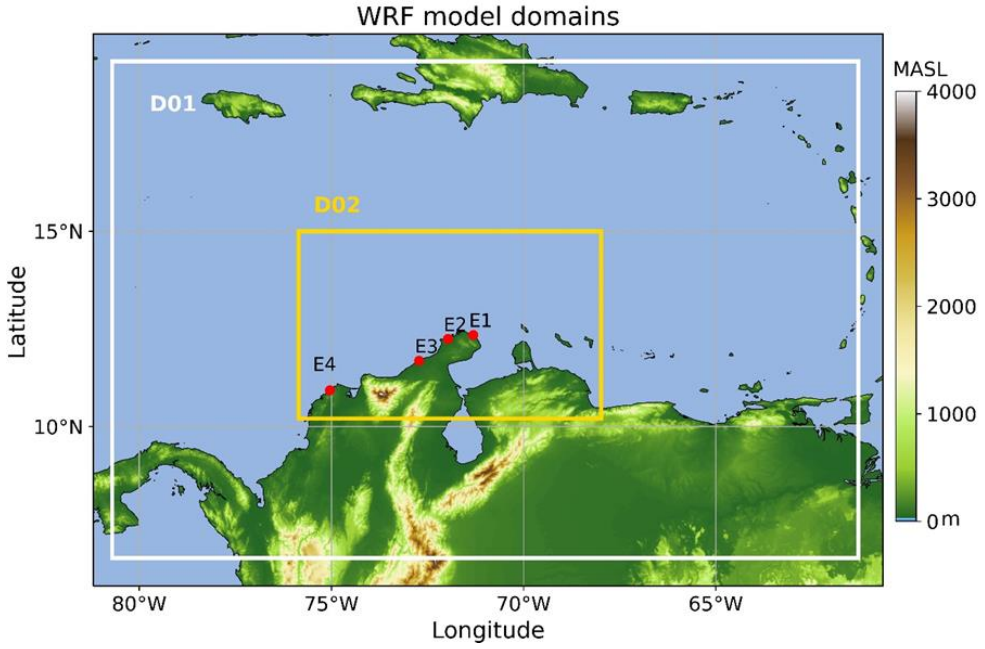

Figure 3.1: ***WRF model domains.***

The nesting of the model was performed in two ways (exchange of information between domains). And the terrain was modeled with a spatial representation based on the digital elevation model of the SRTM mission at a resolution of 90 x 90 m and a temporal representation of 45 seconds for the domain D01 and 15 seconds for the domain D02. Table 3.1 lists the physics parameterizations used in the model.

Table 3.1 ***: Physics parameterizations.***

Process	Scheme
Microphysics	Morrison double-moment scheme
Longwave radiation	RRTMG scheme
Shortwave radiation	RRTMG shortwave
Land surface	Noah land surface model
Cumulus (Only D01)	A newer Tiedtke scheme

For the initial and boundary conditions, we used ERA5 reanalysis data (ECMWF, 2017; Hersbach et al., 2020), which have a grid resolution of 0.25° x 0.25° and 137 vertical levels, ranging from 0.02 hPa to 1013.25 hPa. For boundary conditions assimilation we used a three-hour time step.

The monthly simulations of wind speed and direction in WRF produced gridded outputs at a time resolution of 15 minutes for domain D02 and of an hour for domain D01. To compare the outputs with the observed data at the meteorological stations, we used the WRF's time series option that generates the time series for the grid point nearest to the point of the station. The time series were generated for each time step of the model integration, according to the domain (45 s for D01 and 15 s for D02). The four shoreline meteorological stations shown in Figure 3.1 and Table 3.2 are operated by DIMAR (General Maritime Directorate of Colombia).

Table 3.2 : ***Meteorological stations.***

Number	Name	Latitude	Longitude	Av. wind ($m\ s^{-1}$)	Av. Temp (°C)	Av. Press P (hPa)	Years with records
1	Puerto Estrella	12.36	-71.31	8.3	28.3	1010.75	4
2	Puerto Bolivar	12.26	-71.97	8.4	27.8	1010.37	3
3	Ballenas	11.70	-72.72	6.9	27.9	1009.65	4
4	Puerto Velero	10.94	-75.04	6.0	28.3	1008.94	3

3.3.3 Boundary layer parameterizations

Since atmospheric boundary layer interactions (transport of turbulent fluxes of heat, moisture, and momentum) affect directly the wind speed and direction at heights of interest for the wind industry (around 100 m height), we evaluated the performance of the three PBL schemes presented in Table 3.3, based on previous recommendations by Carvalho et al. (2014) and Salvação & Guedes Soares (2018).

The Yonsei University PBL scheme (Hong, Noh, & Dudhia, 2006; Hong, 2010) is a first-order non-local closure scheme with explicit entrainment layer and parabolic K profile which have been widely used in wind resource assessment (Carvalho et al., 2012; Carvalho et al., 2012; Xiao-Ming Hu et al., 2013; Carvalho et al., 2014; Mattar & Borvarán, 2016; Salvação & Guedes Soares, 2018, González-Alonso de Linaje et al., 2019).

The Mellor-Yamada-Janjic scheme (Mellor & Yamada, 1982; Z. I. Janjic, 1994; Janjic, 2002) is a 1.5 order local closure scheme that determines eddy diffusion coefficients from prognostic turbulent kinetic energy (TKE) (Xie, Fung, Chan, & Lau, 2012).

The QNSE is a 1.5 order local spectral closure method developed for a fully three-dimensional, incompressible, turbulent flow field with an imposed homogeneous, vertical, stable temperature gradient (Galperin & Sukoriansky, 2010; Wang et al., 2011).

Table 3.3 : ***Combination of boundary layer and surface layer configuration.***

Planetary boundary layer (PBL) schemes	Surface layer (SL) schemes
YSU - Yonsei University	MM5 Similarity
MYJ - Mellor-Yamada-Janjic	ETA
Quasi–normal Scale Elimination (QNSE) Scheme	QNSE

3.3.4 Model performance

We compared the WRF results in both domains for two extreme months identified in the previous chapter (June for higher winds and October for lower winds) with the ERA5outcomes in coincident pixels and with data from the ground stations. For the comparison, we used the average monthly diurnal cycle (AMDC), divided in time intervals of six hours each (in Local Standard Time or LST). This division provides information about the skill of each WRF scheme to reproduce the observed phase and amplitude of the intra-daily wind speed variations, represented by peaks and valleys, which is of great importance for wind farm planners and operators.

The comparison uses Taylor's diagrams (Taylor, 2001) and the Fractional Bias statistics presented in equation 5.1, where Pre_i and Obs_i are the predicted and observed values for a given time interval.

$$FB = \frac{\sum_i^n (Pre_i - Obs_i)}{0.5 \sum_i^n (Pre_i + Obs_i)} * 100 \qquad (5.1)$$

A second measure of the performance of WRF with the studied PBL and SL schemes is to estimate the wind speed frequency distribution for the observations, ERA5, and WRF simulations through two-parameter Weibull distributions commonly used in the wind energy field to represent wind variability. The probability density function of the Weibull distribution and its cumulative form is expressed as:

$$f(v) = \frac{\kappa}{\lambda}\left(\frac{v}{\lambda}\right)^{\kappa-1} \exp\left\{-\left(\frac{v}{\lambda}\right)^{\kappa}\right\} \qquad k>0, \lambda>0, v>0 \qquad (5.2)$$

$$F(v) = 1 - \exp\left\{-\left(\frac{v}{\lambda}\right)^{\kappa}\right\} \qquad (5.3)$$

Where k = Weibull shape parameter; λ = Weibull scale parameter on (m s^{-1}); v = wind speed (m s^{-1}).

As mentioned in Chapter 4, the Weibull distribution consists of a scale parameter (λ) and a shape parameter (k), with high k values (k >2,5) indicating narrow frequency distributions (v.gr.,

steadier, less variable wind, which sometimes is the case for the trade winds belts), and low values of k ($k < 1{,}5$) indicating greater variability concerning the mean (Burton et al., 2001).

3.3.5 Characterization of the wind potential

The wind power or rate of kinetic energy flow is defined according to equation 5.4. To characterize the availability of wind power, we use the kinetic wind energy flux or Wind Power Density (WPD) defined by equation 5.5. According to Kalmikov (2017), the WPD allows comparing the wind resource independent of the size of the turbines (rotor area), which is appropriate for the classification of the wind resource. This study used the wind power classification proposed by the United States Department of Energy's National Renewable Energy Laboratory (NREL) Gunturu & Schlosser (2012).

$$P = \frac{1}{2} * \rho * A * v^3 * C_p \qquad (W) \qquad (5.4)$$

Where P = wind power (W); ρ = air density (kg m^{-3}); A = sweep area (m^2); v = wind speed (m s^{-1}) and Cp = power coefficient (between 0 and 1).

$$WPD = \frac{1}{2} * \rho * v^3 \qquad (Wm^{-2}) \qquad (5.5)$$

Where WPD = wind power density (W m^{-2}); ρ = air density (kg m^{-3}); v = wind speed (m s^{-1}).

Since WRF provides diagnostic variables of the atmosphere such as temperature, atmospheric pressure, and vapor mixing ratio for each time step, it is possible to consider the direct influence of the air density in the WPD. This consideration adds value to the study since previous research by Floors & Nielsen (2019) and Ulazia et al. (2019) highlight the importance of using air density as a variable and not as a unique standard value for the WPD and wind power calculations.

3.4 Results and discussion

Since wind energy availability, demand, and grid operation highly correlate with the wind diurnal cycle but also with the daily cycle of energy demand (i.e., demand curves), we analyzed the ability of the WRF model to reproduce the average monthly diurnal cycle in comparison to the meteorological stations and the ERA5 reanalysis. Using the Weibull probability density functions (PDF), we characterize the wind speed distribution generated by WRF PBL schemes and compared them to observed data and the ERA5 reanalysis. As a result, we present the wind speed fields and the WPD fields with their associated standard deviations and the yearly WPD duration curves.

3.4.1 Average monthly diurnal cycle (AMDC)

Puerto Estrella Station

Figure 3.2 shows the average monthly diurnal cycle generated by WRF parameterizations in both domains and the generated by ERA5, compared to data of Puerto Estrella station for the extreme months of June and October.

For June, on the one hand, WRF schemes MY and QNSE in both domains generate higher amplitudes most of the day, in comparison with station data, whereas the YSU scheme show less amplitude along the day, except for the time interval between 6 h -11 h LST (D01 with FB = 6.59% and D02 with FB = 2.80%). On the other hand, ERA5 presents higher amplitudes than station data in the first quarter (FB = 11.86%) and last quarter of the day (FB = 9.25%).

Regarding the frequency and phase in the average monthly diurnal cycle for June, the higher winds speeds along the day at Puerto Estrella station, occur between 11 h and 15 h LST, whereas MY scheme for both domains shows his occurrence in the second quarter of the day (6 h - 12 h), QNSE for both domains generates the daily wind speed peak in the third quarter of the day (as is reported by the station); YSU scheme in both domains generates the maximum wind speeds between 6 h and 14 h LST. Finally, ERA5 generates the maximum diurnal wind speed for June in the time interval between 17 h and 23 h LST.

Table 3.4 summarizes the Bias and the Fractional Bias (FB) for the mean daily estimations and intraday estimations. In most cases, the fine domain (D02) performs better than the coarse domain (D01) for the same scheme. ERA5 shows a lower FB at mean daily level than the WRF schemes, but at the intra diurnal level, most of the times WRF performs better than ERA5.

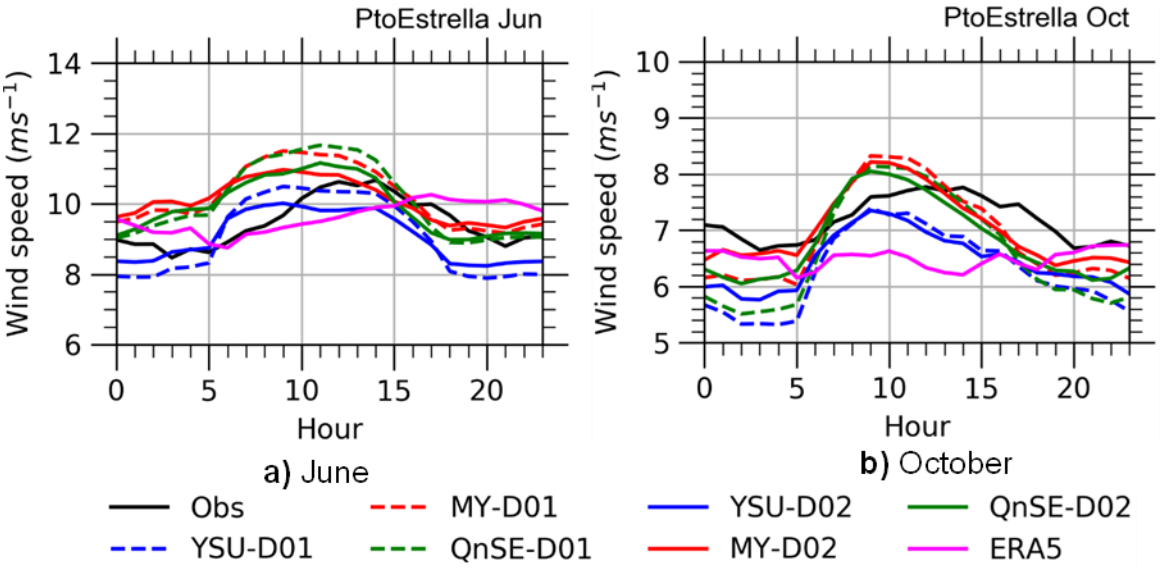

Figure 3.2: ***WRF average monthly diurnal cycle comparison at Pto Estrella station.***

Table 3.4: ***WRF diurnal cycle Bias for June at Pto Estrella station.***

Model	Bias	Daily	0 h to 6 h	7 h to 12 h	13 h to 18 h	19 h to 23 h
YSU D01	Bias	-0.44	-0.67	0.60	-0.45	-1.17
	FB %	-4.61	-7.56	6.59	-4.20	-12.85
YSU D02	Bias	-0.42	-0.22	0.22	-0.82	-0.84
	FB %	-4.39	-2.15	2.80	-8.13	-8.87
MY D01	Bias	0.71	0.97	1.57	0.27	0.14
	FB %	7.47	10.99	15.67	2.88	2.27
MY D02	Bias	0.61	1.18	1.18	-0.13	0.29
	FB %	6.44	13.09	12.04	-1.07	3.79
QnSE D01	Bias	0.60	0.66	1.60	0.38	-0.16
	FB %	6.24	7.58	15.80	3.95	-1.08
QnSE D02	Bias	0.44	0.82	1.16	-0.07	-0.06
	FB %	4.67	9.23	11.73	-0.50	-0.12
ERA5	Bias	0.07	1.04	-0.58	-0.97	0.81
	FB %	1.09	11.86	-5.57	-9.56	9.25

Figure 3.3 shows the Taylor's diagram for June at the Puerto Estrella Station. In this case, ERA5 has the worst performance for the amplitude pattern (standard deviation), whereas the finer WRF domain (D02) represents the amplitude better. In terms of correlation coefficient (pattern similarity), WRF schemes vary between 0.46 and 0.76, with the YSU scheme for the larger domain (D01) offering the best performance (r = 0.76). ERA5 correlation is in this case negative (r = 0.72). Relative to the RMSD, ERA5 presents the larger value (1.056), while all WRF schemes have values between 0.73 and 0.55, with the YSU scheme for D02 presenting the lower value (0.55).

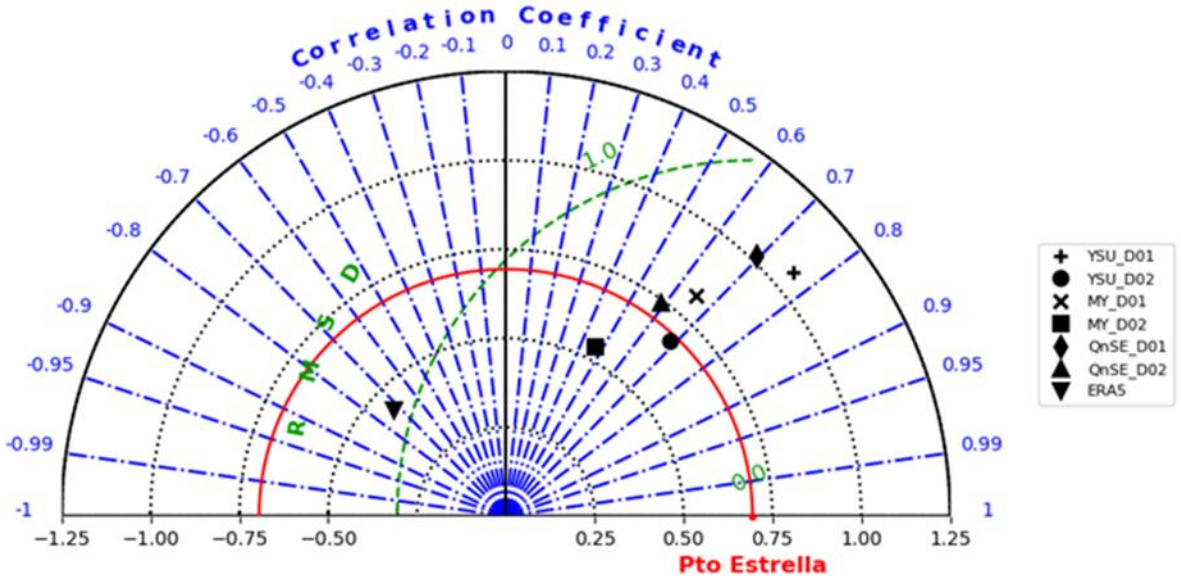

Figure 3.3 : ***Taylor diagram for June diurnal average monthly cycle at Pto Estrella station.***

For the month with lower wind speeds (October) at station 1 (Figure 3.2), the WRF schemes MY and QNSE in both domains also generate higher amplitudes than the registered in the station, but in this case, only for the time interval between 6 h to 12 h LST. In all cases, for the WRF model, the diurnal peak of wind speed (before 10 h LST) is out of phase with the data station (around 13 h LST). In the first and last quarters of the day, all the models present lower amplitudes than the station. ERA5 does not represent the mean diurnal cycle, and even for the interval between 12 h

and 18 h LST, ERA5 is in counter phase with station data (FB = -11.3% - Table 3.5). Table 3.5 shows that during the interval from 06 h to 18 h LST, ERA5 has a higher bias (up to 11%) than the WRF model with the studied schemes.

Table 3.5: ***WRF diurnal cycle Bias for October at Pto Estrella station (1).***

Model	Bias	Daily	0 h to 6 h	7 h to 12 h	13 h to 18h	19 h to 23 h
YSU D01	Bias	-1.11	-0.92	-0.36	-0.55	-0.60
	FB %	-18.66	-16.63	-6.05	-8.43	-9.73
YSU D02	Bias	-0.95	-0.69	-0.34	-0.59	-0.49
	FB %	-15.67	-11.72	-5.24	-8.94	-7.62
MY D01	Bias	-0.47	-0.54	0.06	-0.18	-0.43
	FB %	-9.01	-9.75	-0.05	-3.08	-8.06
MY D02	Bias	-0.34	-0.33	0.06	-0.24	-0.34
	FB %	-6.64	-5.81	0.50	-3.72	-6.30
QnSE D01	Bias	-0.75	-0.78	-0.03	-0.27	-0.58
	FB %	-13.11	-14.98	-1.16	-4.35	-9.77
QnSE D02	Bias	-0.56	-0.50	-0.02	-0.35	-0.40
	FB %	-9.95	-10.00	-0.65	-5.51	-6.65
ERA5	Bias	-0.85	-0.23	-0.64	-0.67	-0.34
	FB %	-14.09	-2.39	-10.07	-11.30	-5.40

Figure 3.4 shows the Taylor´s diagram of the behavior of the models in the representation of the mean diurnal cycle during October at Puerto Estrella, the standard deviation (representing variations of amplitude along the day) registered by the station is lower than the generated by the WRF model but higher than the generated by ERA5. All WRF models report correlation coefficients (r) above 0.83, being the higher the r = 0.89 generated with the MY scheme for the larger domain (D01). By contrast, ERA5 presents an r = -0.26, showing the lower (and also inverse) correlation with station data. The lower RMSD value (0.28) is generated by the WRF model with the YSU scheme for the finer domain (D02), while ERA5 presents an RMSD of 0.46.

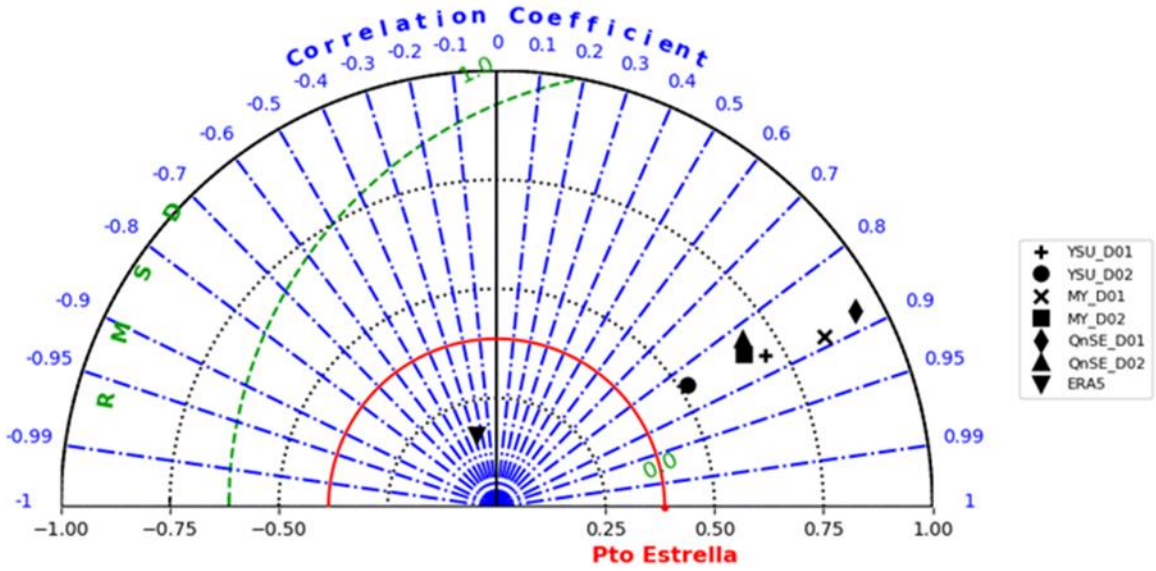

Figure 3.4: ***Taylor diagram for October diurnal average monthly cycle at Pto Estrella station (1).***

Puerto Bolivar station

Figure 3.5 shows the average monthly diurnal cycle of wind speed at Puerto Bolivar station in comparison to those generated by the WRF model with the analyzed combinations of PBL, and by ERA5.

For the month with high wind speeds (for June), the WRF model present lower amplitudes along the diurnal cycle than the station, except for the MY scheme in the interval 06 h to 12 h LST (with FB equal to 3.88% for D01 and equal to 3.67% for D02). ERA5 amplitudes along the diurnal cycle present lower FB in the first, second, and last quarter of the day compared to the WRF model with all the schemes, whereas in the third quarter of the day, the FB of ERA5 is higher than any of those generated by WRF.

The daily peak of wind speeds with all the WRF schemes occur in the period 12 h to18 h LST, meaning that WRF combinations are in phase with the station at the time of reproducing this characteristic of the diurnal cycle, which is not the case with ERA5 that generates the daily peak in the period 18 h to 24 h LST. Both WRF and ERA5 shows a second, less intense wind peak in the period 06 h to 12 h LST which is not registered by Puerto Bolivar Station. Table 3.6 shows the Bias and the FB for all WRF combinations and the ERA5 reanalysis along the diurnal cycle.

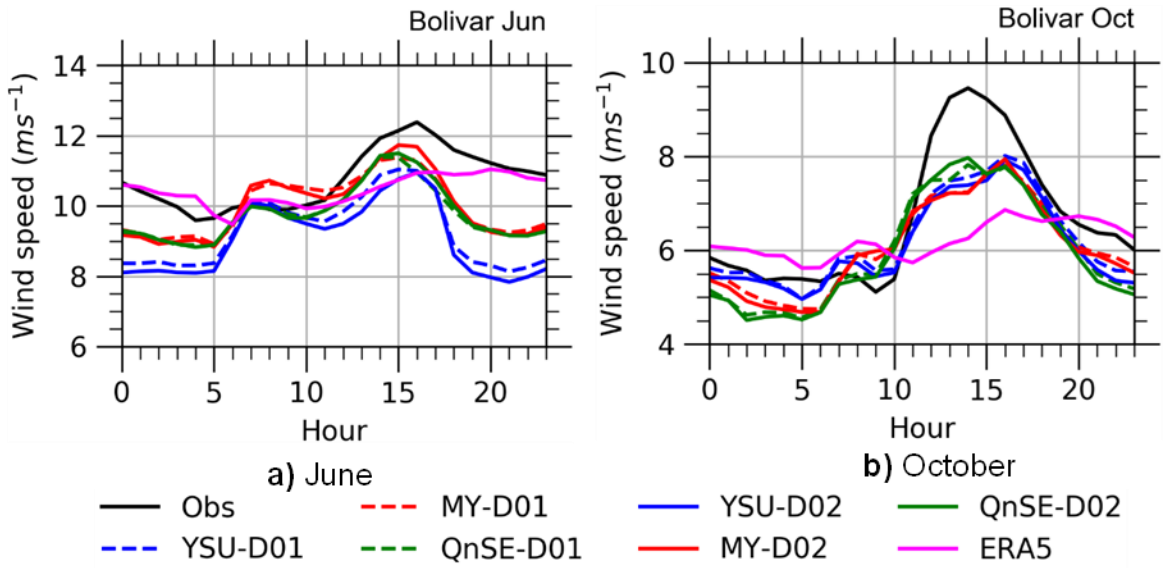

Figure 3.5 : ***WRF average monthly diurnal cycle comparison at Pto Bolivar station.***

Table 3.6: ***WRF diurnal cycle Bias for June at Pto Bolivar station (2).***

Source	Bias	Daily	0 h to 6 h	7 h to 12 h	13 h to 18 h	19 h to 23 h
YSU D01	Bias	-1.51	-1.73	-0.26	-1.18	-2.78
	FB %	-15.29	-18.76	-2.14	-10.53	-28.70
YSU D02	Bias	-1.73	-1.96	-0.38	-1.43	-3.07
	FB %	-17.84	-21.69	-3.41	-13.00	-32.24
MY D01	Bias	-0.79	-0.96	0.34	-0.74	-1.70
	FB %	-7.91	-10.08	3.88	-6.56	-16.67
MY D02	Bias	-0.80	-1.07	0.32	-0.61	-1.74
	FB %	-8.06	-11.40	3.67	-5.41	-17.18
QnSE D01	Bias	-1.02	-1.04	-0.20	-0.91	-1.82
	FB %	-10.13	-11.01	-1.50	-8.07	-17.92
QnSE D02	Bias	-0.99	-1.06	-0.22	-0.79	-1.80
	FB %	-9.92	-11.29	-1.77	-7.01	-17.78
ERA5	Bias	-0.34	0.67	0.04	-1.64	-0.48
	FB %	-3.14	6.58	1.17	-14.95	-4.22

The Taylor diagram in Figure 3.6 shows how the WRF model generates a lower RMSD (between 0.61 and 1.03) than the ERA5 model. In this case, the QNSE scheme for the finer domain (D02) generates the lower RMSD (0.61) as well as the higher r coefficient (r = 0.72). For the standard deviation, all WRF models are closer to the station amplitudes than the ERA5 model (sd = 0.43), being the MY scheme for domain D02 (sd = 0.89) the closer model to the station value (sd = 0.85). From WRF configurations, the YSU scheme exhibits the higher values of sd, whereas the other two schemes present values closer to the ones registered in the station.

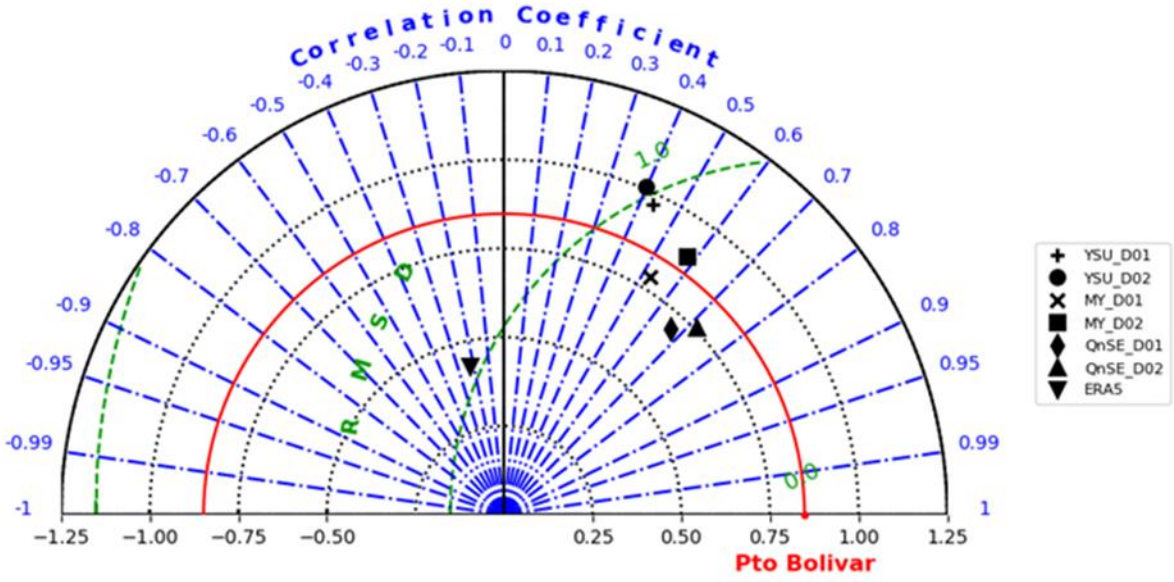

Figure 3.6: ***Taylor diagram for June diurnal average monthly cycle at Puerto Bolivar station.***

For October at Puerto Bolivar station, in Figure 3.5 all WRF schemes are in phase with the station data, especially between 12 h and 18 h LST (period of the daily peak in wind speed at the station). However, for most of the day the WRF models are below the amplitude of the station data (Table 3.7), with a negative FB for all WRF combinations during the entire diurnal cycle. ERA5 is out of phase with the station, especially in the period of high wind speeds, for which ERA5 shows the lower amplitude between all the analyzed models, while for the period 0 h to 11 h the amplitude of ERA5 is higher than the amplitude in the station and in the WRF schemes.

Table 3.7 : ***WRF diurnal cycle Bias for October at Pto Bolivar station (2).***

Model	Bias	Daily	0 h to 6 h	7 h to 12 h	13 h to 18 h	19 h to 23 h
YSU D01	Bias	-0.55	-0.16	-0.03	-0.71	-0.26
	FB %	-8.12	-0.25	-1.11	-9.14	-4.15
YSU D02	Bias	-0.68	-0.21	-0.08	-0.77	-0.35
	FB %	-9.65	-1.17	-1.49	-9.69	-5.23
MY D01	Bias	-0.66	-0.33	0.02	-0.81	-0.31
	FB %	-11.96	-6.67	-1.16	-10.56	-6.45
MY D02	Bias	-0.72	-0.40	0.02	-0.81	-0.37
	FB %	-12.49	-7.93	-0.62	-10.42	-6.64
QnSE D01	Bias	-0.74	-0.44	-0.04	-0.70	-0.41
	FB %	-12.48	-7.86	-0.72	-9.20	-7.92
QnSE D02	Bias	-0.81	-0.48	-0.09	-0.69	-0.48
	FB %	-12.97	-8.53	-1.30	-8.70	-8.67
ERA5	Bias	-0.57	0.40	0.04	-1.58	-0.08
	FB %	-9.57	9.45	1.08	-23.93	-1.40

With regard to the performance for October at Puerto Bolivar station, Figure 3.7 shows how the WRF schemes perform better on the Pearson correlation coefficient (r between 0.92 and 0.95) than

ERA 5 (r = -0.15). In the standard deviation WRF also performs better than ERA5. Among the WRF schemes, the QNSE for domain D02 has higher performance (sd station = 1.43, and sd QNSE D02 = 1.21). The QNSE scheme for domain D02 also performs better in the RMSD criterion with a value of error equal to 0.49 showing ERA5 the worst performance among all analyzed models with an RMSD of 1.54.

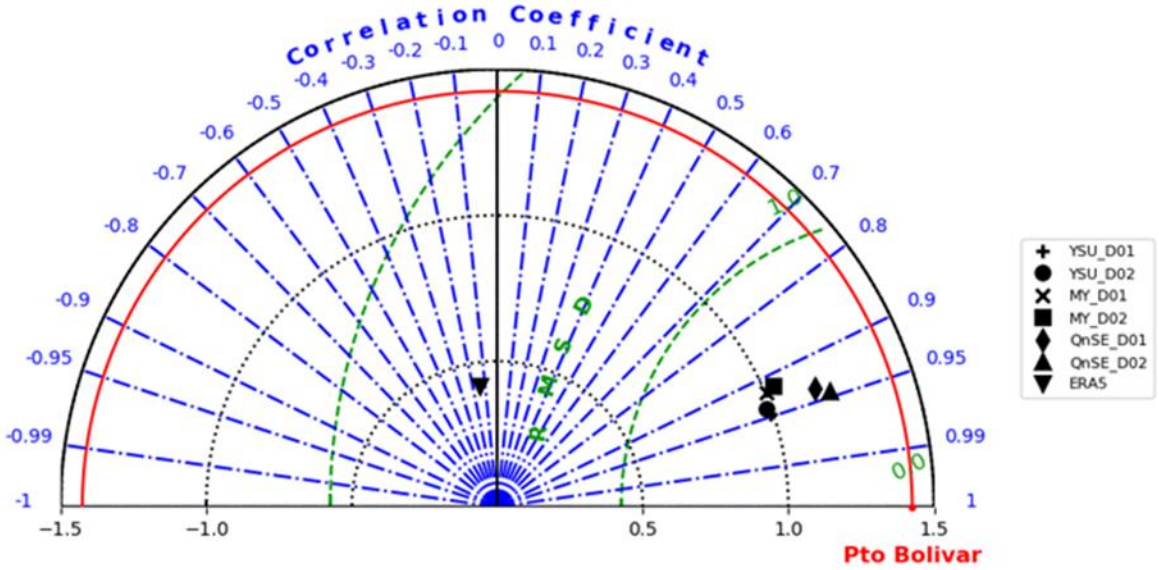

Figure 3.7: ***Taylor diagram for October diurnal average monthly cycle at Pto Bolivar station.***

Ballenas station

Figure 3.8 shows the average monthly diurnal cycle at Ballenas station for the months of high (June) and low (October) wind speeds compared to those generated by both ERA5 and WRF.

For June, the daily maximum wind speed occurs in the interval 06 h t0 12 h LST, with a second, less intense peak in the interval 12 h to 18 h. In this month, WRF generates amplitudes close to the registered in the station in the first two-fourths of the diurnal cycle, with amplitudes that are lower than the registered in the last two fourths. Therefore, WRF simulations do not represent the second daily peak of wind speeds. For the interval between 0 h and 12 h, the WRF schemes QNSE and MY in the finer domain present the lower FB (Table 3.8). ERA5 presents in turn low variations throughout the day. For the first fourth of the day and for the time interval between 22 h and 23 h, ERA5 shows high amplitudes than the observed (FB = 32.1 %), and also than the modeled with WRF, whereas the amplitudes generated by ERA5 are lower than the ones reported by the station at the interval between 06 h and 18 h (FB 0f -24.9 % and -19.3 %).

Regarding the phase along the diurnal cycle during June, WRF simulations show a good agreement for the time interval between 0 h and 12 h, whereas for the time interval between 15 h and 20 h the WRF results are in counter phase with the station, which mean a negative FB as shown in Table 3.8. In this case, ERA5 generates an almost invariable pattern around the 8 m s^{-1} for the entire diurnal cycle, producing high FB (Table 3.8).

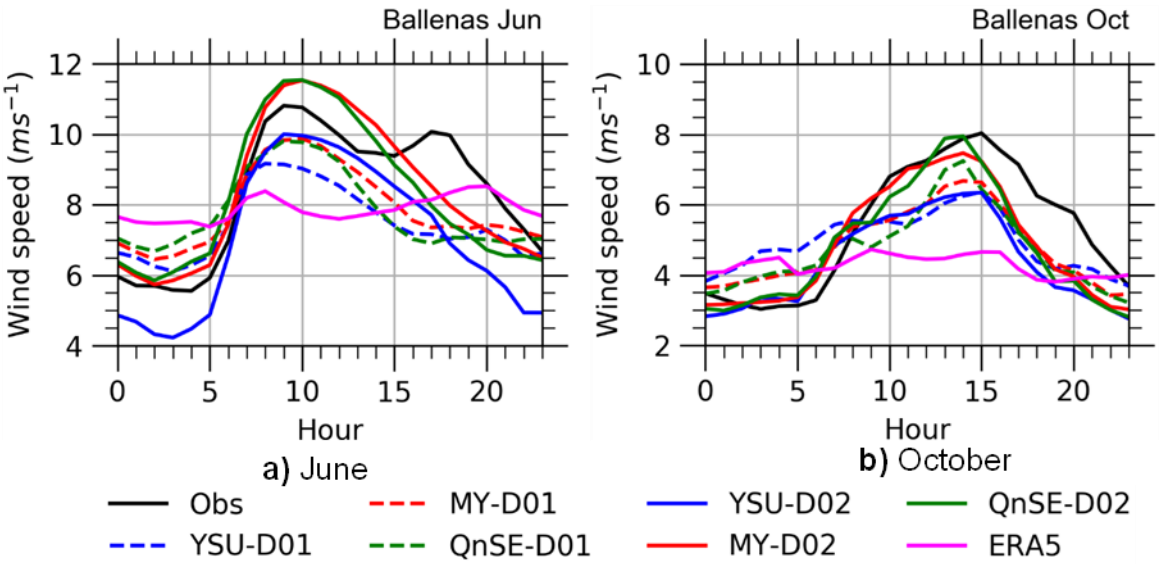

Figure 3.8 : ***WRF average monthly diurnal cycle comparison at Ballenas station.***

Table 3.8 : ***WRF diurnal cycle Bias for June at Ballenas station (3).***

Model	Bias	Daily	0 h to 6 h	7 h to 12 h	13 h to 18 h	19 h to 23 h
YSU D01	Bias	-0.90	0.64	-0.96	-1.97	-1.33
	FB %	-11.64	11.72	-10.22	-23.21	-17.87
YSU D02	Bias	-1.32	-1.18	-0.62	-0.96	-2.43
	FB %	-17.81	-22.56	-6.21	-10.63	-35.10
MY D01	Bias	-0.48	0.96	-0.48	-1.39	-0.95
	FB %	-6.51	15.99	-4.95	-16.27	-13.05
MY D02	Bias	-0.03	0.28	0.62	0.22	-1.10
	FB %	-1.14	4.49	6.52	1.89	-15.15
QnSE D01	Bias	-0.57	1.24	-0.39	-1.84	-1.23
	FB %	-7.74	19.81	-3.91	-21.73	-17.54
QnSE D02	Bias	-0.11	0.48	0.88	-0.18	-1.45
	FB %	-2.19	7.13	9.04	-2.26	-21.28
ERA5	Bias	-0.51	2.12	-2.17	-1.70	-0.36
	FB %	-6.14	32.07	-24.90	-19.27	-4.31

The Taylor diagram for the diurnal cycle during June at the Ballenas station (Figure 3.9) shows how WRF simulations for the fine domain (D02) agree well with station data compared to the simulations for the coarse domain. For instance, the standard deviation of the models on the domain D01 varies between 0.99 and 1.1, whereas for the domain D02 it varies in the range 1.99 to 2.07, while the standard deviation of the observed data is 1.88, being the QNSE scheme the closest. In the correlation parameter, the WRF PBL schemes in domain D02 obtain higher values (between 0.83 for QNSE and 0.92 for YSU) than in domain D01 (between 0.63 and 0.81). The same happens with the RMSD, with the WRF's models performing better in D02, being YSU the scheme with the lower value (0.82). All WRF simulations show a much better performance than ERA5, which presents higher errors, lesser correlation, and a limited representation of the standard deviations (Figure 3.9).

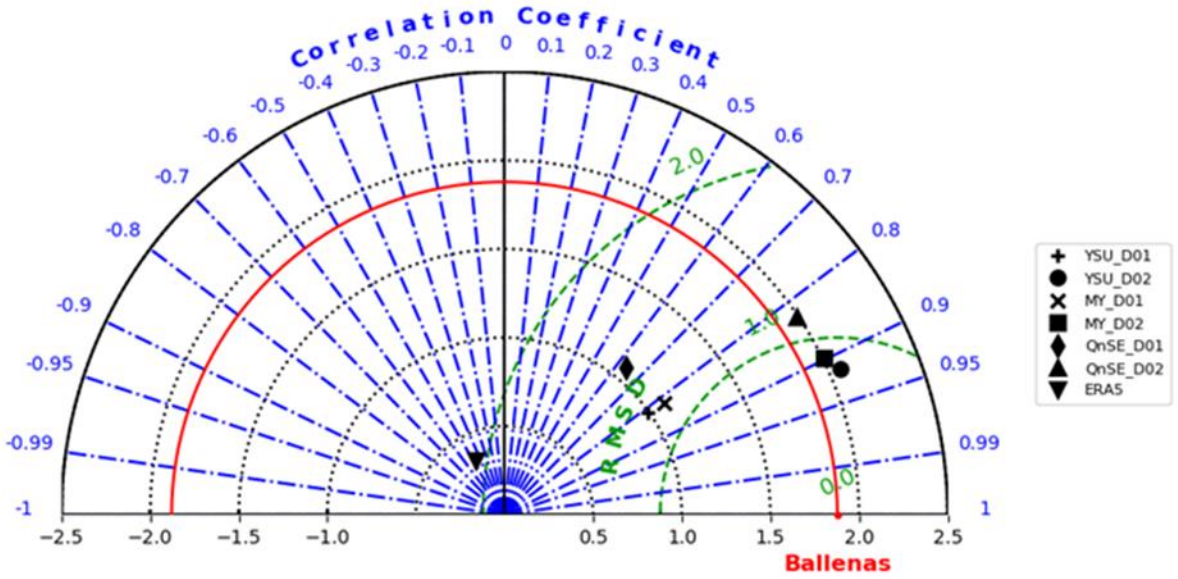

Figure 3.9: ***Taylor diagram for June diurnal average monthly cycle at Ballenas station.***

For October at Ballenas station (Figure 3.8), the maximum daily wind speed occurs between 12 h and 18 h (around 15 h). The simulations with WRF schemes MY and QNSE are in phase with the station data and, in the case of the domain D02, these two schemes also have good agreement in amplitude between 00 h and 16 h. The simulations, however, show a drop of wind speeds after that time interval, although they remain in phase with the station data. These results can be appreciated in the high FB (between 11% and 20%) for the interval between 18 h and 23 h, as shown in Table 3.9. The WRF simulation performed with the YSU scheme shows the higher FB between WRF simulations in the third-fourth of the day, which means a poor performance in the representation of the amplitude during the interval of occurrence of the maximum daily wind speed. ERA5 presents the higher FB for the mean daily wind speed and for the time interval between 6 h and 18 h, showing the lack of capacity of ERA5 to reproduce the amplitude of the mean diurnal cycle along the month of lower wind speeds.

Table 3.9 : ***WRF diurnal cycle Bias for October at Ballenas station (3).***

Model	Bias	Daily	0 h to 6 h	7 h to 12 h	1 h to 18 h	19 h to 23h
YSU D01	Bias	-0.32	0.60	-0.14	-0.93	-0.51
	FB %	-9.47	11.17	-4.54	-14.58	-11.48
YSU D02	Bias	-0.88	-0.12	-0.29	-0.94	-0.89
	FB %	-20.18	-8.25	-6.65	-14.16	-20.34
MY D01	Bias	-0.47	0.30	-0.30	-0.74	-0.58
	FB %	-12.60	4.00	-7.90	-11.45	-14.16
MY D02	Bias	-0.39	-0.05	0.01	-0.37	-0.71
	FB %	-9.69	-5.35	-0.30	-5.55	-16.59
QnSE D01	Bias	-0.55	0.30	-0.40	-0.74	-0.66
	FB %	-14.08	3.70	-11.35	-11.12	-15.08
QnSE D02	Bias	-0.47	-0.03	-0.09	-0.35	-0.83
	FB %	-11.46	-4.89	-3.60	-4.93	-19.21
ERA5	Bias	-1.02	0.40	-0.84	-1.79	-0.41

FB %	-26.52	5.55	-21.32	-34.67	-5.91

The Taylor diagram of the diurnal average monthly cycle at Ballenas station during the month of lower wind speeds , (Figure 3.10) shows that the WRF simulations with the QNSE and MY schemes, for the domain D02, have the higher performance with regard to the standard deviation (1.67 and 1.65 respectively, with1.77 for the station data) and the RMSD, with a value of 0.78 for the QNSE scheme and of 0.67 for the MY scheme. In terms of Pearson correlation coefficient, all WRF simulations have high values (between 0.78 and 0.92). ERA5, by contrast, shows the worst performance with a lower standard deviation, higher error, and lower correlation coefficient among the analyzed models.

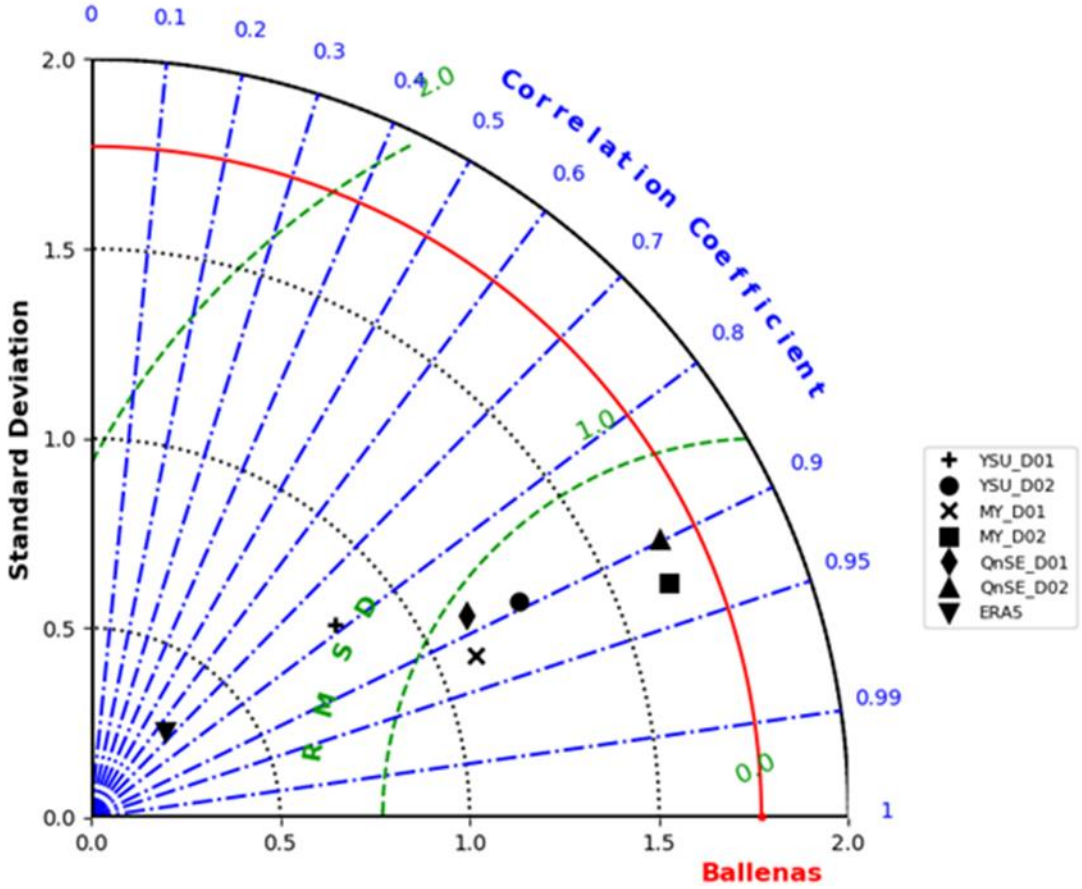

Figure 3.10: ***Taylor diagram for October diurnal average monthly cycle at Ballenas.***

Puerto Velero station

Figure 3.11 shows the observed and simulated average monthly diurnal cycle of wind speed during the extreme months of June and October for Puerto Velero station.

For June, which is the month of high wind speeds, the station reports a daily peak, above 8 m s^{-1} between 12 h and 18 h. The WRF simulations are almost in phase with the station data, although for the beginning of the day (0 h to 6 h) the coarse domain (D01) presents a higher amplitude than the observed one (Table 3.10). The simulations in the fine domain (D02) fit better with the station

data for this period of the day. For the rest of the day, the WRF simulations maintain a similitude with the phase reported by the station, but their amplitudes are lower than the recorded (which generates a FB up to -47 %), with the exception of the domain D01 which in the last fourth of the day increases the amplitude and exceeds the station values. For the entire diurnal cycle, the WRF simulations for domain D01 have an amplitude higher than the one generated for the domain D02. With ERA5, the oscillation in wind speed is in counter phase with the reported by the station between 6 h and 23 h. Along the day, the ERA5 data presents FB up to 43.5%.

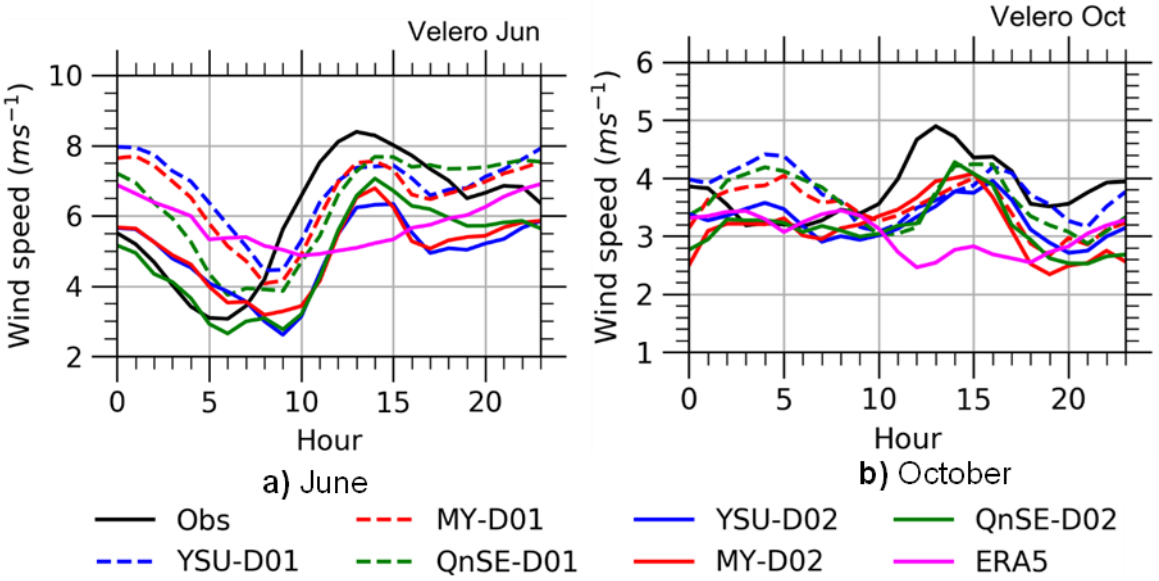

Figure 3.11: ***WRF average monthly diurnal cycle comparison at Pto Velero station.***

Table 3.10 : ***WRF diurnal cycle Bias for June at Pto Velero station (4).***

Model	Bias	Daily	0 h to 6 h	7 h to 12 h	13 h to 18 h	19 h to 23h
YSU D01	Bias	0.72	3.06	0.18	-0.83	0.55
	FB %	9.31	53.92	1.03	-11.12	4.40
YSU D02	Bias	-1.11	0.67	-1.65	-2.17	-1.33
	FB %	-21.49	17.13	-39.02	-31.30	-24.89
MY D01	Bias	0.46	2.69	-0.24	-0.92	0.38
	FB %	5.11	47.15	-7.64	-12.53	1.46
MY D02	Bias	-1.01	0.69	-1.55	-2.09	-1.12
	FB %	-19.68	15.38	-36.60	-30.14	-21.34
QnSE D01	Bias	0.24	1.69	-0.81	-0.63	0.74
	FB %	1.99	33.04	-21.33	-8.13	8.24
QnSE D02	Bias	-1.12	-0.13	-1.91	-1.58	-0.92
	FB %	-21.53	-1.28	-47.79	-21.72	-17.07
ERA5	Bias	-0.29	2.02	0.83	-2.74	-1.29
	FB %	-5.27	41.20	15.11	-43.54	-21.42

The Taylor diagram of the average monthly diurnal cycle at the Velero station for June (Figure 3.12) shows how the QNSE scheme for both domains offers the best performance about standard deviation and RMSD. For instance, the standard deviation of the simulations with the QNSE scheme have values of 1.47 for domain D01 and 1.41 for domain D02 compared to 1.72 of the station data. For WRF simulations, the RMSD varies between 1.70 and 0.98, being the lower

RMSD generated by the QNSE scheme. WRF simulations have Pearson correlations in the range of 0.33 and 0.82, with the QNSE scheme for domain D02 having the higher value of the parameter. ERA5 by contrast, presents a strong inverse correlation and, a high value of error, and the lower value of standard deviation between all the analyzed models.

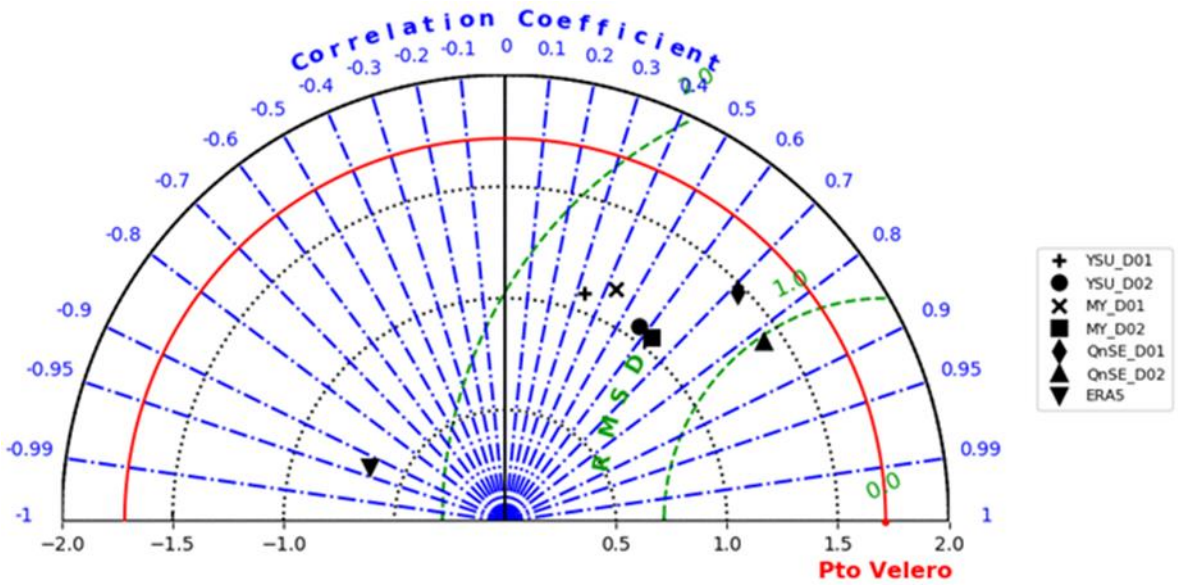

Figure 3.12: ***Taylor diagram for June diurnal average monthly cycle at Pto Velero station.***

For October at Puerto Velero station (Figure 3.11), WRF simulations for the domain D01 show two peaks of wind speed, the first between 0 h and 6 h and the second between 12 h and 18 h. In this case, the WRF simulations are out of phase with the first peak of station data, which also show two peaks but between 21 h and 0 h and between 12 h and 18 h, with the maximum value around 13 h, whereas WRF simulations for D01 present the highest values around 16 h. WRF simulations present major amplitudes than the station only for the first fourth of the day. WRF simulations for domain D02 only captures the peak of the station data between 12 h and 18 h, but with less amplitude than the registered by the station. For the first half of the day, the simulations for domain D02 present amplitudes similar to the registered by the station. ERA5 is in counter phase with the station data during the time interval with the peak and for the rest of the diurnal cycle ERA5 shows amplitudes similar to the registered, therefore the FB of ERA5 is in the order of magnitude of the FB for the WRF simulations, except for the time interval between 12 h and 18 h (Table 3.11)

Table 3.11 : ***WRF diurnal cycle Bias for October at Pto Velero station (4).***

Model	Bias	Daily	0 h to 6 h	7 h to 12 h	13 h to 18 h	19 h to 23 h
YSU D01	Bias	-0.14	0.47	-0.05	-0.42	-0.14
	FB %	-4.11	8.28	-2.30	-9.52	-4.32
YSU D02	Bias	-0.64	-0.06	-0.35	-0.55	-0.51
	FB %	-15.87	-1.50	-10.12	-11.71	-13.55
MY D01	Bias	-0.42	0.18	-0.05	-0.55	-0.47
	FB %	-12.22	0.86	-1.50	-14.95	-15.50
MY D02	Bias	-0.77	-0.28	-0.26	-0.54	-0.75
	FB %	-20.04	-7.68	-6.94	-12.52	-22.27
QnSE D01	Bias	-0.28	0.29	-0.09	-0.39	-0.34
	FB %	-7.35	6.16	-3.13	-8.08	-11.13
QnSE D02	Bias	-0.73	-0.24	-0.34	-0.50	-0.66
	FB %	-18.65	-6.32	-10.00	-10.56	-19.64
ERA5	Bias	-0.81	-0.29	-0.15	-0.94	-0.69
	FB %	-25.87	-13.11	-10.40	-25.47	-20.90

The Taylor diagram of the diurnal average monthly cycle for October at Puerto Velero station (Figure3.13) shows that the schemes that better represent the observed standard deviation (0.51) are the MYJ (0.49) for domain D02 and the QNSE for both domains (0.46 and 0.47 respectively). The higher Pearson correlations correspond to the simulations for the domain D02. However, compared with the other analyzed sites with WRF, in this case, the r values are relatively low. The RMSD of the simulations for the domain D02 also performed better than the simulations for the coarse domain D01. ERA5 shows the lower performance for standard deviation (0.30) and correlation coefficient (0.05), but not so in the case of the RMSD parameter, where simulations with the YSU and QNSE schemes present a larger error.

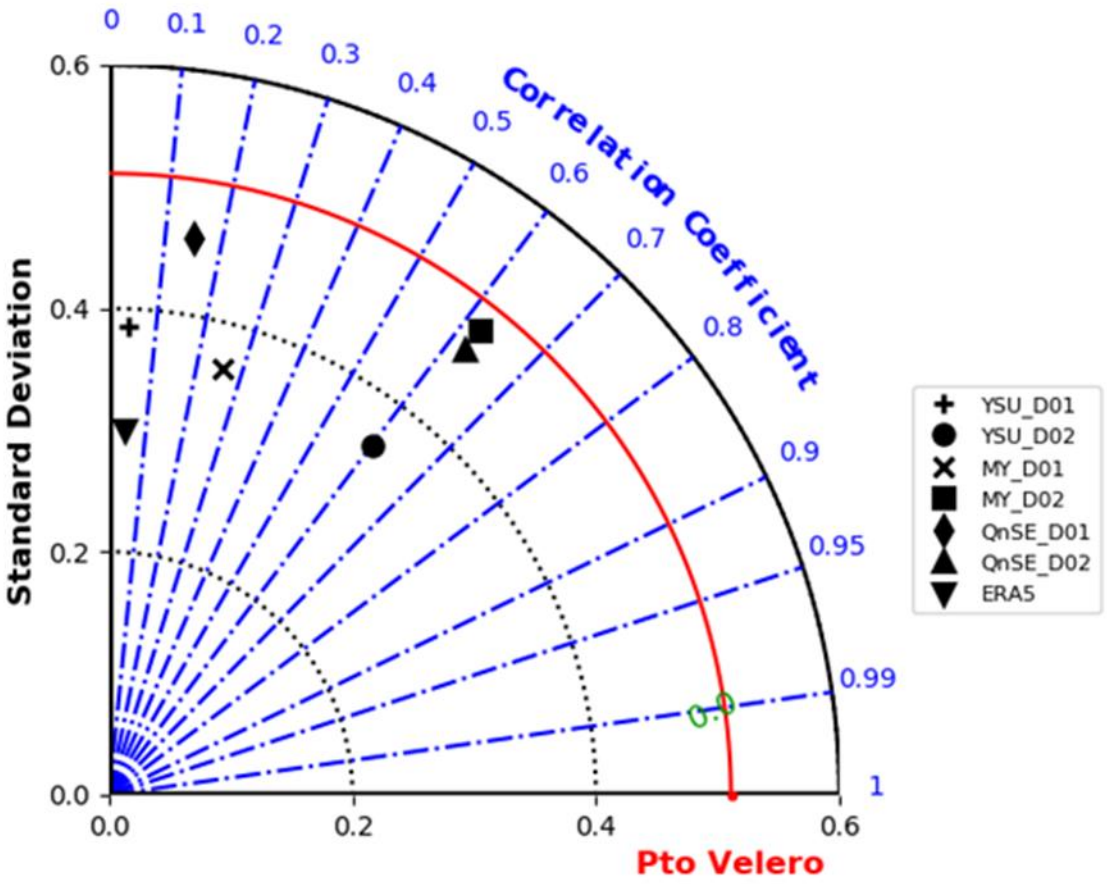

Figure3.13: ***Taylor diagram for October diurnal average monthly cycle at Pto Velero station.***

To select the best PBL scheme for the studied area, according to the results presented in this chapter, we take into account that the performance of each scheme varies according to the analyzed site. Although all measurement sites are located along the shoreline, each one differs in its surrounding topography, land cover, and relative location respect to wind streams generated by forcing mechanisms such as trade winds. Table 3.12 summarizes the number of times in which each model (PBL schemes per grid size, and ERA5) performs better than the others relative to the parameters contemplated in the Taylor diagrams. The QNSE scheme for the grid domain D02 is the one that most times (9 times) performs better than the others. Although the QNSE performance regarding standard deviation, crmsd, and Pearson correlation does not necessarily occur simultaneously, we consider that is very representative, since no model was the best for the three parameters at the same time for a particular site. In the case of ERA5, the performance of the reanalysis product was the worse between the analyzed models since it did not outperform the others in any metric or site.

Table 3.12 : ***Number of times in which each scheme and grid size perform better about Taylor's diagram parameters.***

PBL scheme - Grid size	June			October		
	Parameter			Parameter		
	sd	crmsd	ccoef	sd	crmsd	ccoef
YSU-D01	0	0	1	0	0	1
YSU-D02	1	2	1	1	2	0
MY-D01	0	0	0	0	0	1
MY-D02	1	0	0	1	1	1
QnSE-D01	1	0	0	0	0	0
QnSE-D02	1	2	2	2	1	1
ERA5	0	0	0	0	0	0

Wind direction

To compare the ability of WRF to reproduce the monthly mean diurnal cycle of wind direction, we present the hodographs for the extreme months in station Pto Estrella (Figure 3.14 and Figure 3.15). Compared with the stations, the fine domain (D02) represents better the amplitude of the diurnal cycle than the coarse domain D01 and ERA5. In both months (June and October), ERA5 exhibits a lack of capacity to present the intra-diurnal variability. Since this pattern is repeated in the other stations, we omit to present the graphs corresponding to the other stations.

As mentioned before, in this region exist local wind systems such as land-sea breezes (Pérez et al. 2018.) and low-level jets (Whyte et al., 2008), whose behavior is of interest for wind energy generation.

For the land-sea breeze system, the WRF model with any of the analyzed PBL schemes can reproduce the intra diurnal variability of wind direction, showing the occurrence of north-east winds (counterclockwise) during most of the day, while late at night and in the early hours of the morning the wind direction changes to southeast winds. This behavior repeats in both extreme months, but in October with a less strong u-wind component.

In June, the analyzed station shows strong -u wind at 12 h LST, while the YSU and MYJ schemes show its occurrence at 09 h LST, and the QNSE scheme shows the occurrence of the strong -u wind at 11 h LST. The v wind component presents two peaks during the diurnal cycle, the +v wind component (south winds) which occurs around 06 h LST in the station and is captured by the YSU scheme, but not by the MYJ and QNSE schemes that detect it around 08 h LST. The maximum value of -v wind component (north winds) occurs around 16 h LST in the station, while for WRF PBL schemes, it occurs around 15 h LST.

Figures 3.14 and 3.15, show the behavior of the wind components (u and v), generated by WRF, with very similar occurrences of maximum intra diurnal values during both extreme months of June and October.

For both moths, ERA5 shows a clockwise behavior of the intra diurnal winds, which is the opposite of what the station shows. The magnitude of the wind components remains similar in the three sources (observations, WRF, and ERA5), although the hodographs generated by ERA5 are considerably narrower than the observed while the hodographs generated by WRF are wider than the observed in the station. These differences are due to the variation in the amplitude of the daily oscillation inherent to each source.

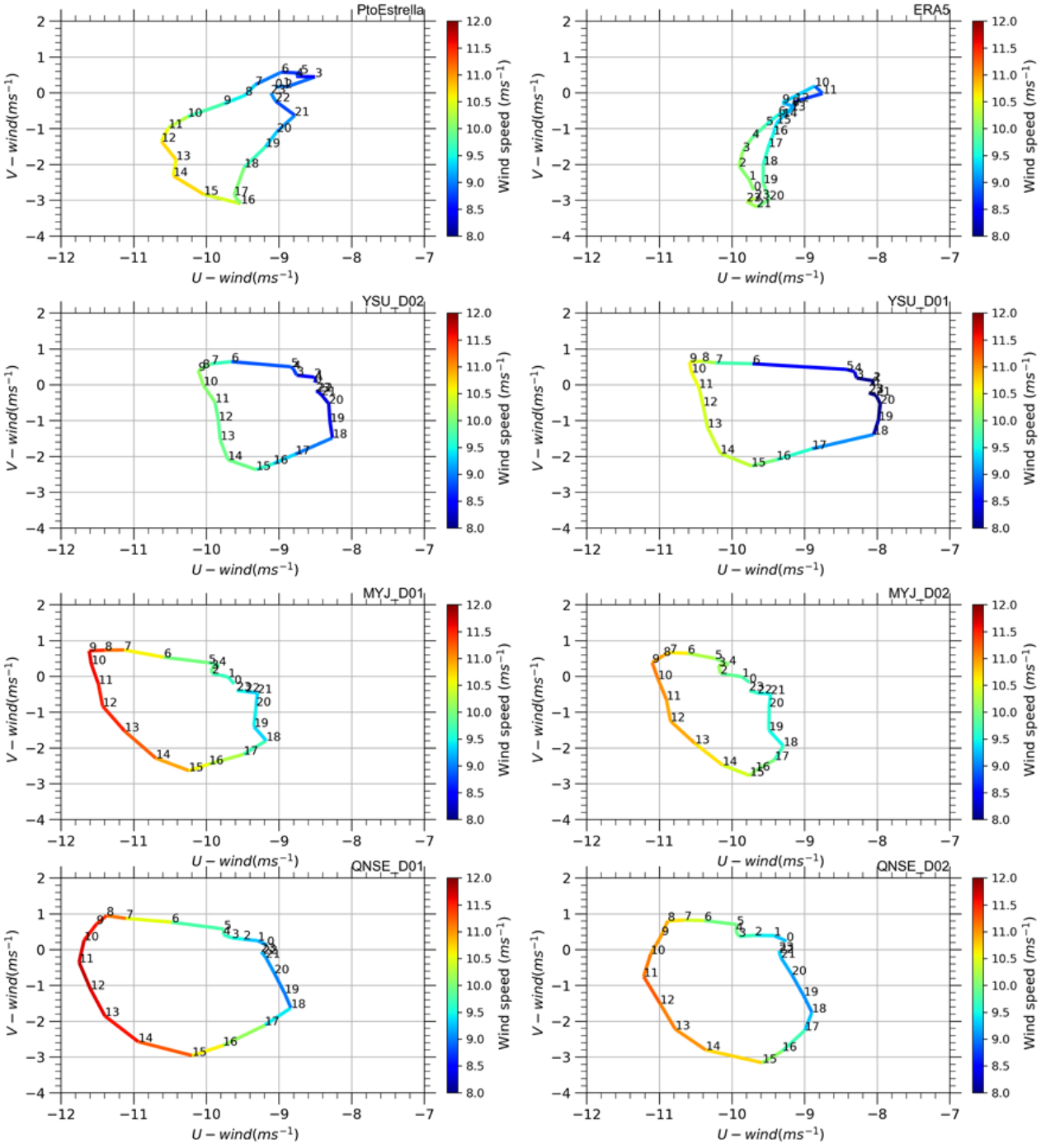

Figure 3.14 : ***Hodographs for June at Pto Estrella station.***

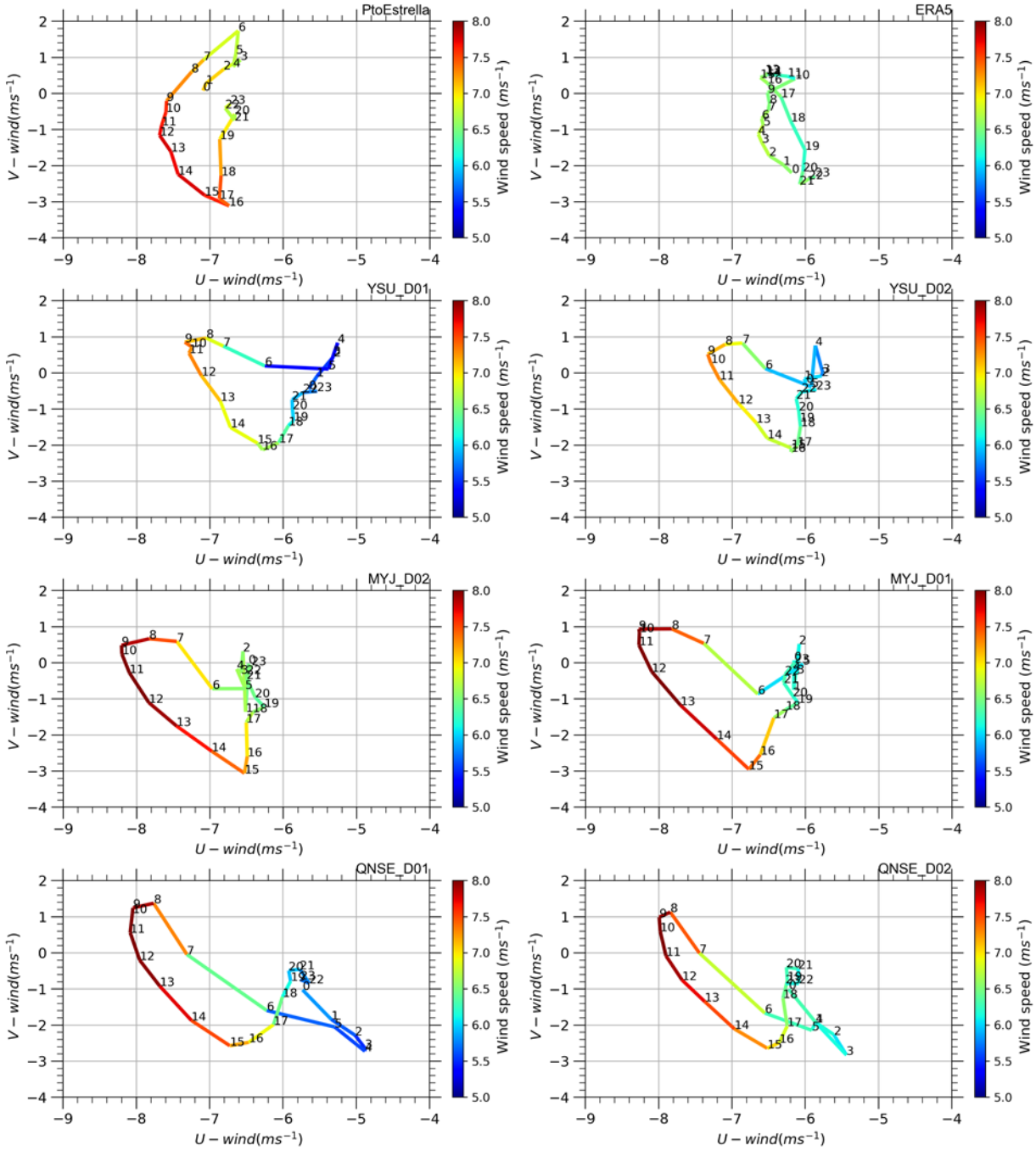

Figure 3.15 : *Hodographs* for October at Pto Estrella station.

3.4.2 Wind speed frequency distribution

We compared the WRF simulations performed with the proposed PBL schemes and using Weibull's PDF of the wind speed frequency distribution of the WRF simulations with ERA5 data and with stations data, for the two months representative of extreme wind conditions in the studied

area. Since Weibull distribution does not consider the temporal simultaneity of measured and simulated wind speed, as remarked by Carvalho et al. (2014), this analysis is complementary to the presented in the previous numeral.

Figure 3.16 shows the Weibull distributions for the meteorological station data, ERA5 and each of the WRF simulations in both domains. The performance of the WRF schemes for wind speed distribution varies according to the month, the site, and the grid resolution.

In the case of Puerto Estrella station, located further north of the studied region, for June, the wind speeds generated with MY and QNSE schemes for both domains tend to overestimate the wind speed whereas the YSU scheme underestimates it. In terms of the shape of the distribution, in all cases, wind speeds generated with WRF fit better the observed distributions compared to ERA5. In this case, ERA5 is unable to represent the high wind speeds, whereas overestimates the lower wind speeds. For October, in this station, all models overestimate the occurrence of low wind speeds, whereas only the YSU scheme and ERA5 also underestimate the high wind speeds. In this case, the distribution of ERA5falls closer to the WRF distributions and to the observed distribution at the station.

Regarding the wind speed PDFs at Puerto Bolivar station, for June, both WRF and ERA5 underestimate the wind speed. However, ERA5 exhibits a narrow shape of the speed distribution (which overestimate the frequency of intermediate speeds), showing less variability of the wind speed. Among WRF simulations, the YSU is the scheme that underestimates wind speeds the most. For October at Puerto Bolivar station all models underestimate the strong wind speeds and overestimate the low speeds. However, in this month all models show a distribution of wind speeds close to the observations, especially when compared with the results for the month of high wind speeds (June).

For the wind speed frequency distribution at Ballenas station, during June, the WRF simulations with QNSE and MY schemes for domain D02 show an almost perfect fit with the distribution of observed data. In this case, ERA5 overestimates the frequency of intermediate wind speeds, whereas underestimates strong and weak wind speeds. The YSU scheme once more underestimates the wind speeds for both domains. For the wind speed frequency during October at this site, all models overestimate the frequency of weak wind speeds while they underestimate the frequency of strong wind speeds. The shape of the distributions in all models is closer to the observed data, compared with June.

For the site located farthest south of the studied area (Pto Velero station), during June, the wind speeds generated within the larger domain shows a good fit to the station data distribution, whereas the speeds generated with WRF within the finer domain exhibit a systematic bias and underestimation of the wind speeds. In this case, ERA5 overestimates the intermediate wind speeds. For October at this site, as in the other sites, all models tend to underestimate wind speeds, although the models fit the observed distributions better than in the case of the month of high wind speeds (June).

Tables 3.13 and 3.14 summarize the results described in the previous paragraphs, presenting the differences in percentage of some important statistics, including shape and scale parameter of Weibull distribution, compared to the observed data for the extreme months.

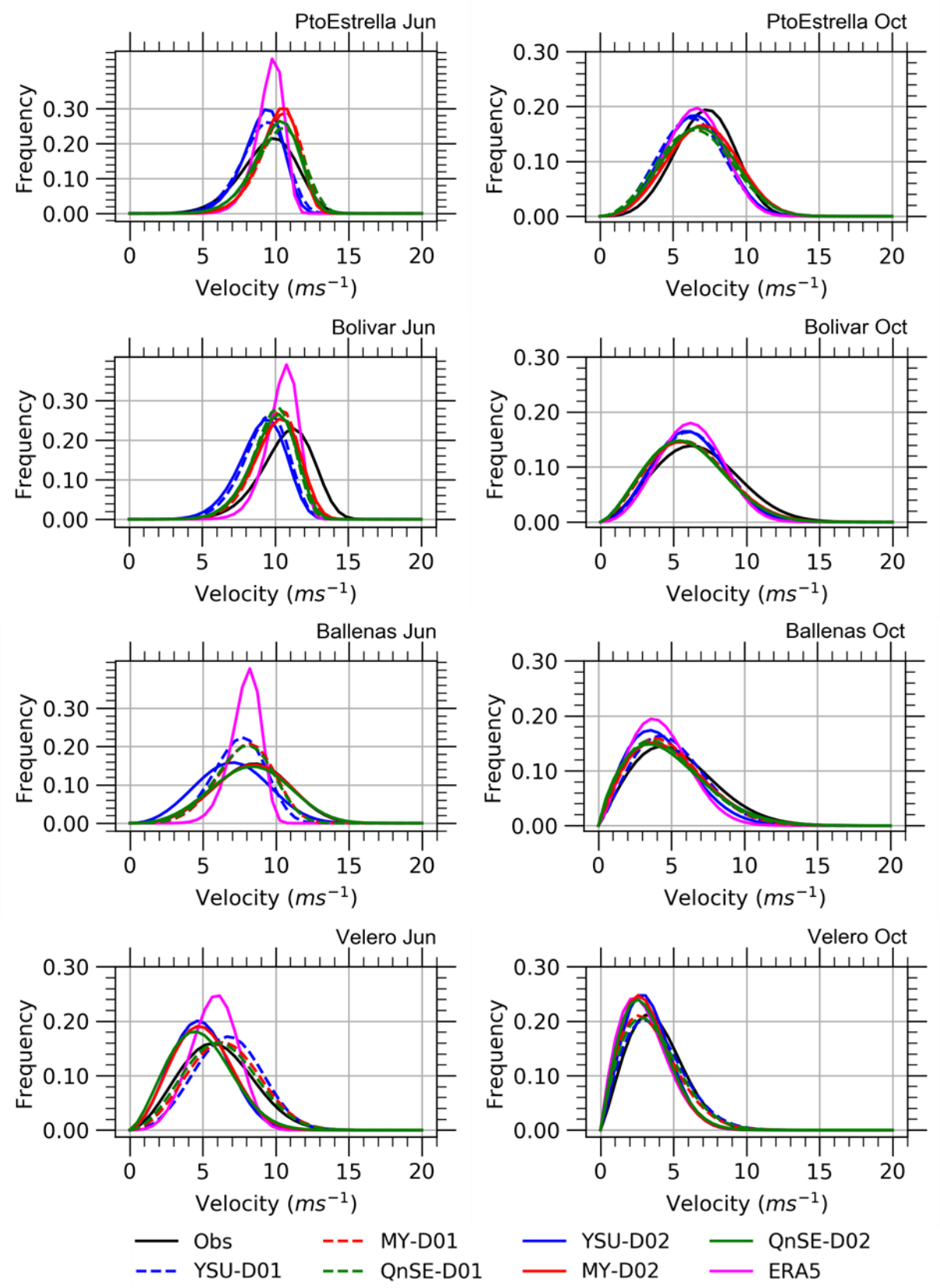
PtoEstrella Jun
PtoEstrella Oct
Bolivar Jun
Bolivar Oct
Ballenas Jun
Ballenas Oct
Velero Jun
Velero Oct
Frequency
Velocity (ms^{-1})
Obs
YSU-D01
MY-D01
QnSE-D01
YSU-D02
MY-D02
QnSE-D02
ERA5

Figure 3.16: ***Weibull distribution of wind speed for different PBL schemes compared with observed data and ERA5 data.***

Table 3.13 : ***Differences in % of Weibull distribution statistics for June.***

Statistics	Station	Station Data	Differences in %						
			YSU D01	YSU D02	MY D01	MY D02	QNSE D01	QNSE D02	ERA5
k	Puerto Estrella (1)	5.87	17	32	44	50	21	28	106
λ (m s^{-1})		10.21	5	6	6	4	5	4	2
mean		9.46	4	4	8	7	6	5	1
variance		3.49	31	46	41	46	21	31	74
skewness		-0.36	25	44	56	61	31	40	98
k	Puerto Bolivar (2)	7.05	0	6	12	3	12	6	63
λ (m s^{-1})		11.48	14	16	8	7	10	9	5
mean		10.74	14	16	7	7	9	9	3
variance		3.21	26	20	31	19	33	25	63
skewness		-0.47	0	8	13	4	13	6	49
k	Ballenas (3)	3.76	28	15	26	2	22	6	141
λ (m s^{-1})		9.25	12	15	7	0	8	1	10
mean		8.35	11	16	6	0	7	1	6
variance		6.15	50	5	42	3	40	9	82
skewness		-0.04	537	389	498	40	438	144	1562
k	Puerto Velero (4)	2.69	28	15	26	2	22	6	141
λ (m s^{-1})		6.74	12	15	7	0	8	1	10
mean		5.99	11	16	6	0	7	1	6
variance		5.76	50	5	42	3	40	9	82
skewness		0.28	537	389	498	40	438	144	1562

Table 3.14 : ***Differences in % of Weibull distribution statistics for October.***

Statistics	Station	Station Data	Differences in %						
			YSU D01	YSU D02	MY D01	MY D02	QNSE D01	QNSE D02	ERA5
k	Puerto Estrella (1)	4.02	20	15	21	16	26	21	8
λ (m s^{-1})		7.87	11	9	2	0	6	3	9
mean		7.14	12	10	3	1	7	5	9
variance		3.97	15	9	42	34	47	39	4
skewness		-0.09	206	148	220	164	289	224	74
k	Puerto Bolivar (2)	2.59	12	11	3	6	4	6	24
λ (m s^{-1})		7.51	7	9	9	9	10	11	8
mean		6.67	7	9	9	9	10	11	7
variance		7.63	29	30	12	9	13	11	41
skewness		0.32	38	33	11	21	16	21	67

Statistics	Station	Station Data	Differences in %						
			YSU D01	YSU D02	MY D01	MY D02	QNSE D01	QNSE D02	ERA5
k	Ballenas (3)	2.05	7	2	1	7	8	12	11
λ (m s^{-1})		6.05	8	18	10	9	12	10	20
mean		5.36	8	18	10	9	11	10	20
variance		7.48	24	30	17	5	9	3	47
skewness		0.60	14	4	3	16	18	30	22
k	Puerto Velero (4)	2.18	8	2	14	5	11	9	12
λ (m s^{-1})		4.30	1	14	9	17	6	17	20
mean		3.80	1	14	8	17	5	17	20
variance		3.39	14	29	10	25	11	19	20
skewness		0.52	22	4	38	12	30	22	33

3.4.3 Fields of average wind speed

This section presents the fields of monthly average wind speed at 10 meters above ground level and their corresponding standard deviations for the extreme months of June and October, generated by ERA5 and by each one of the WRF PBL schemes.

These wind fields are strongly influenced by synoptic-scale phenomena like the trade winds, the Caribbean low-level jet, and the displacement of the ITCZ throughout the year. Besides, due to its nature as a coastal area, the studied winds are also influenced by the local phenomenon of land-sea breezes, but also the orography, the landcover and the shape of the coastline. Therefore, detailed wind fields like the ones presented in this section are very valuable resource.

Performances in the month of higher average wind speeds (June)

Figure 3.17shows the fields of average wind speed at 10 m generated through the studied PBL schemes and ERA5 for June in the domain D02. For the land portion located farther north (La Guajira region) during June, both the QNSE and the MYJ schemes generate a very similar pattern of monthly mean wind speed spatial distribution (this similarity can be appreciated better in Figure 3.21).

According to the WRF schemes QNSE and MYJ, the values of mean wind speed range from 9 m s^{-1} to 13 m s^{-1}(Figure 3.17). The standard deviations (Figure 3.18) for this land region with these two schemes, vary between 1 m s^{-1} and 3.5 m s^{-1}. For this area, the YSU scheme generates values of mean wind speed in the interval of 6 m s^{-1} to 10 m s^{-1}, with standard deviations ranging from 1.5 m s^{-1} to 4 m s^{-1}. In the three cases, wind speed increases in a south-north direction, and from east to west, as expected for the region.

In the offshore regions, the mean wind speeds generated by the three schemes reach values of up to 11 m s^{-1} for a large zone located between 76°W and 72°W and above 12°N, with standard deviations under 1.5 m s^{-1}, which indicate propitious conditions for the development of offshore wind energy with high wind speeds and low variability. In the same zone under 12 N, the mean

wind speeds are still above 6 m s^{-1}, but the standard deviations are higher than 1.5 m s^{-1}. Over the sea, the wind speed decreases towards the south and increases from east to west. Furthermore, for the region between 72 W to 70 W, and 11 N to 12 N, which encompasses the Gulf of Venezuela, the three schemes show mean wind speeds between 11 m s^{-1} and 12 m s^{-1}, with standard deviations between 1 m s^{-1} and 2 m s^{-1}, which is indicative of excellent offshore wind potential.

Figure 3.17 shows how ERA5 underestimates the average wind speed onshore over La Guajira region, compared to the QNSE and MYJ schemes, whereas in comparison with the YSU scheme, ERA5 slightly overestimates the average wind speed in this land portion. Compared with WRF, as expected, ERA5 cannot represent the influence of local factors such as the topography and land cover on the wind speed. Therefore, ERA5 is unable to represent wind variations associated with these factors. Regarding offshore winds, ERA5 presents wind patterns that are similar to those generated by WRF models.

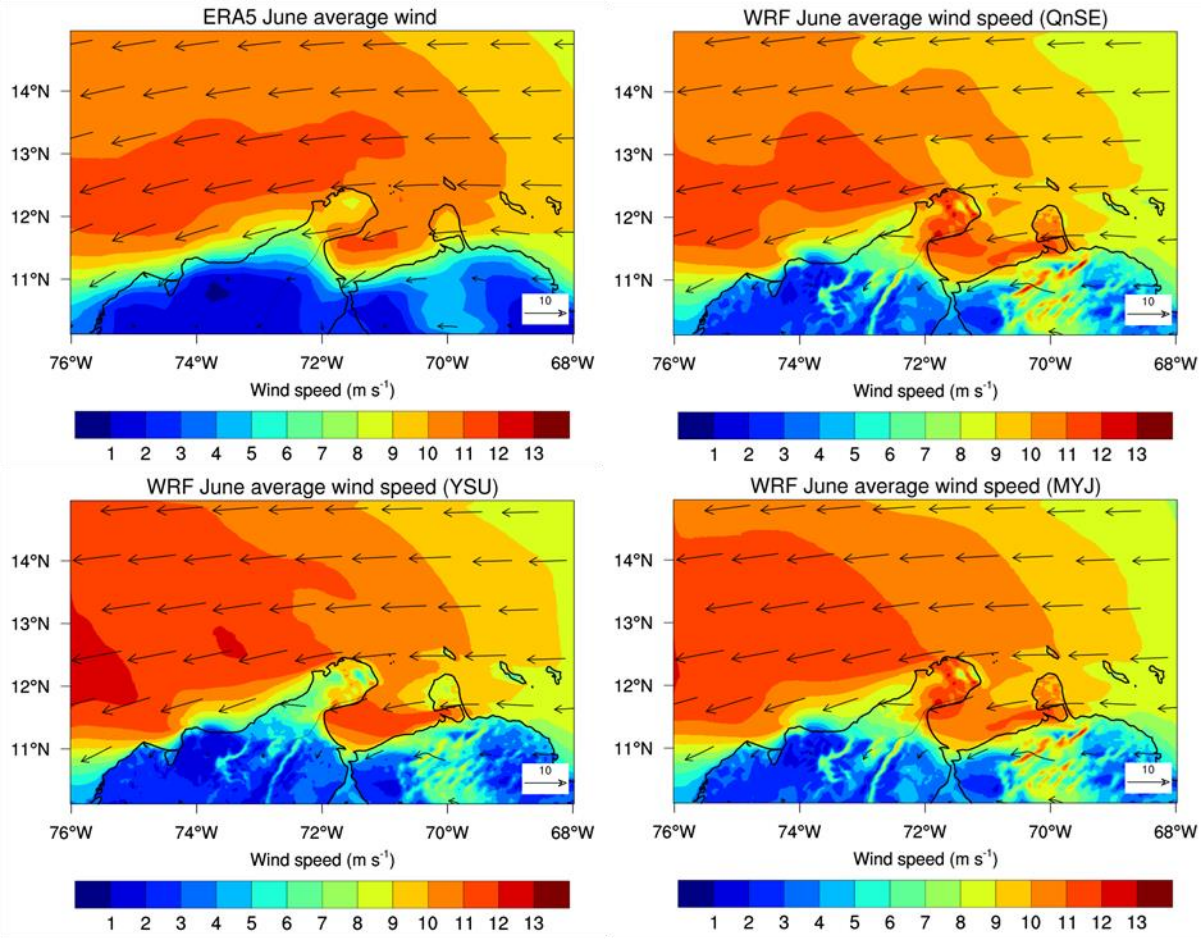

Figure 3.17 : ***Average wind speed for June – Comparison between ERA5 and WRF with analyzed schemes.***

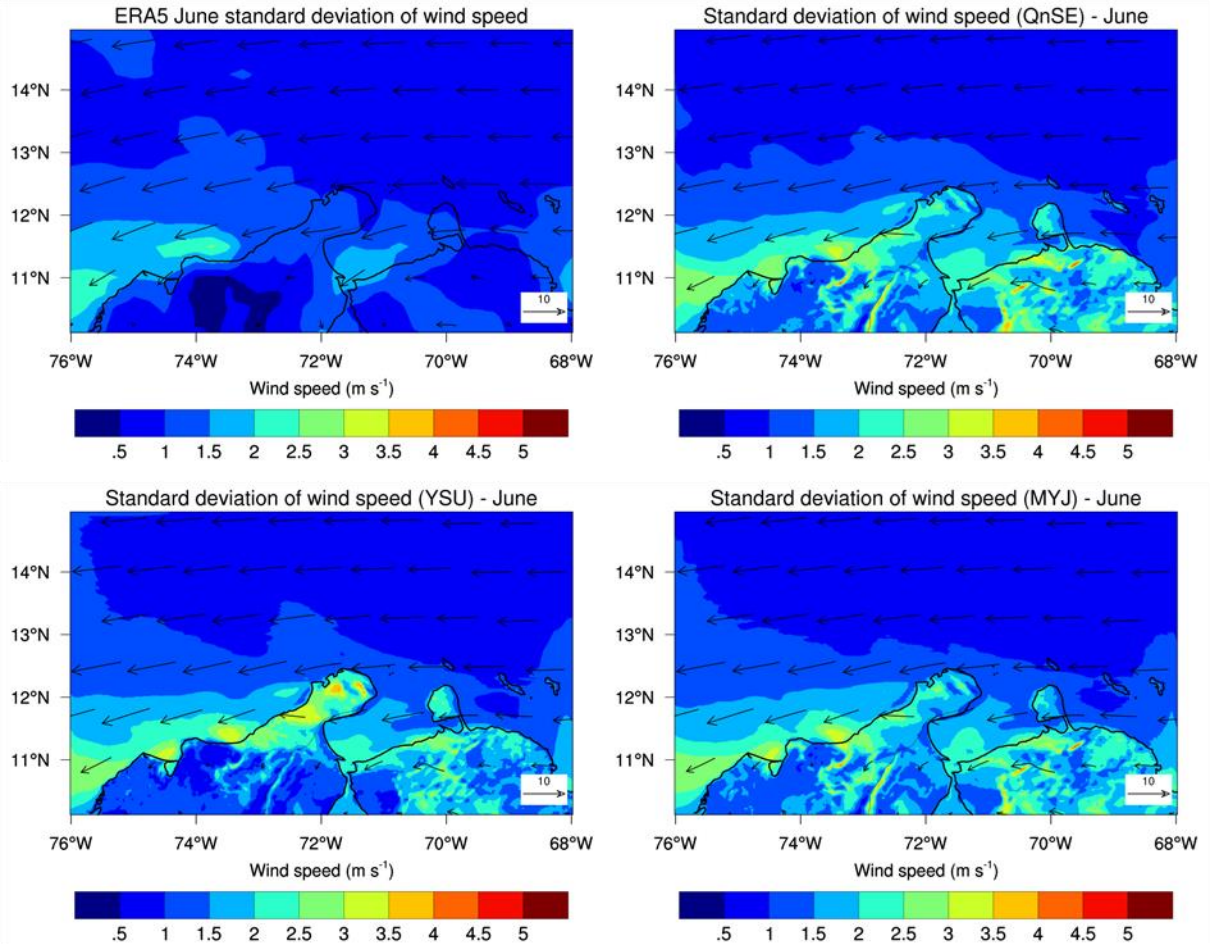

Figure 3.18 : ***Standard deviation of wind speed for June – Comparison between ERA5 and WRF with analyzed schemes.***

Performances in the month of lower average wind speeds (October)

For the onshore region, during the month of lower wind speeds, the schemes QNSE and MYJ, as in the case of June, generated a very similar pattern of mean wind speed for the land portion located at the north (La Guajira region), with mean wind speeds between 5 m s^{-1} and 8 m s^{-1} (Figure 3.19). In the case of the YSU scheme, the mean wind speeds on the same region vary between 4 m s^{-1} and 6 m s^{-1}. Regarding the standard deviations of wind speeds (Figure 3.20), the QNSE scheme generates the higher values varying between 2.5 m s^{-1} and 3.5 m s^{-1}, while for MYJ the standard deviation is in the range of 2.5 m s^{-1} to 3 m s^{-1}. The YSU scheme generate the lower standard deviations between 2 m s^{-1} and 3 m s^{-1}.

For the offshore winds during the month of lower wind speeds (Figure 3.19), in the areas mentioned above, the three schemes generate values of mean wind speed between 5 m s^{-1} and 8 m s^{-1}, with standard deviations between 1.5 m s^{-1} and 3.5 m s^{-1}. As in the case of June, wind speeds increase from east to west and decrease from north to south.

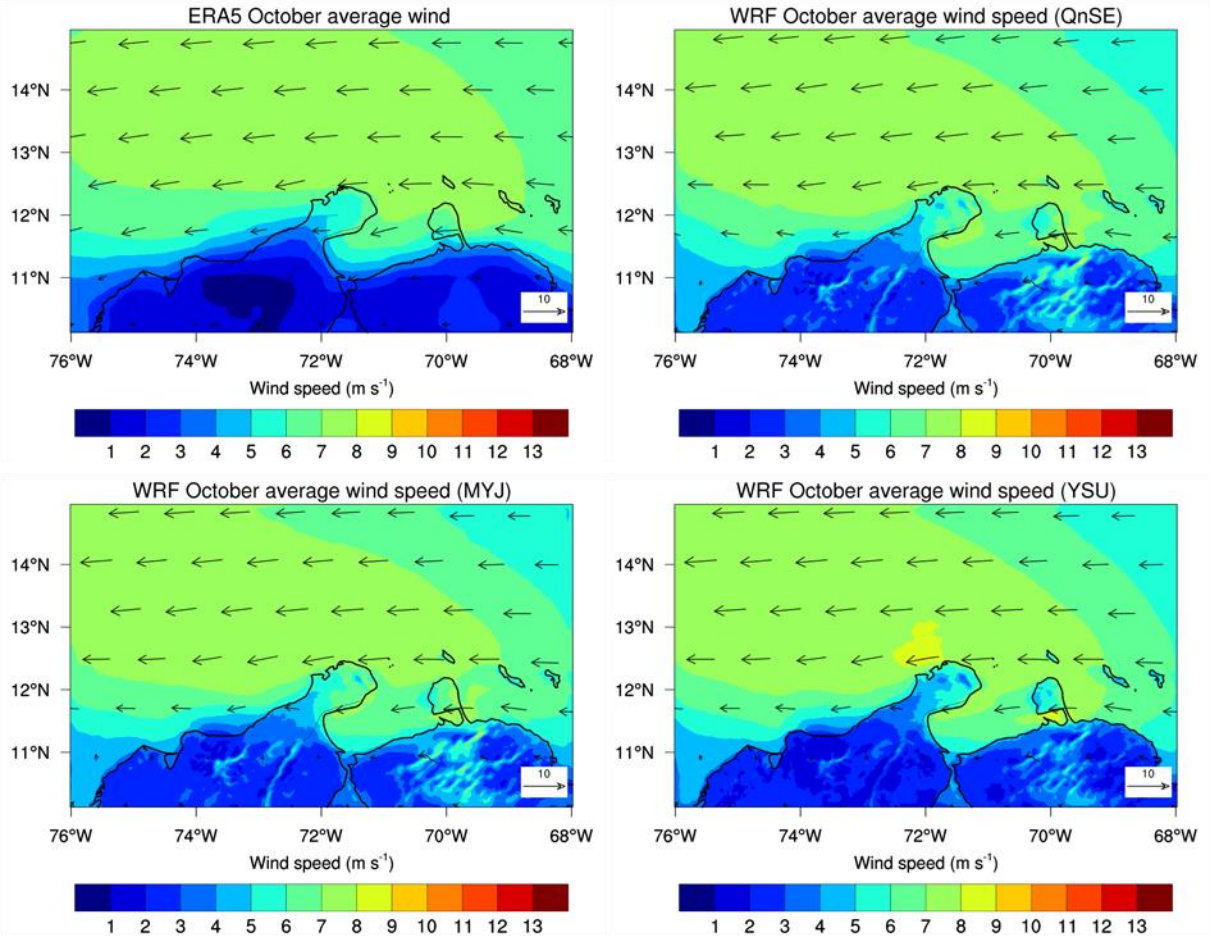

Figure 3.19 : ***Average wind speed for October – Comparison between ERA5 and WRF with analyzed schemes.***

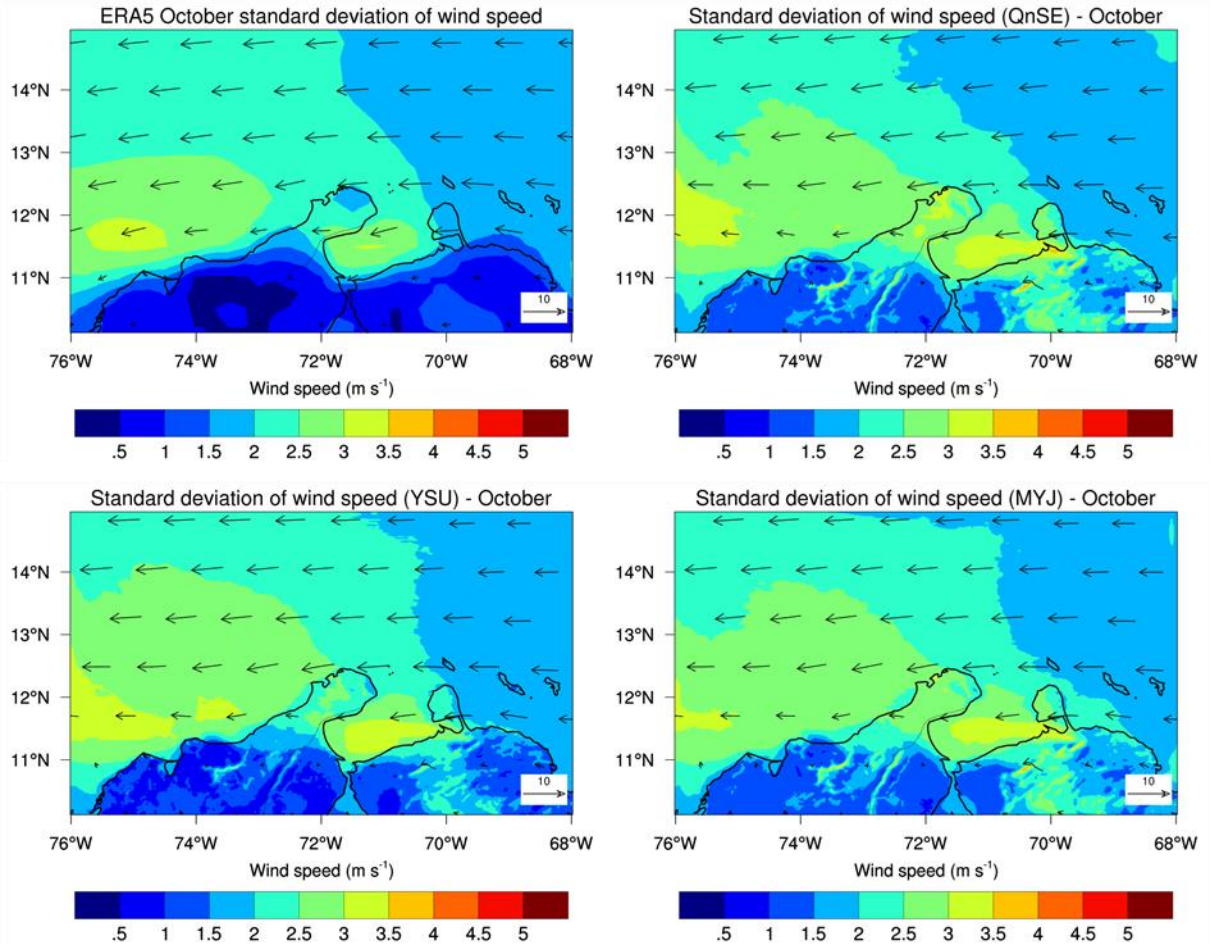

Figure 3.20 : ***Standard deviation of wind speed for October – Comparison between ERA5 and WRF with analyzed schemes.***

Since each analyzed PBL scheme solves the closure problem with a different approach, then each PBL scheme presents different strengths and weaknesses. While the local closure schemes aim at representing small eddies, the nonlocal ones work with the superposition of large and small eddies. To compare the PBL schemes between them, we present Figure 3.21, in which we calculated the difference of the YSU (first-order non-local closure scheme) and MYJ (1.5 order local closure) schemes regarding the QNSE (1.5 order local closure) scheme, which was selected as the best-performed scheme regarding the meteorological stations. For June, the YSU scheme underestimates the wind speed onshore, reaching differences of 3 m s^{-1} in some regions, otherwise for large areas of the offshore domain YSU presents higher wind speeds than the QNSE scheme (in the range of 0,5 m s^{-1} to 1 m s^{-1}). For October, the difference between YSU and QNSE schemes decreases almost for the entire domain and remains only in the inland places that are associated with topographic factors such as mountain chains. The MYJ scheme performs in a very similar way, barely showing differences with the QNSE scheme for the two analyzed months. This similarity between QNSE and MYJ is due to the nature of these two parameterization schemes since both are 1.5 order local closure schemes. The best performing QNSE scheme was designed for stable conditions (Cohen e al., 2015).

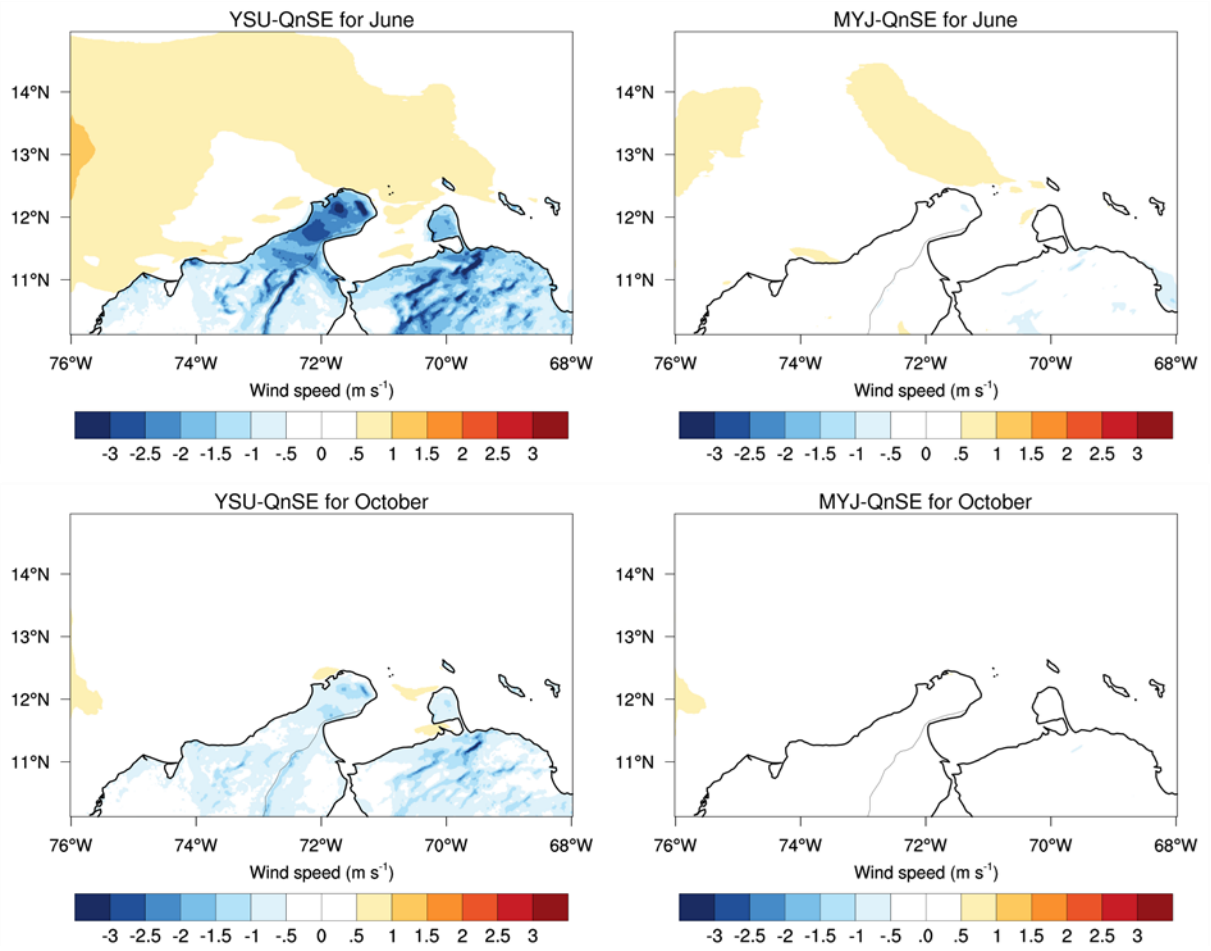

Figure 3.21 : ***Differences of monthly average wind speed with the best performing scheme (QnSE).***

Intra diurnal cycle of wind speeds

Figure 3.22 shows the monthly average wind speed for the interval 13 h to 18 h LST during June, generated by each one of the three PBL schemes. Such time interval is important for the assessment of wind power potential and the operation of wind farms since it coincides with a time interval in which the daily demand for energy in Colombia is high and sustained. In the northern land portion (La Guajira region) the YSU scheme generates lower wind speeds than the QNSE and MYJ schemes, whereas for the sea portion of the analyzed domain, the QNSE scheme generates a pattern with lower average wind speeds than the other two schemes.

For this intra-diurnal interval, the scheme that generates a higher standard deviation in La Guajira region is the YSU scheme. The calculated standard deviations show that the offshore areas with high wind speeds (> 11 m s^{-1}) present lower wind variability than onshore areas with also high wind speeds.

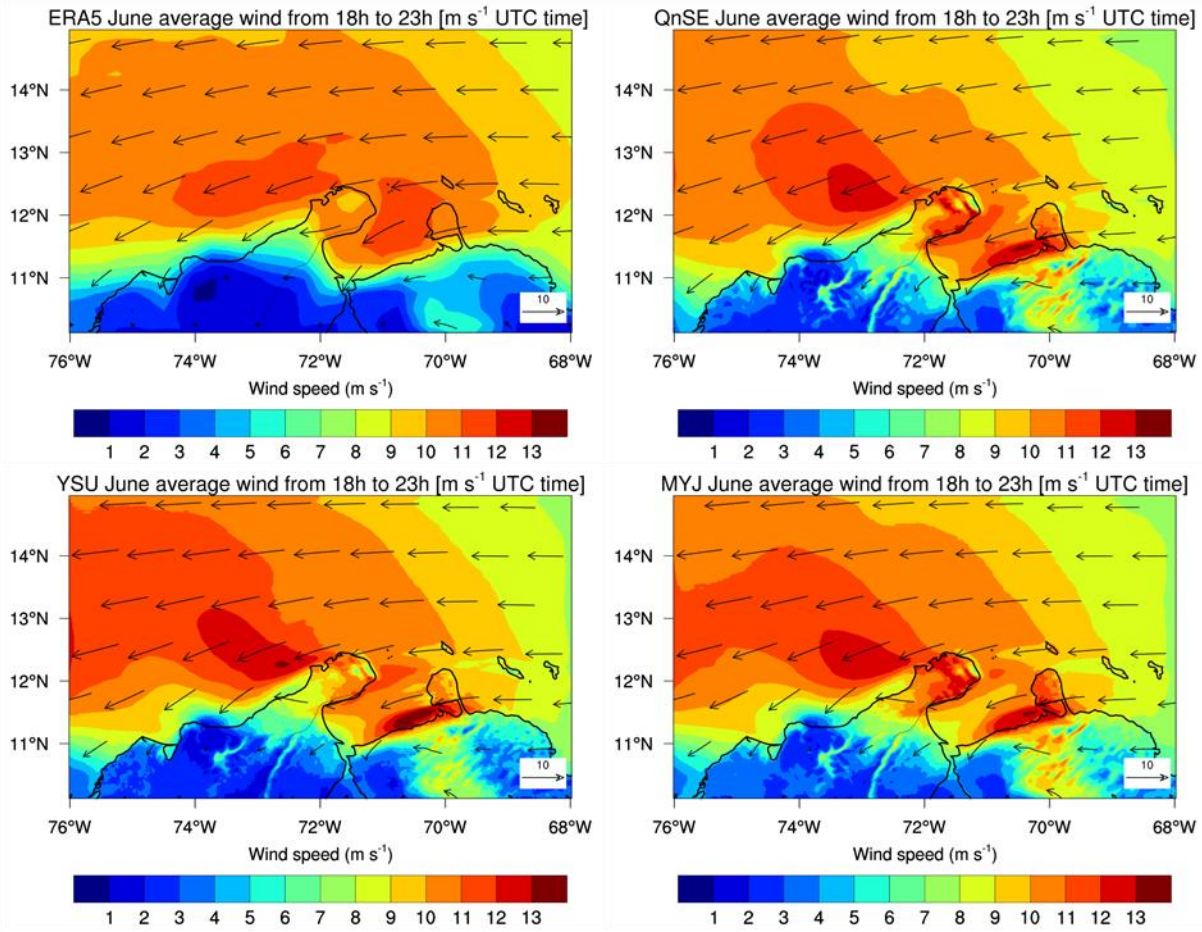

Figure 3.22 : ***Monthly average wind speed for the interval 13 h to 18 h LST for ERA5 and the three PBL schemes (a, b, c) during June.***

For the intra-diurnal cycle (interval 13 h to 18 h LST) for October (the month with lower wind speeds) (Figure 3.23), the YSU scheme generates the lower wind speeds for the land portion of La Guajira region, whereas the wind patterns are very similar for the three schemes in the offshore area. The standard deviations of the three schemes for wind speeds during October (1.5 m s^{-1} to 3.5 m s^{-1}) present higher variability in both land and sea regions compared with the standard deviations generated during June (0.5 m s^{-1} to 2.0 m s^{-1} for most areas).

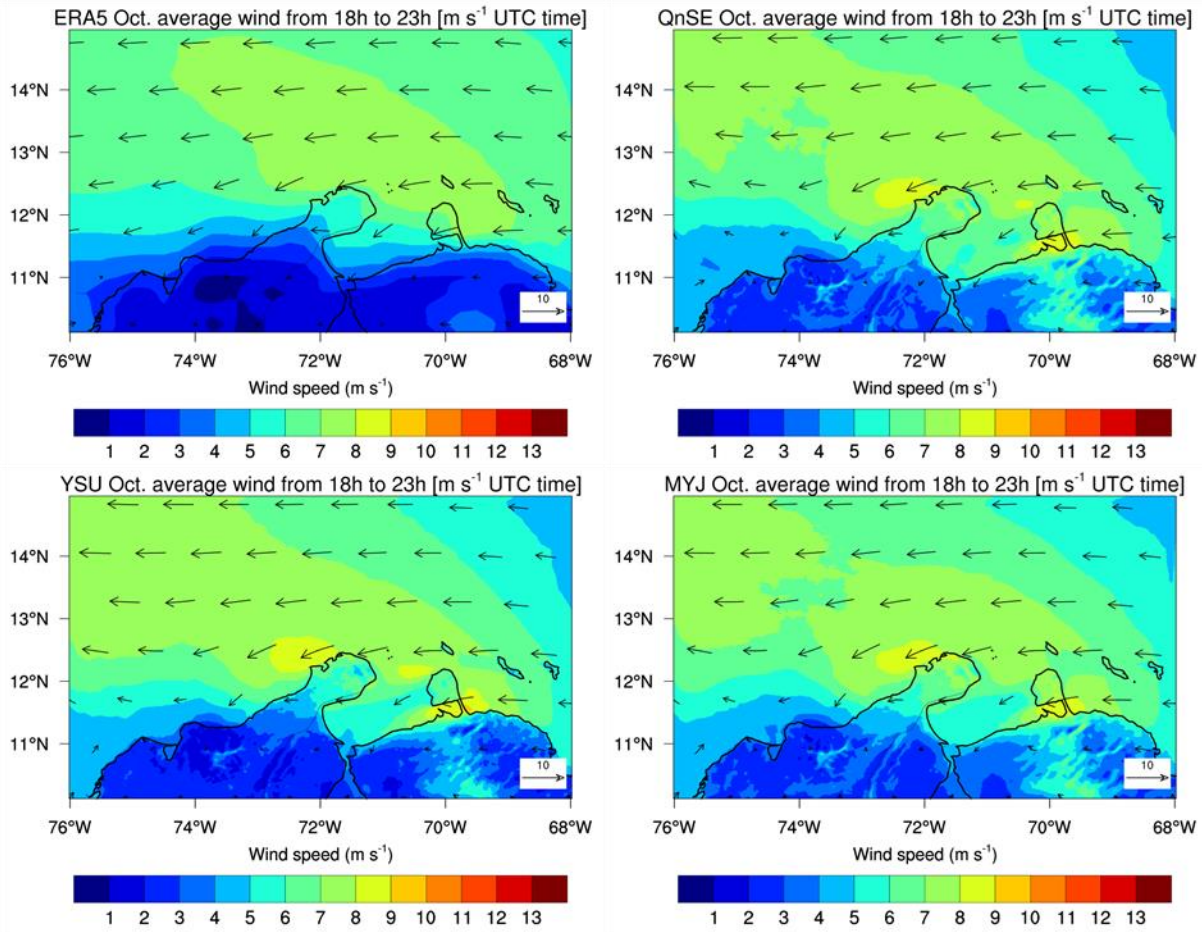

Figure 3.23 : ***Monthly average wind speed for the interval 13 h to 18 h LST for ERA5 and the three PBL schemes during October.***

In both cases (the months with the low and high wind speeds), the WRF model improves significantly the representation of wind patterns compared with ERA5 for the interval 13 h to 18 h. This is due to because the ability of WRF to detail local factors such as topography and land cover in the wind fields, whereas ERA5 does not capture the subtleties of such effects. This capabilities of WRF are viewed also in the case of the monthly wind speed average.

Figure 3.24 shows the differences between the QNSE scheme with regard to the YSU and the MYJ schemes for the analyzed interval of the diurnal cycle. As in the case of the entire monthly average, there are notable differences between the QNSE and the YSU schemes. For instance, the QNSE scheme generates higher wind speeds in the land portion while the YSU scheme does the same (but in lower amplitude), for the offshore domain. These differences are higher for the windier month of June.

The MYJ scheme for June in the analyzed time interval generates higher wind speeds (up to 1.5 m s^{-1}) than the QNSE scheme in the onshore region (in the case of the entire monthly average wind speed the schemes do not show differences – Figure 3.21). During October, the performance of the two schemes is very similar.

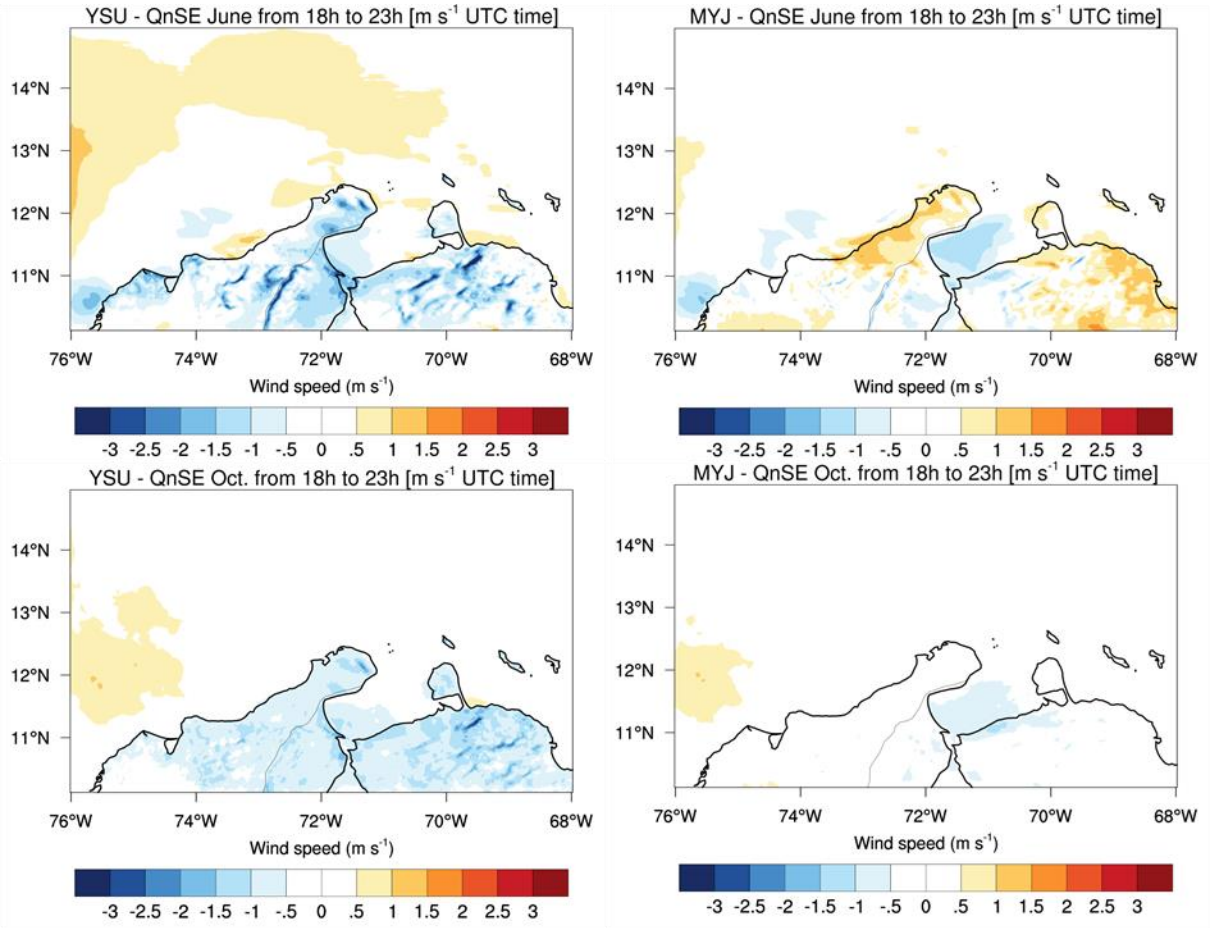

Figure 3.24 : ***Differences of monthly average wind speed in the interval 13 h to 18 h LST with best performing scheme* (*QnSE*).**

Comparison between WRF and ERA5

The results obtained with the schemes in the nested domains show a definite improvement in the spatial representation of wind magnitude, variability, and patterns, when compared with the lower resolution offered by ERA5, which allows to appreciate the added value of running WRF with factors such as a better-defined topography and land cover. In general terms, ERA5 underestimates wind speed for both months and for the intraday time intervals, whereas WRF contributes to generating a more detailed representation of the analyzed variables.

3.4.4 Wind Power Density at 100 m

After selecting the QNSE scheme as the most indicated for representing the wind in the studied area, we proceed to estimate the WPD at 100 meters height, for the analyzed months. In Figure 3.25 we present a comparison between the WPD fields generated by WRF and by ERA5 at 100 meters height. On the one hand, as was expected, the high resolution of the WRF model produces more detailed fields, since the model performs calculations for a grid of 3 x 3 km and therefore can

catch more details of the influence of local factors in regional wind patterns. On the other hand, ERA5 is a valuable reanalysis product that, due to its resolution, cannot present the level of detail offered by WRF. For example, for the month of June, ERA5 underestimates the WPD for the inland portion located farthest north (La Guajira region), showing a quasi-uniform field around 1200 W m^{-2}, whereas the field generated by WRF present values of up to 2000 W m^{-2}. In addition, for the offshore during June, WRF generates higher values of the variable and shows greater variability. For October instead, ERA5 present higher values of the WPD than WRF, both inland and offshore and, for La Guajira region, ERA5 shows a uniform pattern of the WPD, between 400 W m^{-2} and 800 W m^{-2}, whereas WRF shows wide areas of this region with a WPD under 400 W m^{-2}. For the offshore during October, ERA5 also present higher values of the WPD. In both months, WRF can reproduce the influence of local factors such as the coastline and orography in the wind fields and therefore in the WPD fields.

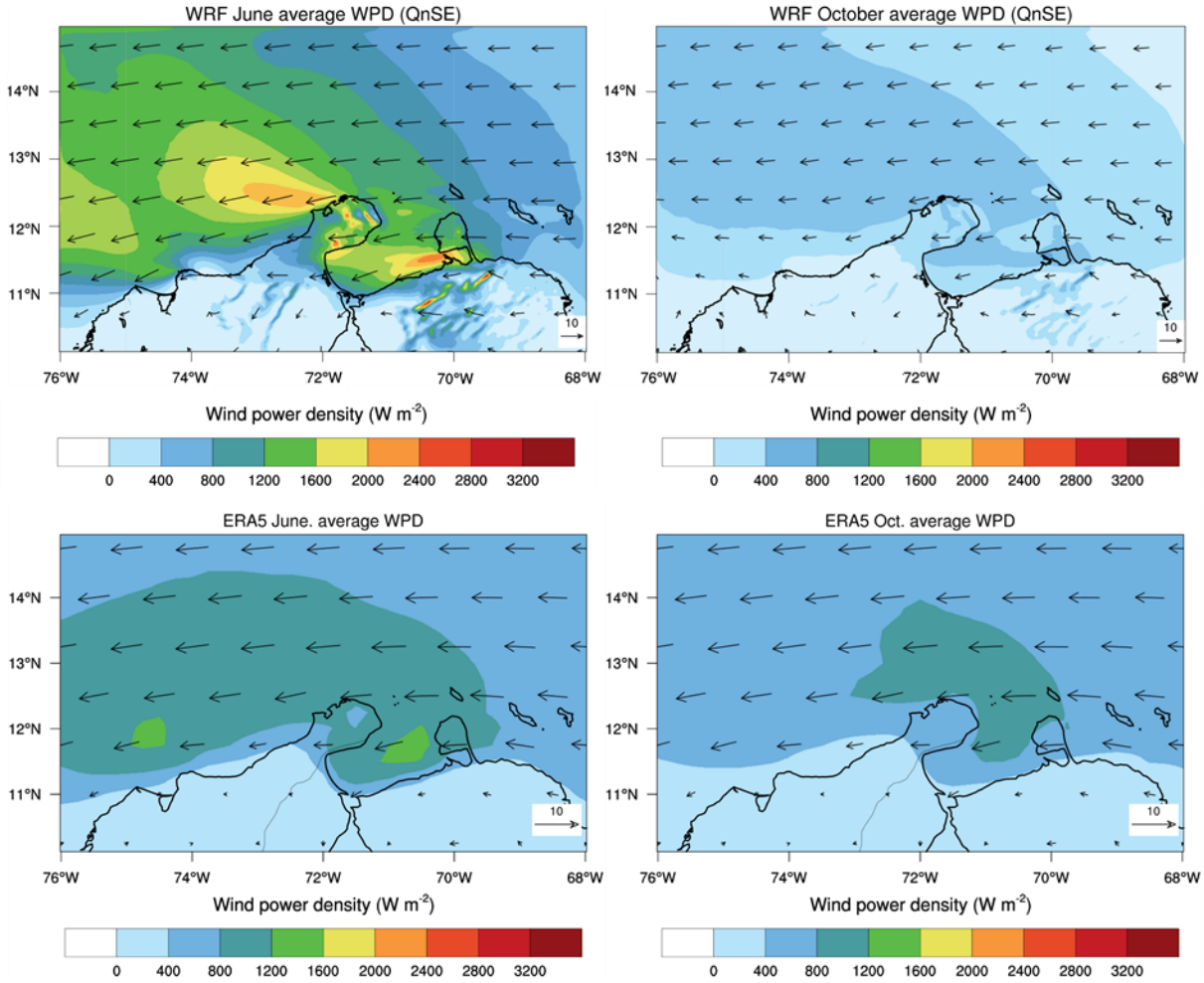

Figure 3.25 : ***Wind power density fields – Comparison with ERA5 data at 100 meters height for June and October.***

In terms of the wind power assessment with WRF, for June (Figure 3.26) the WPD for La Guajira region reaches values up to 1600 W m^{-2} in the shoreline, with standard deviations in the order of 500 W m^{-2}, whereas offshore in promising areas the WPD reaches 2000 W m^{-2} with a maximum standard deviation of 800 W m^{-2}, which indicates a wind potential more than excellent, according

to NREL (Gunturu & Schlosser, 2012). For July, the WPD at offshore reaches values up to 2200 W m^{-2} whereas for the shoreline the values of WPD remain very close to those reached in June, about the standard deviation of WPD in July this reaches values up to 1000 W m^{-2}.

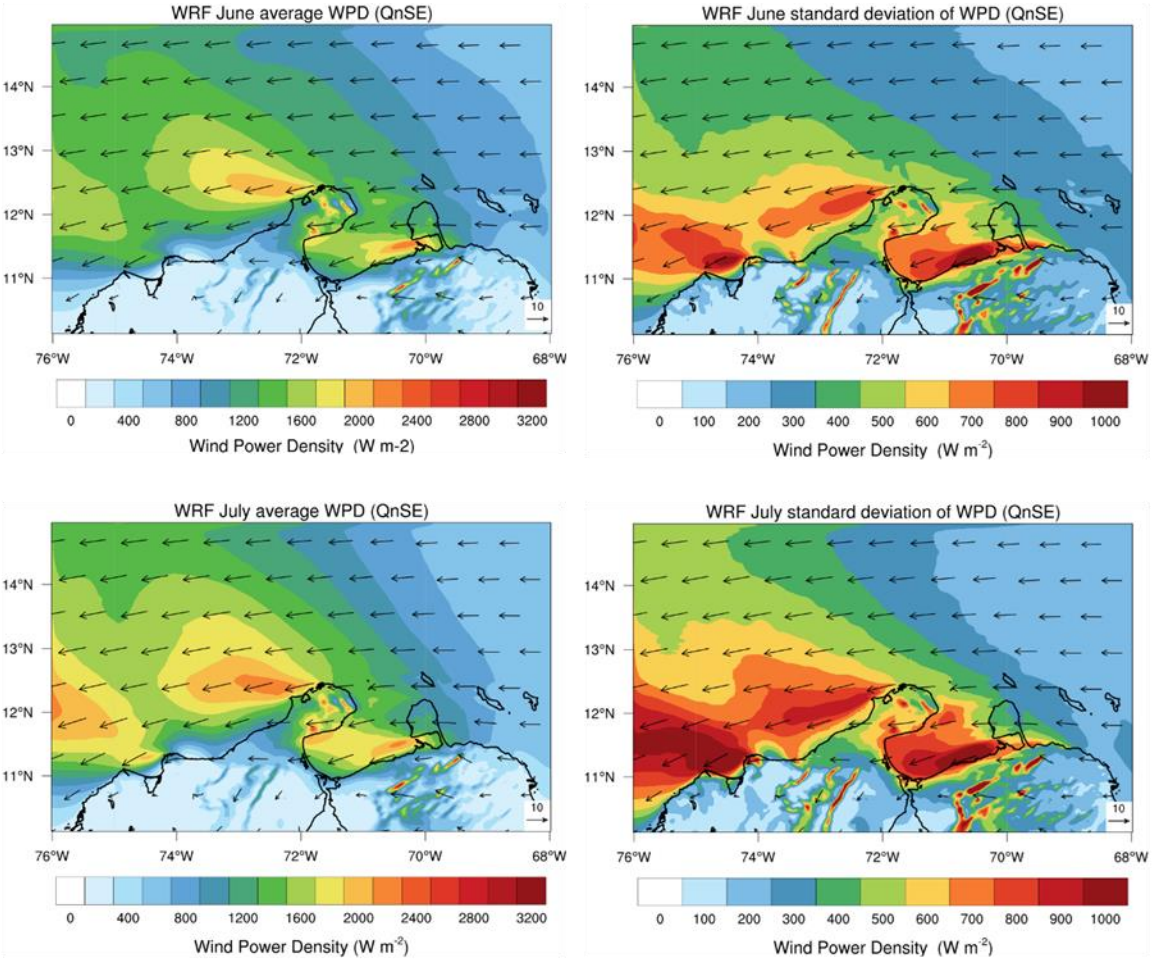

Figure 3.26 : ***Wind power density and its standard deviation at 100 meters height for June and July.***

For October (see Figure 3.27) the WPD descend to a range between 800 W m^{-2} and 600 W m^{-2} for the shoreline, and also for the offshore regions, presenting a standard deviation up to 400 W m^{-2} for the onshore and shoreline, whereas for offshore the standard deviation reaches values between 400 W m^{-2} and 600 W m^{-2}. That means that, even in the month of lower wind speeds, the wind potential for the shoreline and onshore of La Guajira region is between good and excellent (according to NREL). For November, at the offshore the values of both WPD and its standard deviation begin to be greater than the presented during October, whereas for the inland and shoreline these remain similar to those presented in October.

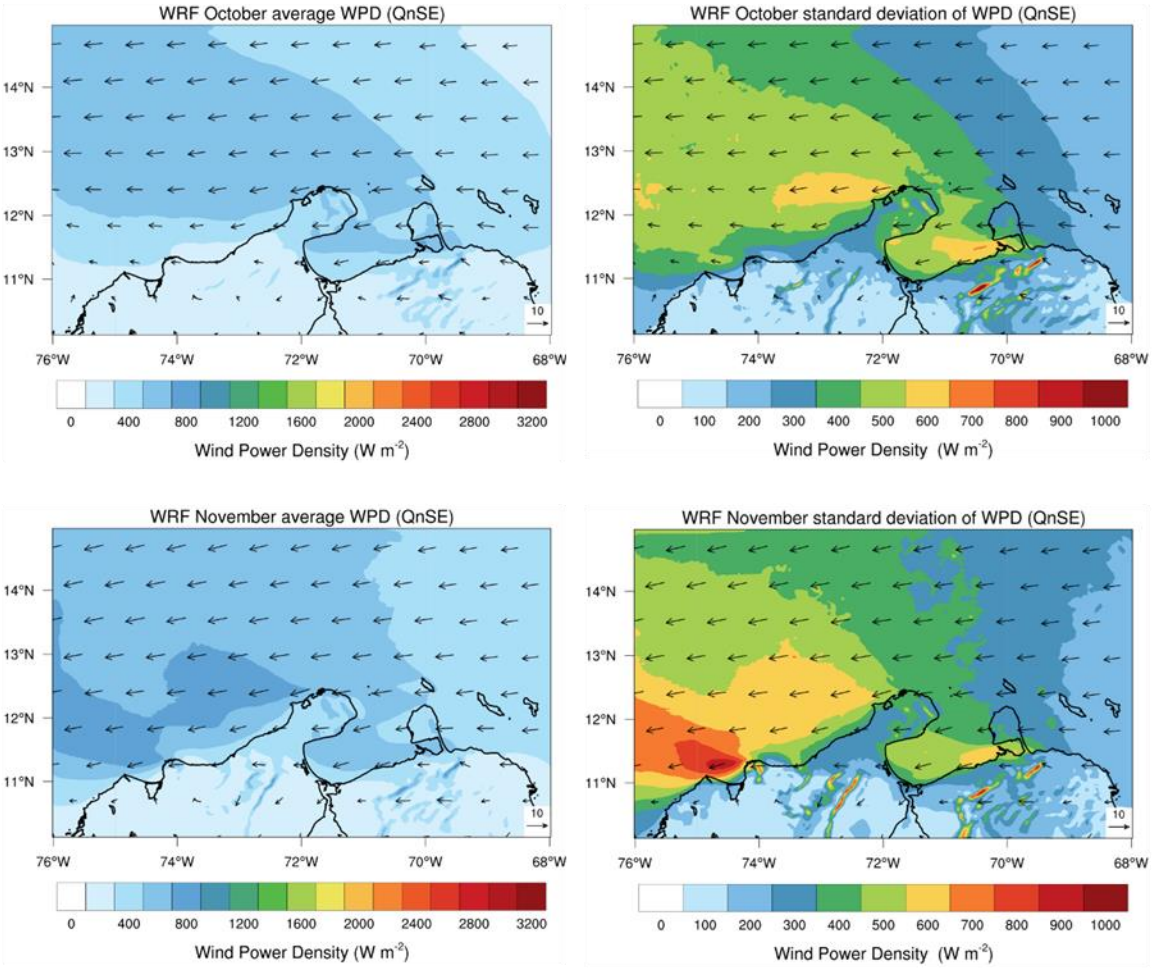

Figure 3.27 : ***Wind power density and its standard deviation at 100 meters height for October and November.***

The wide variability of the monthly WPD is a great indicator of the necessity of an adequate assessment of the wind potential from the point of view of the operation of the whole electrical grid, an also for individual wind farms, which shows the need for future developments in wind energy forecasting for periods on the weekly, daily, and intraday scales.

About the expected improvement in the estimation and representation of the WPD with the WRF model, according to the results presented in Figure 3.25, WRF produced a significant improvement in the representation of the WPD both in spatial variability and availability of wind resource across the studied region. In addition, there are additional and significant improvements in the representation of the influence of local factors such as the coastline and local topography, also since the calculations performed with WRF consider the intra hourly variations of wind speed and air density, which generates more accurate and reliable results.

Annual cycle and duration curves of Wind Power Density

The annual WPD (at 100 m) was estimated for the entire domain and for the nearest points to the meteorological stations. For point estimates was used data generated with the Tslist option of the WRF model to obtain time series of wind speed, temperature, atmospheric pressure, and mixing

ratio at specific sites. The time step for the point calculations was the 10-minute average, despite comparing the estimations with the ones obtained from meteorological stations and ERA5(for ERA 5, the one-hour averages were used).

The WPD estimated with WRF was compared with estimations of WPD performed with data from ERA5, and the meteorological stations, using the duration curves, as shown in Figure 3.28. The results show that WRF can represent relatively well, both in time and magnitude, the availability of WPD in the studied sites, although the WRF skill varies according to the place, and even can be worse than ERA5 in some cases. As was shown previously, ERA5 has a good capability for representing the mean wind speed in some of the analyzed sites (although it has serious problems with the representation of the diurnal cycle), which can explain the good performance of ERA5 in the site of Pto Velero station (Figure 3.28 d). In the case of Pto Bolivar station (Figure 3.28 b), both ERA5 and WRF do not fit well with the station's WPD, whereas at Pto Estrella(Figure 3.28 a) and Ballenas (Figure 3.28 c) stations WRF outperforms ERA5 in representing the variability of the observed WPD.

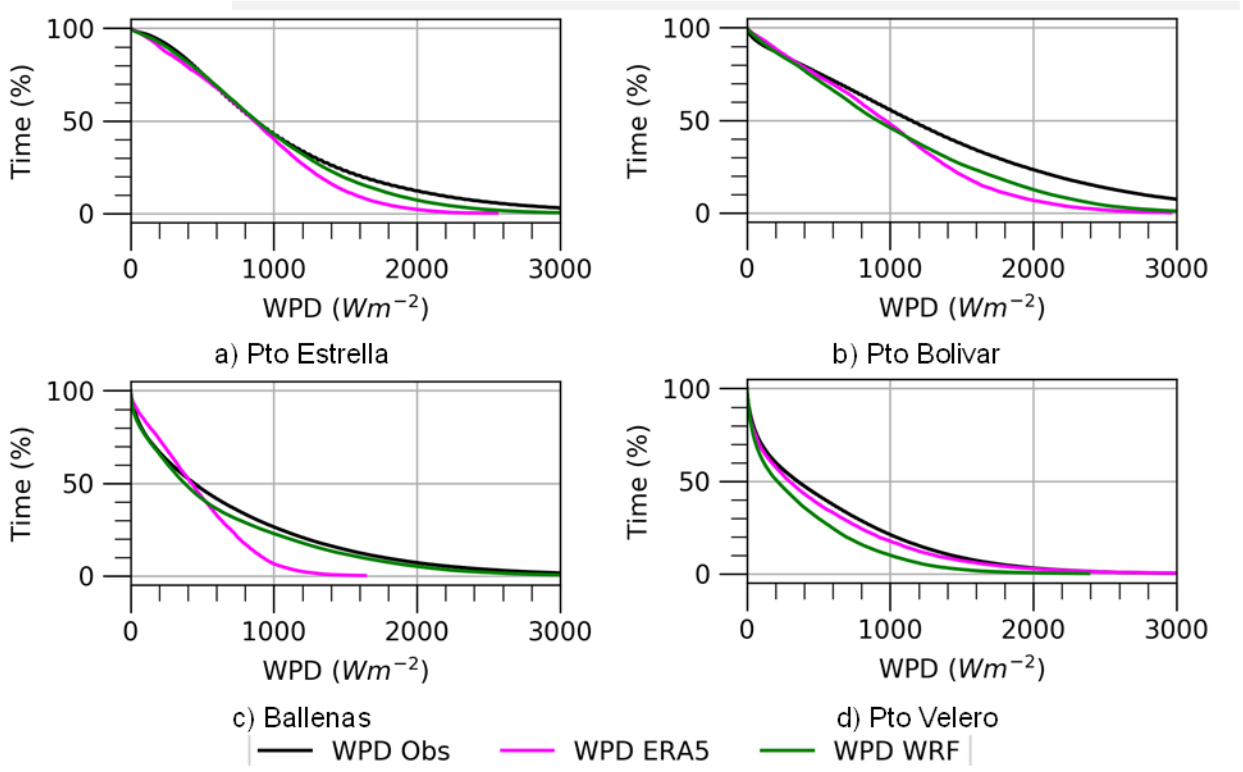

Figure 3.28: ***Duration curves of WPD for the whole year.***

Figure 3.29 shows the annual regime of WPD at 100 meters height for the studied area. Throughout the year values of WPD over 400 W m^{-2} are observed in La Guajira region, being this an indicator of the economic viability of the wind resource. For the period between December and September (10 months) the WPD for inland of the La Guajira region stays over 800 W m^{-2} (Outstanding quality according to NREL), whereas for the shoreline the WPD reaches values up to 1600 W m^{-2} during March, April, June, and July. Besides the presented annual regime of WPD shows the

availability of a Superb quality wind class (WPD > 800 W m $^{-2}$, according to NREL classification) throughout the year for the wide offshore areas identified previously in this study.

The monthly standard deviation of the WPD is presented in Figure 3.30, this source adds context to the annual regime of WPD presented in Figure 3.29. For the inland of La Guajira region, the standard deviation of the WPD maintain values between 300 W m^{-2} and 600 W m^{-2} for most of the area, whereas in the months with higher WPD appears some areas with higher values in the standard deviation. For the offshore the values of the standard deviation vary throughout the year, reaching values between 400 W m^{-2} and 1000 W m^{-2}. The results presented in these two figures allow us to conclude that wind energy in the area has a strong seasonality component that is function of the ITCZ displacement throughout the year.

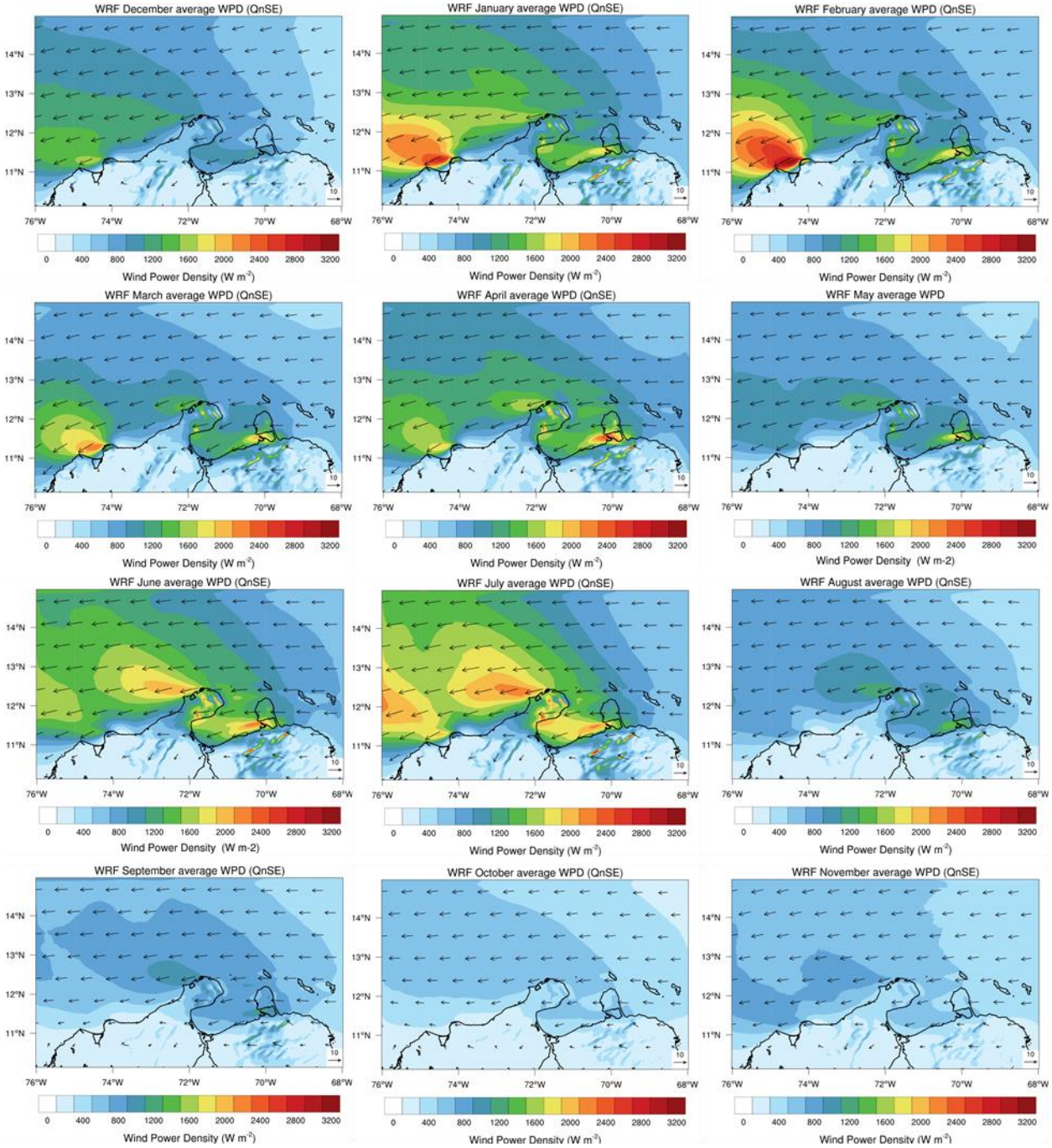

Figure 3.29 : ***Monthly regime of WPD at 100 meters height estimated with WRF.***

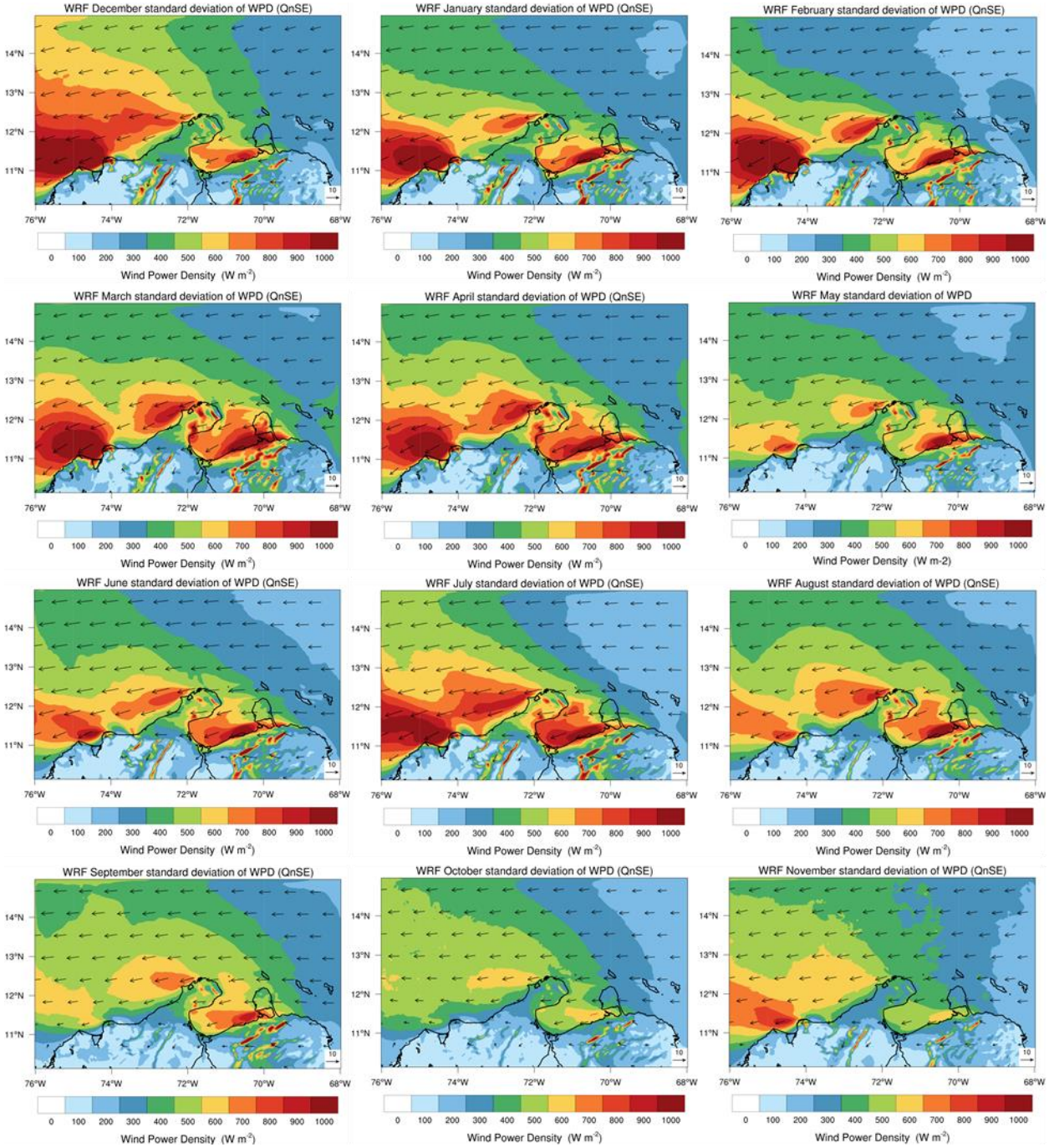

Figure 3.30 ***: Standard deviation of the monthly WPD.***

Intraday Wind Power Density

In Figure 3.31 (for June) and Figure 3.32 (for October), we present the cross-section of the monthly average of the WPD at 13 h (LST) for the latitudes coincident to Puerto Estrella station (12.35°N) and Ballenas station (11.70°N). These cross-sections have a height between 100 and 1,000 meters.

The higher WPD in June occurs near to -72.7° longitude (offshore), which likely relates to the Caribbean Low-Level Jet (CLLJ) (Whyte et al., 2008). As expected, the values of WPD vary according to latitude and longitude, indicating a high availability of wind energy for this hour of the day in both onshore and offshore locations. Heights up to 140 m can be reached with the available technology.

By contrast, in October the mean values of WPD at 13 h (LST) descend significantly, keeping values that are adequate for wind power generation at 12.35°N. But with only few zones reaching a WPD up to 400 W m^{-2} at11.70°N.

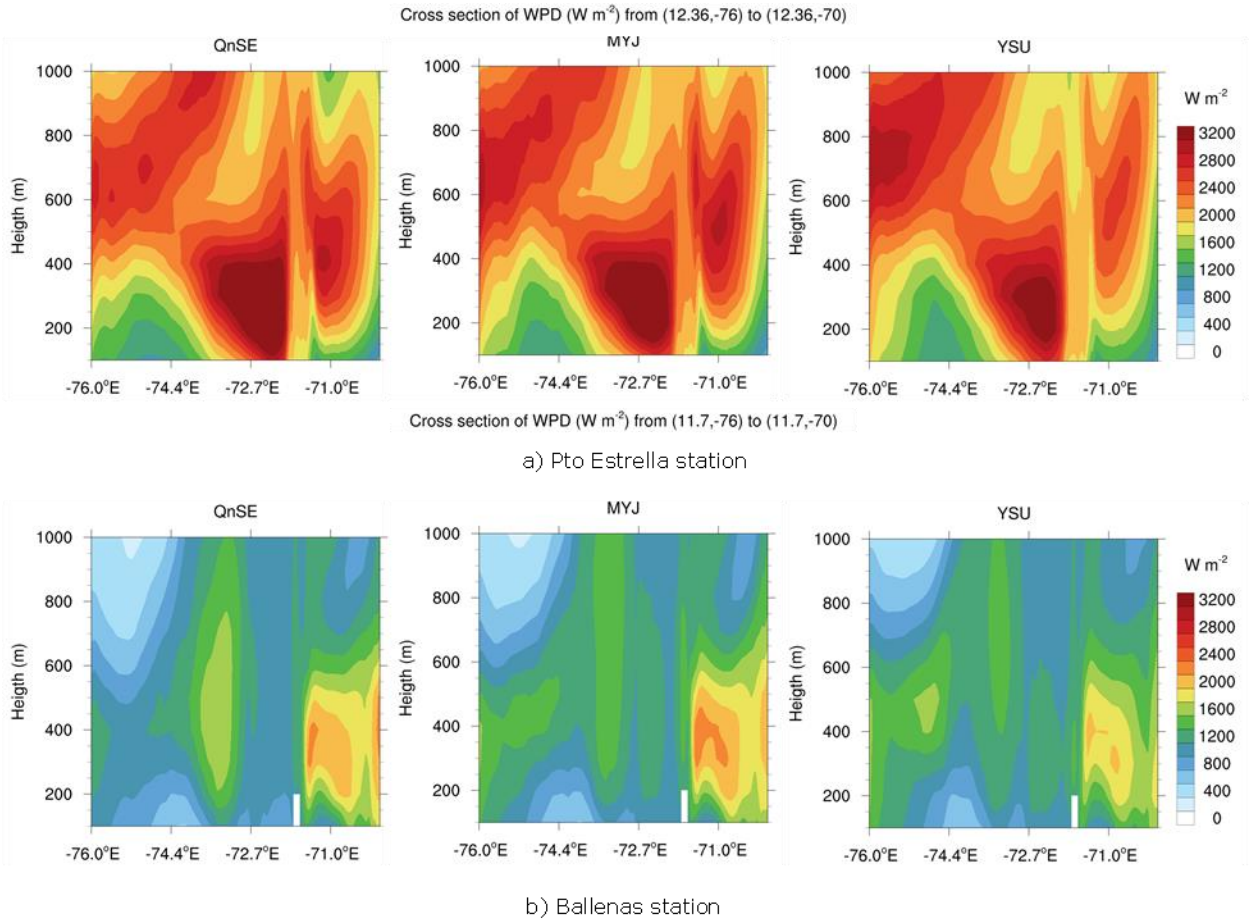

Figure 3.31 : ***Cross-section of the monthly average WPD at 13 h (LST) for June at latitudes 11.70 °N and 12.35°N (stations 1 and 2).***

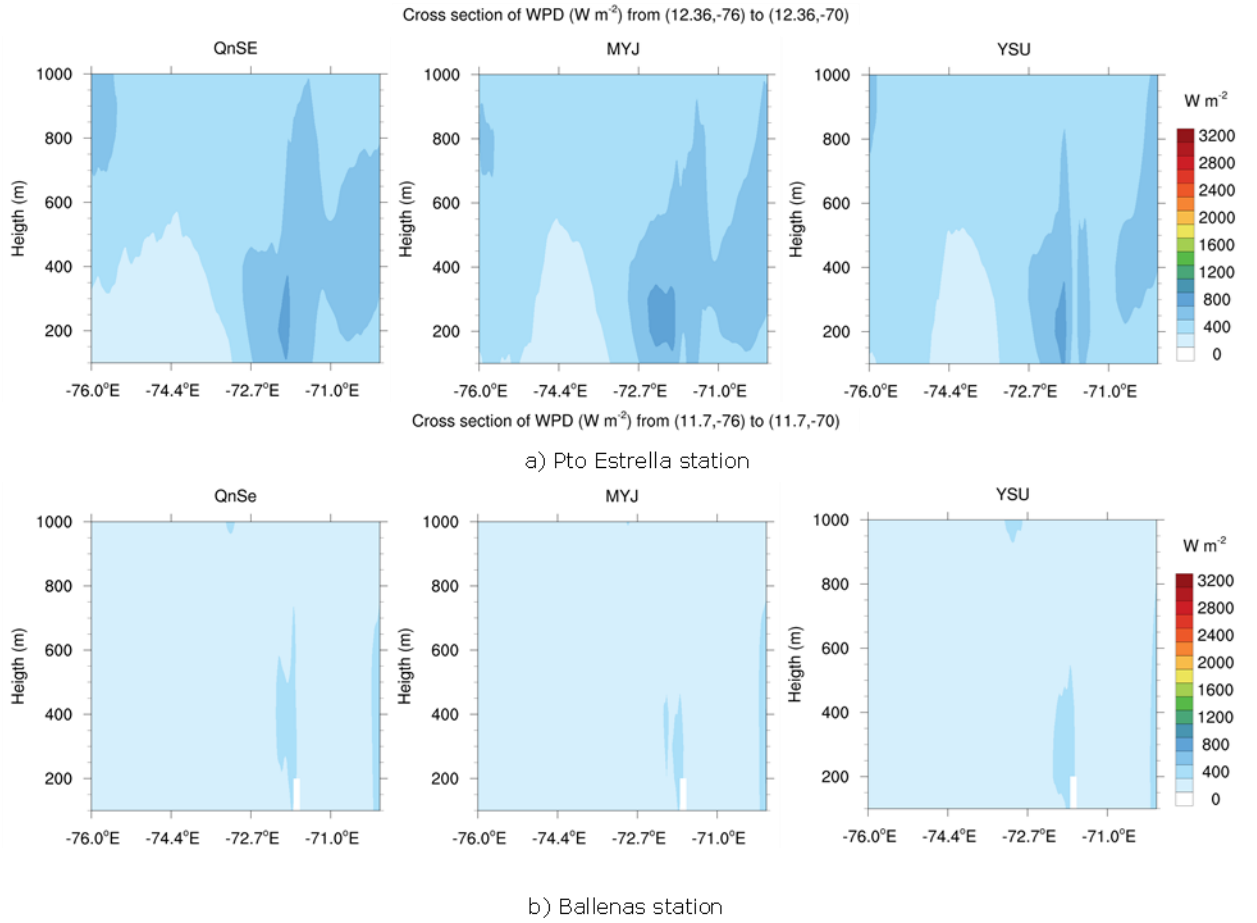

Figure 3.32 : ***Cross-section of the monthly average WPD at 13 h (LST) for October at latitudes 11.70 °N and 12.35°N (stations 1 and 2).***

3.5 Conclusions

In this study, we evaluated the performance of three planetary boundary layer (PBL) schemes implemented in WRF to represent surface winds in the Caribbean region of Colombia. We compared the performances against data from four meteorological stations and data from ERA5 reanalysis. We chose the scheme with the best performance to determine the wind power potential of the region, using WPD fields and their duration curves for a representative year. To our knowledge, this is the first study of wind potential for the Caribbean region of Colombia that performs a high-resolution numerical simulation of the atmosphere, using the WRF model with two nested domains (9 km and 3 km resolutions) and 50 vertical levels with 15 minutes outputs, analyzing the sensitivity of different PBL schemes for two months with extreme wind speeds (June and October), and extending the analysis to other months of the same seasons (with July and November fields of WPD) and for the whole year through the WPD duration curves and the WPD annual cycle.

We found that the WRF model (for the studied region with any of the analyzed schemes and in both grid resolutions), significantly improves the representation, in phase and amplitude, of the intra diurnal wind patterns observed in complex topographic sites along the shoreline, compared to the ERA5 reanalysis. This is particularly evident in the low fractional bias obtained by the WRF schemes for the analyzed intra-day intervals.

Regarding the ability of the PBL schemes to reproduce the phase and amplitude of the mean diurnal cycle of wind speed observed in the meteorological stations, the QNSE scheme outperforms the YSU and MYJ schemes, being the MYJ local closure scheme the one with the worst performance. Overall, in the analyzed cases the nested domain with higher grid resolution performs better than the external domain with lower grid resolution. For the finer grid resolution, the averaged FB (over intra diurnal intervals and months) was 9.88% for the QNSE scheme, 9.95% for MYJ, and 13.02% for YSU (compared to 14.60% for ERA5), whereas for the 9-km domain the averaged FB was 10.20% for the QNSE scheme, 9.50% for MYJ, and 10.83% for YSU respectively. These results show that, under the FB metric, in some cases the raw domain performs better than the finer domain.

For the analyzed sites, the WRF model is able to represent both timing and magnitude of the land-sea breeze circulation systems, performing better than ERA5, which presents narrow hodographs with counterclockwise rotation patterns. However, the WRF hodographs still show wider patterns than the observed in the stations, even though their wind rotation pattern is clockwise like the observed. In this regard, the higher grid resolutions of the model slightly improve performance over low resolutions.

The wind speed frequency distributions generated with WRF vary widely with the site, the month, and the PBL scheme as well as with the grid resolution. Overall: i) for the month of lower wind speeds, the PDFs from WRF and ERA5 fit well the observed data, although WRF outperforms ERA5; ii) for the month of higher wind speeds, WRF's PDFs varies considerably, and the best fit changes with the location and the domain, whereas ERA5 distributions are narrow around the mean, at the analyzed points; iii) WRF, with both grid resolutions, performs better than ERA5, since the reanalysis product lacks the capacity to represent the frequency of occurrence of both low and high wind speeds, while ERA5 overestimates the occurrence of mean speeds.

The wind fields generated with WRF show more details in the wind patterns and its variability, at the offshore, onshore, and across the shoreline. This feature stands from the high-resolution simulation of fluid and local factors such as topography, shoreline, and land cover. In principle, a pattern closer to reality is expected from these additional details. Despite the difference in the level of detail reached by WRF, at the scale of the model domain, the average wind fields generated by ERA5 are not very different from those of WRF. Instead, WRF presents fields with higher standard deviations than ERA5. At the intra-diurnal level, the WRF fields are stronger than those from ERA5, especially for La Guajira Region and the continental portion of the domain. These differences are connected with the broader WRF PDFs compared to ERA5, and with the fact that the WRF PDFs are similar to the observed ones on the available stations, which suggests that the standard deviation might be better captured in WRF than in ERA5.

For the wind fields during the interval between 13 h and 18 h (LST), WRF presents stronger fields than ERA5, including the land portion of La Guajira region, compared to the observation points.

For this interval, ERA5 presented an averaged FB of 21.8% for June and 23.8% for October, whereas QNSE for the finer domain presented a FB of 7.9% and 7.4% respectively (all WRF schemes and domains presented a lower averaged FB than ERA5 for this interval). Therefore, it could be inferred that, compared to ERA5, WRF offers a better representation of the wind field for such interval, at least for the mentioned region. Since the WPD is a function of the cube of wind speed, the accurate representation of the magnitude and variability of winds offers very valuable information for wind energy operators.

Since the YSU scheme is widely used in the specialized literature, it is important to report that, according to our results, the YSU scheme generates weaker wind fields than QNSE and MYJ schemes, for the land portion of the studied domain (for both monthly average and the interval 13 h to 18 h). These differences are persistent in the two analyzed months and may be due to the approximation used to solve the closure problem, given that YSU is a first-order nonlocal closure scheme, whereas QNSE and MYJ both are 1.5 order local closure schemes.

Despite the advantages of using WRF, we must highlight some identified issues. For instance, at the daily average scale, it was common to observe that some WRF schemes, at some points, presented a fractional bias higher than ERA5 (i.e., at station 1, in comparison with the YSU scheme, ERA5 presented a FB of 1% for June and 14.1% for October while the YSU fractional bias for those months was of -4.6% and -18.7% respectively). This behavior was highly variable with the site and the WRF schemes. For the daily average of wind speed both WRF and ERA5 presented a higher negative fractional bias during the month of lower wind speeds. Although for the analyzed intra diurnal interval (six hours), the WRF model appears to stay in phase with the observations at some points (for example Figure 3.5), at the hourly scale the model was not able to reproduce the phase and amplitude of the observed oscillation (i.e., problems of simultaneity in the representation at hourly scale). For the intra diurnal variability, according to the averaged FB, ERA5 was outperformed by all WRF schemes and domains for the periods between 07 h to 12 h and 13 h to 18 h, whereas for the interval between 19 h to 23 h the role was reversed and ERA5 outperformed WRF with an average FB of 9.1% whereas the best WRF model in this interval (MYJ for domain D01) presented an averaged FB of 9.7%, and for the period between 00 h and 06 h, five out of six WRF configurations outperformed the averaged FB of ERA5 (15.3%). We also observed that, in the representation of the diurnal cycle, WRF generates very wide hodographs compared to the observations, while the opposite occurs with ERA5 that generates excessively narrow hodographs. In both cases, they perform away from the observations.

WRF improves significantly the frequency of WPD in both variability and magnitude compared with ERA5 for two of the observation's points (stations 1 and 3). In the case of station 4, ERA5 shows an almost perfect fit with the observations, whereas in station 2, WRF behaves slightly better than ERA5, but both ERA5 and WRF were still far from the observations at this point. The WPD estimates performed with WRF with the three schemes at regional scale generate a similar vertical pattern, with variations at the height of interest (between 100m and 150m). The WPD fields generated with ERA5, at least for large domains (synoptic scale), may provide useful information for the initial identification of areas with wind potential.

The wind fields generated with WRF for monthly mean wind speed, monthly average diurnal cycle, monthly average WPD, and their respective deviations, are very useful for wind power potential identification during the feasibility and planning stages of wind farms, while demonstrating the

feasibility for using WRF to model short-term operation in wind farms. Since the results presented in this study are more centered on the evaluation of the wind potential for feasibility stages of wind farms and for their operation in long time scales (i.e., for maintenance programming yearlong), we highlight the need for the validation of WRF performance in forecasting contexts, focusing on the operation of wind farms in short time scales.

The simulations show wide offshore areas between 76°W and 72°W and above 12°N, and also in the Gulf of Venezuela (between 72 W to 70 W, and 11 N to 12 N) that are feasible for commercial development of the offshore wind industry, reaching values of WPD above 2000 W m^{-2} during months of high wind speeds, and values up to 400 W m^{-2} during months of low wind speeds.

Our results also allow identifying several areas with commercial wind power potential (currently with scarce or null measurement data) both on the shoreline and offshore along the north coast of South America, in the territories of Colombia and Venezuela, and especially in the region of La Guajira.

The results on wind power potential presented in this study are very valuable for the Caribbean region of Colombia, since they came from simulations with a high spatial and temporal resolution, and they considered the variability of the resource. About the results presented for WRF PBL schemes performance, these are very relevant since they constitute a very useful basis for any future implementation of wind power forecasting programs in the region.

4. General Conclusions

This study characterizes the wind regime of the Caribbean coast of Colombia with ten-minute averaged wind speed data from climatological stations and data from the newer ERA5 reanalysis product. This characterization allowed the identification of local wind patterns such as land-sea breezes and the statistical definition of diurnal cycles of wind speed. The characterization not only confirms that the highest average wind speeds occur in La Guajira, (5.5 m s-1 to 8.3 m s^{-1}), but also identifies other places with potential for wind power generation along the coastline of the Magdalena department (6.0 m s^{-1} to 7.1 m s^{-1}), while discarding others such as the coast of the department of Bolivar (2.8 m s^{-1} to 5.4 m s^{-1}), the Gulf of Urabá (2.2 m s^{-1} to 3.2 m s^{-1}), and the archipelago of San Andrés (3.4 m s^{-1} to 4.5 m s^{-1}). As expected, ERA5 shows Pearson correlations with observed data between 0.23 and 0.80, the highest correlations occurring in higher latitudes (under direct influence of the trade winds) and the lower correlations near coastlines with complex shape and topography.

For some places in La Guajira region, the Annual Energy Production (AEP) is up to 17 GWh year, with a capacity factor (CF) up to 50%, whereas for the shoreline of the Magdalena department (to the south) the AEP reaches 9 GWh year, with a capacity factor of 30%. These estimates consider a correction due to operational restrictions, based on the CF reported by the Jepírachi wind farm for 2014. The estimated values of AEP with ERA5 present differences between 11.8% and 25.7% with respect to observations (10 minutes averages).

The atmospheric modeling for La Guajira region with WRF improves the representation, in phase and amplitude, of the intra diurnal wind patterns observed in sites along the shoreline, in comparison with the representation provided by ERA5. For the studied months, in the representation of the diurnal cycle, ERA5 shows an average FB of 14.60% whereas the best-performing WRF configuration for this metric (MYJ-D01) presented an average FB of 9.50%. At the daily average scale, some WRF schemes, at some specific locations, presented a fractional bias higher than ERA5 (e.g., at station 1, in comparison with the YSU scheme, ERA5 presented a FB of 1% for June and 14.1% for October while the YSU fractional bias for those months was of -4.6% and -18.7% respectively). Both WRF and ERA5 present higher averaged FB during the month with low wind speeds.

The analysis of 6-hour windows within the day shows that the diurnal cycle simulated by WRF is, most of the time, nearly in phase with observations, with typical delays between maxima or minima of about 1-3 hours. By contrast, ERA5 appears in counter phase or with a quasi-flat oscillation throughout the day. At the intra-diurnal level, in the six-hour windows, at least one of the WRF schemes outperformed ERA5 in the averaged FB. Furthermore, in some cases, ERA5 was totally out of phase with respect to the observed data. At hourly scale, the patterns in the diurnal cycle generated by WRF also outperform the patterns generated with ERA5, which appear further away from observations.

From the studied PBL schemes, the QNSE performed better than the YSU and MYJ with respect to the metrics of the Taylor diagrams of the mean diurnal cycles, including variability and

correlation. In general, the YSU scheme underestimates the wind speed fields compared to QNSE and MYJ, especially inland.

For the estimation of the WPD, the WRF model presented an almost perfect fit to the observed WPD duration curves in two of the analyzed sites (Pto Estrella, and Ballenas), outperforming ERA5. In Pto. Velero station ERA5 clearly outperformed WRF, whereas at Pto. Bolivar station both models had fair performance, with WRF being slightly better.

Since WRF better represents the influence of local factors in the wind fields, WRF WPD fields are more detailed than those generated by ERA5 (especially along the shoreline and inland). For instance, ERA5 underestimates the WPD on the shoreline during the month of high wind speeds, whereas WRF presents a good agreement with the stations in the phase and amplitude of the diurnal cycle, and in the wind speed frequency distributions. For the month of low wind speeds, ERA5 overestimates the WPD inland and offshore. However, the WPD fields generated with ERA5, at least for large domains (synoptic scale), may provide useful information for the initial identification of areas with wind potential. In this sense, as future venue of research, we highlight the need for the validation of WRF performance in forecasting contexts, focusing on the operation of wind farms in short time scales.

The wind fields and the WPD fields obtained from the atmospheric modeling with WRF provide new information of high resolution about wind variability and availability, which allows the identification of sites with commercial wind potential, but currently with scarce existing information. Many of these sites with commercial WPD (defined by NREL as greater than 500 W m^{-2}) are located in wide offshore areas and along the shoreline and inland of La Guajira Region. This information will be of great help for the planning of new wind farms and even for the operation of existing ones.

The validation of WRF PBL schemes presented in this study will be useful for wind energy forecast systems in wind farms and for the national electric grid operation in short time scales. While ERA5 can provide useful information about WPD for synoptic scales, WRF offer very detailed information for wind power assessment in the local and regional scales. Both combined, serve to identify new sites with wind potential.

5. References

Arslan, T., Bulut, Y. M., & Altin Yavuz, A. (2014). Comparative study of numerical methods for determining Weibull parameters for wind energy potential. Renewable and Sustainable Energy Reviews, 40, 820–825. https://doi.org/10.1016/j.rser.2014.08.009

Benjamin, S. G., Weygandt, S. S., Brown, J. M., Hu, M., Alexander, C. R., Smirnova, T. G., Olson, J. B., James, E. P., Dowell, D. C., Grell, G. A., Lin, H., Peckham, S. E., Smith, T. L., Moninger, W. R., Kenyon, J. S., & Manikin, G. S. (2016). A North American hourly assimilation and model forecast cycle: The rapid refresh. *Monthly Weather Review*, *144*(4), 1669–1694. https://doi.org/10.1175/MWR-D-15-0242.1

Betts, A. K., Chan, D. Z., & Desjardins, R. L. (2019). Near-Surface Biases in ERA5 Over the Canadian Prairies. *Frontiers in Environmental Science*, *7*(September). https://doi.org/10.3389/fenvs.2019.00129

Bonan, G. (2016). Ecological Climatology. https://doi.org/10.1017/CBO9781107339200

Burton, T., Sharpe, D., Jenkins, N., & Bossanyi, E. (2001). Wind Energy Handbook. JOHN WILEY & SONS, LTD. New York: JOHN WILEY & SONS, LTD.

Carvajal-Romo, G., Valderrama-Mendoza, M., Rodríguez-Urrego, D., & Rodríguez-Urrego, L. (2019). Assessment of solar and wind energy potential in La Guajira, Colombia: Current status, and future prospects. *Sustainable Energy Technologies and Assessments*, *36*(August), 100531. https://doi.org/10.1016/j.seta.2019.100531

Carvalho, D., Rocha, A., Go´mez-Gesteira, M., & Silva Santos, C. (2014). Sensitivity of the WRF model wind simulation and wind energy production estimates to planetary boundary layer parameterizations for onshore and offshore areas in the Iberian Peninsula. *Applied Energy*, *135*, 234–246. https://doi.org/10.1016/j.apenergy.2014.08.082

Carvalho, D., Rocha, A., Gómez-Gesteira, M., & Silva Santos, C. (2014). WRF wind simulation and wind energy production estimates forced by different reanalyses: Comparison with observed data for Portugal. Applied Energy, 117, 116–126. https://doi.org/10.1016/j.apenergy.2013.12.001

Carvalho, D., Rocha, A., & Gómez-Gesteira, M. (2012). Ocean surface wind simulation forced by different reanalyses: Comparison with observed data along the Iberian Peninsula coast. *Ocean Modelling*, *56*, 31–42. https://doi.org/10.1016/j.ocemod.2012.08.002

Carvalho, David, Rocha, A., Gómez-Gesteira, M., & Santos, C. (2012). A sensitivity study of the WRF model in wind simulation for an area of high wind energy. *Environmental Modelling and Software*, *33*, 23–34. https://doi.org/10.1016/j.envsoft.2012.01.019

Cohen, A. E., Cavallo, S. M., Coniglio, M. C., & Brooks, H. E. (2015). A review of planetary boundary layer parameterization schemes and their sensitivity in simulating southeastern U.S. cold season severe weather environments. *Weather and Forecasting*, *30*(3), 591–612. https://doi.org/10.1175/WAF-D-14-00105.1

Devis-Morales, A., Montoya-Sánchez, R. A., Bernal, G., & Osorio, A. F. (2017). Assessment of extreme wind and waves in the Colombian Caribbean Sea for offshore applications. Applied Ocean Research, 69, 10–26. https://doi.org/10.1016/j.apor.2017.09.012

Emeis, S. (2013). Wind Energy Meteorology. Springer. https://doi.org/10.2174/97816080528511060101

EPM (2019) https://www.epm.com.co/site/home/nuestra-empresa/nuestras-lantas/energia/parque-eolico

Floors, R., & Nielsen, M. (2019). Estimating air density using observations and re-analysis outputs for wind energy purposes. *Energies*, *12*(11). https://doi.org/10.3390/en12112038

Galperin, B., & Sukoriansky, S. (2010). Geophysical flows with anisotropic turbulence and dispersive waves: Flows with stable stratification. *Ocean Dynamics*, *60*(5), 1319–1337. https://doi.org/10.1007/s10236-010-0325-z

Gil Ruiz, S.A., Cañon, J., Martinez, J.A. (2020) Wind Power Assessment in The Caribbean region of Colombia Using Ten-Minute Wind Observations and ERA5 Data, under review for publication in Journal of Renewable Energy

González-Alonso de Linaje, N., Mattar, C., & Borvarán, D. (2019). Quantifying the wind energy potential differences using different WRF initial conditions on Mediterranean coast of Chile. Energy, 188. https://doi.org/10.1016/j.energy.2019.116027

Gunturu, U. B., & Schlosser, C. A. (2012). Characterization of wind power resource in the United States. Atmospheric Chemistry and Physics, 12(20), 9687–9702. https://doi.org/10.5194/acp-12-9687-2012

Henao, F., Viteri, J. P., Rodríguez, Y., Gómez, J., & Dyner, I. (2020). Annual and interannual complementarities of renewable energy sources in Colombia. *Renewable and Sustainable Energy Reviews*, *134*(December 2019). https://doi.org/10.1016/j.rser.2020.110318

Hersbach, H., Bell, B., Berrisford, P., Hirahara, S., Horányi, A., Muñoz-Sabater, J., Nicolas, J., Peubey, C., Radu, R., Schepers, D., Simmons, A., Soci, C., Abdalla, S., Abellan, X., Balsamo, G., Bechtold, P., Biavati, G., Bidlot, J., Bonavita, M., … Thépaut, J. N. (2020). The ERA5 global reanalysis. Quarterly Journal of the Royal Meteorological Society, 146(730), 1999–2049. https://doi.org/10.1002/qj.3803

Hong, S. Y. (2010). A new stable boundary-layer mixing scheme and its impact on the simulated East Asian summer monsoon. *Quarterly Journal of the Royal Meteorological Society*, *136*(651), 1481–1496. https://doi.org/10.1002/qj.665

Hong, S. Y., Noh, Y., & Dudhia, J. (2006). A new vertical diffusion package with an explicit treatment of entrainment processes. *Monthly Weather Review*, *134*(9), 2318–2341. https://doi.org/10.1175/MWR3199.1

Hoyos Guerrero, B. G., Vélez Macías, F. de J., & Morales Quintero, D. E. (2018). Evaluación del potencial eólico basada en Sistemas de Información Geográfica en La Guajira, Colombia.

IDEAM, UPME, Ruiz M., J. F., Serna C., J., & Zapata L., H. J. (2017). ALTLAS DE VIENTO DE COLOMBIA. Bogota: IDEAM.

IRENA, I. R. E. (2019). Renewable Power Generation Costs in 2018. In International Renewable Energy Agency. https://doi.org/10.1007/SpringerReference_7300

Jacques, R. (2010). Wind Resource Assessment Handbook. AWS Truepower

James, E. P., Benjamin, S. G., & Marquis, M. (2018). Offshore wind speed estimates from a high-resolution rapidly updating numerical weather prediction model forecast dataset. *Wind Energy*, *21*(4), 264–284. https://doi.org/10.1002/we.2161

Janjic, Z. (2002). Nonsingular Implementation of the Mellor-Yamada Level 2.5 Scheme in the NCEP Meso model. *NCEP Office Note*, *437*, 61. http://www.emc.ncep.noaa.gov/officenotes/newernotes/on437.pdf

Janjic, Z. I. (1994). The step-mountain eta coordinate model: further developments of the convection, viscous sublayer, and turbulence closure schemes. *Monthly Weather Review*, *122*(5), 927–945. https://doi.org/10.1175/1520-0493(1994)122<0927:TSMECM>2.0.CO;2

Kalmikov, A. (2017). Wind Power Fundamentals. Wind Energy Engineering, 17–24. https://doi.org/10.1016/B978-0-12-809451-8.00002-3

Kalverla, P. C., Duncan, J. B., Steeneveld, G. J., & Holtslag, A. A. M. (2019). Low-level jets over the North Sea based on ERA5 and observations: Together they do better. Wind Energy Science, 4(2), 193–209. https://doi.org/10.5194/wes-4-193-2019

Kaplan, Y. A. (2017). Determination of the best Weibull methods for wind power assessment in the southern region of Turkey. IET Renewable Power Generation, 11(1), 175–182. https://doi.org/10.1049/iet-rpg.2016.0206

Lee, J., & Zhao, F. (2020). *Global Wind Energy Council |GLOBAL WIND REPORT 2019*.

Mattar, C., & Borvarán, D. (2016). Offshore wind power simulation by using WRF in the central coast of Chile. *Renewable Energy*, *94*, 22–31. https://doi.org/10.1016/j.renene.2016.03.005

Mellor, G. L., & Yamada, T. (1982). Development of a Turbulence Closure Model for Geophysical Fluid Problems. *Reviews of Geophysics*, *20*(4), 851–875. https://doi.org/10.1029/RG020i004p00851

NASA 2020., MERRA-2 reanalysis product., https://gmao.gsfc.nasa.gov/reanalysis/MERRA-2/

Nordex (2019) http://www.nordex-online.com/fileadmin/MEDIA/Produktinfos/EN/Nordex_N60_EN.pdf

Olauson, J. (2018). ERA5: The new champion of wind power modelling? Renewable Energy, 126, 322–331. https://doi.org/10.1016/j.renene.2018.03.056

Pérez, R. A., Ortiz, R. J. C., Bejarano, A. L. F., Otero, D. L., Restrepo, L. J. C., & Franco, A. A. (2018). Sea breeze in the Colombian Caribbean coast. Atmosfera, 31(4), 389–406. https://doi.org/10.20937/ATM.2018.31.04.06

Pielke, R. A., & Segal, M. (1986). Mesoscale Meteorology and Forecasting. Mesoscale Meteorology and Forecasting. https://doi.org/10.1007/978-1-935704-20-1

Pichugina, Y. L., Banta, R. M., Bonin, T., Brewer, W. A., Choukulkar, A., McCarty, B. J., Baidar, S., Draxl, C., Fernando, H. J. S., Kenyon, J., Krishnamurthy, R., Marquis, M., Olson, J., Sharp, J., & Stoelinga, M. (2019). Spatial variability of winds and HRRR–NCEP model error statistics at

three doppler-lidar sites in the wind-energy generation region of the Columbia River Basin. *Journal of Applied Meteorology and Climatology*, *58*(8), 1633–1656. https://doi.org/10.1175/JAMC-D-18-0244.1

Poveda, G. (2004). La hidroclimatología de Colombia, una síntesis desde la escala inter-decadal.pdf. Revista Academia Colombiana de Ciencias, XXVIII (107), 201–222.

Ranjha, R., Svensson, G., TjernströM, M., & Semedo, A. (2013). Global distribution and seasonal variability of coastal low-level jets derived from ERA-interim reanalysis. Tellus, Series A: Dynamic Meteorology and Oceanography, 65. https://doi.org/10.3402/tellusa.v65i0.20412

Rife, D. L., Pinto, J. O., Monaghan, A. J., Davis, C. A., & Hannan, J. R. (2010). Global distribution and characteristics of diurnally varying low-level jets. Journal of Climate, 23(19), 5041–5064. https://doi.org/10.1175/2010JCLI3514.1

Rueda-Bayona, J. G., Guzmán, A., Eras, J. J. C., Silva-Casarín, R., Bastidas-Arteaga, E., & Horrillo-Caraballo, J. (2019). Renewables energies in Colombia and the opportunity for the offshore wind technology. Journal of Cleaner Production, 220, 529–543. https://doi.org/10.1016/j.jclepro.2019.02.174

Ricciardulli, Lucrezia & National Center for Atmospheric Research Staff (Eds). Last modified 27 Feb 2017. "The Climate Data Guide: CCMP: Cross-Calibrated Multi-Platform wind vector analysis." Retrieved from https://climatedataguide.ucar.edu/climate-data/ccmp-cross-calibrated-multi-platform-wind-vector-analysis.

Salvação, N., & Guedes Soares, C. (2018). Wind resource assessment offshore the Atlantic Iberian coast with the WRF model. *Energy*, *145*, 276–287. https://doi.org/10.1016/j.energy.2017.12.101

Shetland Aerogenerators (2019) https://www.burradale.co.uk/

Shi, J., & Erdem, E. (2017). Estimation of Wind Energy Potential and Prediction of Wind Power. Wind Energy Engineering, 25–49. https://doi.org/10.1016/B978-0-12-809451-8.00003-5

Skamarock, W. C., Klemp, J. B., Dudhia, J. B., Gill, D. O., Barker, D. M., Duda, M. G., Huang, X.-Y., Wang, W., Powers, J. G., Liu, Z., & Berner, J. (2019). A description of the Advanced Research WRF Version 4, NCAR Technical Notes TN-556+STR. Technical Report, March, 113.

Smets, A., Jäger, K., Isabella, O., Van Swaaij, R., & Zeman, M. (2016). Solar Energy: The Physics and Engineering of Photovoltaic Conversion, Technologies, and Systems. (UIT Cambridge, Ed.). Cambridge.

Stull, R. B. (1988). An Introduction to Boundary Layer Meteorology.

Taylor, K. E. (2001). in a Single Diagram. *Journal of Geophysical Research*, *106*(D7), 7183–7192. https://doi.org/10.1029/2000JD900719

Ulazia, A., Sáenz, J., Ibarra-Berastegi, G., González-Rojí, S. J., & Carreno-Madinabeitia, S. (2019). Global estimations of wind energy potential considering seasonal air density changes. *Energy*, *187*. https://doi.org/10.1016/j.energy.2019.115938

Ulazia, A., Sáenz, J., Ibarra-Berastegi, G., González-Rojí, S. J., & Carreno-Madinabeitia, S. (2019). Global estimations of wind energy potential considering seasonal air density changes. Energy, 187. https://doi.org/10.1016/j.energy.2019.115938

UPME (2020) https://www1.upme.gov.co/PromocionSector/Subastas-largo-plazo/Paginas/Subasta-CLPE-No-02-2019.aspx

Vergara, W., Deeb, A., Toba, N., Crampton, P., & Leino, I. (2010). Wind energy in Colombia A framework for Market Entry. Washington, DC.

Wang, C., Hu, J., Feng, S., Jin, S., Zhang, F., & Liu, C. (2011). Comparing different boundary layer schemes of WRF by simulation the low-level wind over complex terrain. *2011 2nd International Conference on Artificial Intelligence, Management Science and Electronic Commerce, AIMSEC 2011 - Proceedings*, *20100211110012*, 6183–6188. https://doi.org/10.1109/AIMSEC.2011.6009632

Whyte, F. S., Taylor, M. A., Stephenson, T. S., & Campbell, J. D. (2008). Features of the Caribbean low-level jet. International Journal of Climatology: A Journal of the Royal Meteorological Society, 28(1), 119-128.

Wind-turbine-models.com (2019). https://en.wind-turbine-models.com/turbines/1248-vestas-v117-3.45)

Wilczak, J., Finley, C., Freedman, J., Cline, J., Bianco, L., Olson, J., Djalalova, I., Sheridan, L., Ahlstrom, M., Manobianco, J., Zack, J., Carley, J. R., Benjamin, S., Coulter, R., Berg, L. K., Mirocha, J., Clawson, K., Natenberg, E., & Marquis, M. (2015). The wind forecast improvement project (WFIP): A public-private partnership addressing wind energy forecast needs. Bulletin of the American Meteorological Society, 96(10), 1699–1718. https://doi.org/10.1175/BAMS-D-14-00107.1

Whyte, F. S., Taylor, M. A., Stephenson, T. S., & Campbell, J. D. (2008). Features of the Caribbean low-level jet. International Journal of Climatology: A Journal of the Royal Meteorological Society, 28(1), 119-128.

Xie, B., Fung, J. C. H., Chan, A., & Lau, A. (2012). Evaluation of nonlocal and local planetary boundary layer schemes in the WRF model. *Journal of Geophysical Research Atmospheres*, *117*(12), 1–26. https://doi.org/10.1029/2011JD017080

XM (2019)

https://www.xm.com.co/EnMovimiento/Documents/Boletin335/ResumenEenrgiaRenovable.pdf

XM (2019) https://www.xm.com.co/Paginas/Consumo/historico-de-demanda.aspx

XM (2019) http://informesanuales.xm.com.co/2014/SitePages/operacion/2-13-Anex-Generacion-por-recurso.aspx - https://www.xm.com.co/Paginas/Consumo/historico-de-demanda.aspx

XM (2019) http://informesanuales.xm.com.co/2014/SitePages/operacion/2-13-Anex-Generacion-por-recurso.aspx